PERFORMANCE INVESTIGATION OF INDUCTION MOTOR WITH DIRECT TORQUE CONTROL

A DISSERTATION

Submitted in partial fulfillment of the requirements for the award of the degree of

MASTER OF TECHNOLOGY

In

ELECTRICAL ENGINEERING

(With Specialization in Power Apparatus and Electric Drives)

By

KONDA REDDY POLU

DEPARTMENT OF ELECTRICAL ENGINEERING
INDIAN INSTITUTE OF TECHNOLOGY ROORKEE
ROORKEE-247 667 (INDIA)

JUNE, 2006

ID NO: MT-340 | 2006-35 | KRP - PA-SPG

Candidate's Declaration

I here by declare that the work which has being presented in the Dissertation Report entitled **"Performance Investigation of Induction Motor with Direct Torque Control"** in partial fulfillment of the requirements for the award of the degree **Master of Technology** in **Electrical Engineering** with specialization in **Power Apparatus and Electric Drives,** submitted in the **Department of Electrical Engineering, Indian Institute of Technology, Roorkee, INDIA – 247 667**. This is an authentic record of my own work carried out in the period of last two semesters from Aug 2005 to June 2006, under the supervision of **Dr Pramod Agarwal,** Professor and **Dr. S P Gupta,** Professor and Head of the Department, Department of Electrical Engineering, Indian Institute of Technology, Roorkee, INDIA – 247 667.

The matter embodied in this Dissertation Report has not been submitted by me for the award of any other degree or diploma.

P. Konda Reddy

(Konda Reddy Polu)

Date: 29/08/06

Place: ROORKEE

This is to certify that the above statements made by the candidate are correct to the best of my knowledge.

(Dr. Pramod Agarwal)
Professor,
Department of Electrical Engineering,
Indian Institute of Technology, Roorkee

S. P. Gupta

(Dr. S P Gupta)
Professor and Head of the Department,
Department of Electrical Engineering,
Indian Institute of Technology, Roorkee

Acknowledgements

I wish to place on record my deep sense of gratitude and in debt ness to my guides, **Dr. Pramod Agarwal, Professor and Dr. S P Gupta, Professor and Head of the Department, Department of Electrical Engineering, Indian Institute of Technology Roorkee, Roorkee** for their whole heartedness and high dedication with which they involved in this work. I am grateful for hours they spent in discussing and explaining even the minute details of the work in spite of their hectic schedule of work in the department. They listened patiently and authoritatively as they guided me and made their valuable suggestions.

I am grateful to all my teachers of the PAED group for their suggestions and constant encouragement. I am also grateful to all Research Scholars of the PAED group for their suggestions and constant encouragement.

Timely assistance and help from the laboratory staff of Drives Lab, Stores, and Workshop is sincerely acknowledged. Grateful acknowledgements also to my friends and other well wishers whose timely help has gone a long way in this work.

P.Kondareddy

(Konda Reddy Polu)

M.Tech (Elect.) PAED

Date: 29/06/06

Place: ROORKEE

Abstract

Induction motors are widely used in many industrial applications due to their mechanical robustness and low cost. However a draw back of induction machines is that precise torque control can not easily be achieved. In order to overcome this difficulty vector control of pulse width modulation (PWM) inverter fed IM drives which guarantees high dynamic and static performance has been developed. The draw backs of this method are dependency on the rotor resistance value and computational requirements and time delay due to the use of current control loops and axes transformations. Direct torque control (DTC) has a relatively simple control structure yet performs at least as good as vector control technique.

In the present work the Direct Torque Controlled induction motor drive operating principle is briefly studied and the various forms of direct torque controlled induction motor drives that are reported in literature have been reviewed. The implementation of simulation of the drive is done using MATLAB/SIMULINK toolbox with a speed sensor and without speed sensor. The implementation aspects of the simulation and the obtained results are discussed. The drive simulation is done for starting from rest, sudden changes in load torque, speed reversal and the speeds above the base speeds operating the induction motor in the field weakening region. A hybrid fuzzy controller for direct torque control induction motor drive is also presented. The features of the presented hybrid fuzzy controller will be highlighted by comparing the performance of various control approaches, including PI control, PI-type fuzzy logic control (FLC), proportional-derivative (PD) type FLC, and combination of PD-type FLC and I control, for DTC-based induction motor drives.

Contents

List of Figures

List of Tables

Nomenclature

R_s, L_{ls}	Stator resistance and leakage inductance
R_r', L_{lr}'	Rotor resistance and leakage inductance
L_m	Magnetizing inductance
V_{qs}, i_{qs}	Quadrature axis stator voltage and current
V'_{qr}, i'_{qr}	Quadrature axis rotor voltage and current
V_{ds}, i_{ds}	Direct axis stator voltage and current
V'_{dr}, i'_{dr}	Direct axis rotor voltage and current
ψ_{qs}, ψ_{ds}	Stator quadrature and direct axis fluxes
ψ'_{qr}, ψ'_{dr}	Rotor quadrature and direct axis fluxes
W_m	Angular velocity of the rotor
P	Number of pole pairs
W_r	Electrical angular velocity of the rotor
T_e	Electromagnetic torque developed by the motor
T_L	Torque applied on the shaft
J	Inertia coefficient of the combined rotor and load
Kp	Proportional gain of the PI speed controller
K_i	Integral gain of the PI speed controller
Sa, Sb, Sc	Inverter switching functions
$d\psi_s$	Stator flux error
PI	Proportional Integral
dT_e	Torque error
V_{dc}	Dc link voltage
VSI	Voltage source inverter
ΔT_e, $\Delta\psi_s$	Torque and flux hysteresis bands
i_{sa}	Instantaneous current in phase A
i_{sb}	Instantaneous current in phase B
i_{sc}	Instantaneous current in phase C
V_{an}	Instantaneous voltage in phase A
V_{bn}	Instantaneous voltage in phase B
V_{cn}	Instantaneous voltage in phase C

Chapter 1

Introduction

1.1 Introduction

Major improvements in modern industrial processes over the past 50 years can be largely attributed to advances in variable speed motor drives. Prior to the 1950's most factories used DC motors because three phase induction motors could only be operated at a unique frequency. Due to rapid increase of the power range of controllable semi conductors (like IGBT's, IGCT's) ,it is nowadays viable to handle high power conversion applications employing these kinds of semi conductors instead of more traditional ones(like thyristors or GTO's),whose dynamic and static performances are still limited. The technical improvement on the semiconductors allows feeding the induction motor with voltage source inverters (VSI), which in turn makes possible the usage of standard torque and flux control methods based on pulse width modulation (PWM) or, more recently, direct torque control.

Direct torque control of induction motor has been first reported ten years ago ,and it was inherently developed for breaking through a common sense in those days ,which was like that "there is nothing but field oriented control to obtain a quick torque response with the induction motor".

Direct torque control (DTC) has a relatively simple control structure yet performs at least as good as FOC technique. It is also known that DTC drive is less sensitive to parameter detuning. The control technique is based on limit cycle control and it makes possible both quick response and high efficiency operation at the same time. In the direct torque control system the instantaneous values of the flux and the torque are calculated from only primary variables. They can be controlled directly and independently by the selection of optimum inverter switching states. The selection is made so as to restrict the errors of the flux and the torque with in the hysteresis bands and to obtain the fastest response and highest efficiency at every instant. It enables both quick torque response, in the transient operation and the reduction of the harmonic losses and acoustic noise.

1.2 State of Art

The AC asynchronous motor, also known as induction motor, has become the most widespread electric motor in use today. The increase in the use of induction motors was largely attributed to major oil and mining companies converting existing diesel and gas powered machinery to run off electricity. Over the past five years, the area of AC motor control has continued to expand because induction motors are excellent drives for use in Electric or Hybrid electric vehicles. These facts are due to the advantages of induction motors over the rest of the motors. The main advantage is that induction motors do not require an electrical connection between the stationary and the rotating parts of the motor. Therefore, they do not need any mechanical commutator leading to the fact that they are maintenance free. Induction motors also have low weight and inertia, high efficiency and a high overload capability. Therefore, they are cheaper and more robust, less prone to any failures at high speeds and can work in explosive environments.

Before the days of power electronics, a limited speed control of induction motor was achieved. The methods usually adopted during those days for the speed control include the following:

1. Switching the three stator windings from stator connection to delta connection, allowing the voltage at the motor windings to be reduced.
2. Induction motors manufactured with more than three stator windings for changing the number of pole pairs.
3. Speed control in wound rotor induction motor where the rotor winding ends are brought out to slip rings.

At that time the above described methods were the only available methods of induction motor speed control where as infinitely variable speed drives with good performances for Dc motors already existed. These drives not only provided good operation but also covered a wide power range. Moreover, they had a good efficiency and with a suitable control even good response. But the main drawback is the compulsory requirement of brushes and maintenance costs.

1.2.1 DC Drive

In the DC drive the torque is directly proportional to armature current in the motor. By using an inner current loop the DC drive system can directly control the torque.

Likewise the constant magnetic field orientation which is achieved through the commutator action makes the direct flux given. Thus two primary factors insuring responsive control i.e., both direct torque and direct flux control are both present in Dc drive. The relatively simple electronics required to implement the DC drive represents another advantage. On the negative side, both the initial and maintenance cost of the DC motors are high and high speed accuracy performance can only be achieved if an encoder is included for feedback.

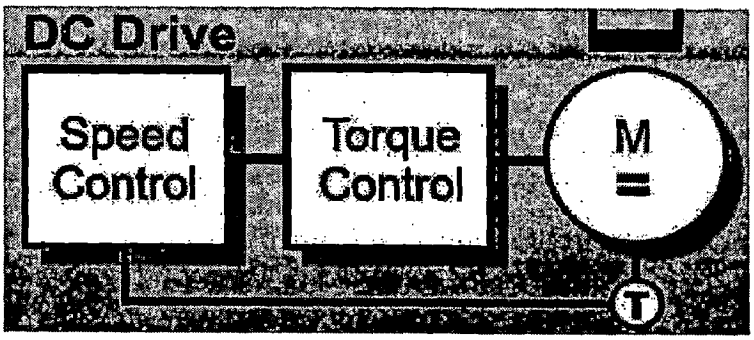

Fig 1.1 DC motor drive

1.2.2 Scalar Frequency Control

Scalar frequency control offers the advantage of operation with out an encoder. On the negative side, torque and flux neither directly nor indirectly controlled. A frequency and voltage reference generator instead provides control with constant volts per hertz output, which then drives the pulse width modulated inverter. Although simple this arrangement provides limited speed accuracy and poor response. Flux and torque levels are dictated by the response of the motor to the applied frequency and voltage and are not under the control of the drive.

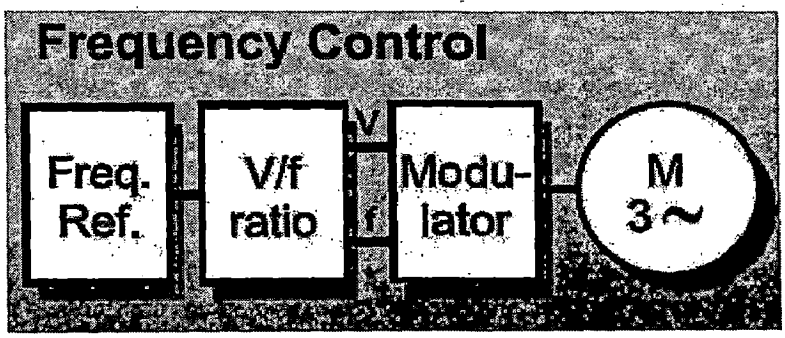

Fig 1.2 Block diagram of scalar frequency control

1.2.3 Flux Vector Control

Flux vector control reestablishes one of the advantages of the Dc drives through implementation of flux control. The spatial angular position of the rotor flux vector is calculated and controlled by the drive based on a relative comparison of the known stator field vector to feedback of rotor angular position and speed. The motor's electrical characteristics are mathematically modeled with processor techniques to enable processing of data. Torque control is indirect because of its position in the control algorithm prior to the vector control process; however good torque response is achieved. Inclusion of pulse encoder insures high speed and torque accuracy. The biggest disadvantage of flux vector is the mandated inclusion of the pulse encoder. Another minor disadvantage is that torque is indirectly rather than directly controlled. The inclusion of the PWM modulator, which processes the voltage and frequency outputs of the vector control stage, creates a signal delay between the input references and the resulting stator voltage vector produced. Thus the ultimate ability of the flux controlled drive to achieve very rapid flux and torque control is limited because of the last two factors.

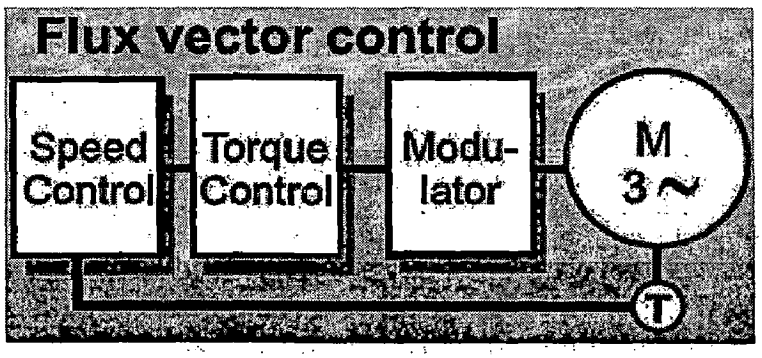

Fig 1.3 Block diagram of field oriented controlled drive

1.2.4 Field Acceleration Control

This method is based on avoiding the electromagnetic transients in the stator currents keeping its phase continuous. Therefore, the equation used can be simplified saving the vector transformation in the controllers. This method mainly achieved some computational reduction, overcoming the main problem in the vector controllers and then becoming an important for the vector controllers.

1.2.5 Direct Torque Control

Direct torque control also reestablishes direct flux control in addition to the implementation of direct torque control. Direct torque control has emerged over the last decade to become one possible alternative to the well known vector control of induction machines. Its main characteristic is the good performance, obtaining results as good as the classical vector control but with several advantages based on it simple structure and control diagram.

A hysteresis controller controls the flux and the torque directly by selecting the appropriate inverter state. The method still requires further research in order to improve the motor performance as well as achieve a better environmental capability that is essential now a days for all industrial applications.

The main features of DTC are as follows:

1) Direct control of flux and torque
2) Indirect control of stator voltages and currents
3) Approximately sinusoidal stator fluxes and currents
4) High dynamic performance even at stand still

The advantages of the DTC are as follows:

1. Absence of coordinate transforms
2. Absence of voltage modulation block, as well as other controllers PI controller for flux and torque.
3. Minimal torque response time even better than either with DC of flux vector control.
4. The delays associated with the PWM modulator stage are removed since the PWM modulator is replaced by an optimal switching logic.
5. Assuming moderate speed accuracy is acceptable the need for a speed encoder is eliminated.

The disadvantages of the DTC drive are:

1. Possible loss of flux control during starting
2. Requirement of flux and torque estimators, implying consequent parameters identification.
3. Inherent torque and flux ripple.

The original benefits associated with dc drive of direct torque control, direct flux control and high responsiveness are thus reestablished. Torque response is better than that available with either or flux vector control.

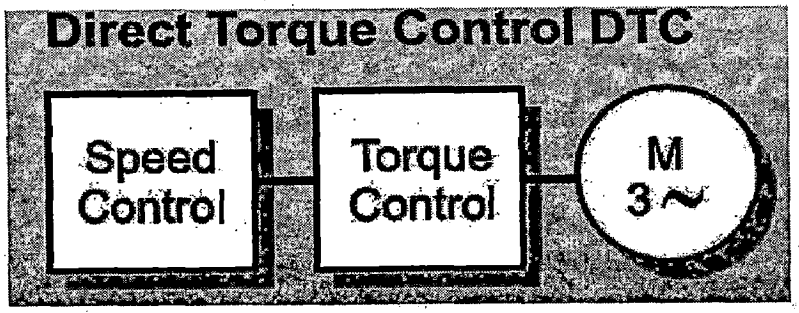

Fig 1.4 Block diagram of direct torque controlled drive

Since the concept of direct torque control has been presented it has been used in many ac drives because it provides fast torque response and robustness against machine parameter variations with out speed sensor. Having passed more than ten years since the technique was first reported there has been a significant advancement of the technology and the technique has given a systematic solution to improve the operating characteristics of not only the motor but also the PWM inverter. Several methodologies for the drive implementation have been reported which have enhanced the performance of the drive compared to what was reported initially.

Although in the recent years the high performance induction machine drives market has been dominated by the rotor flux oriented vector control technique, there has been a growing interest in the direct torque control technique which offers simple control architecture with a dynamic performance to vector control. The reason for this is simple architecture and reduced parameter dependence of the direct torque control technique over the vector control technique. In spite of this superiority of direct torque control there are still two sets of scientists preferring vector control whilst the other prefers direct torque control, the switching losses, torque and flux ripples are of major concern. The table below gives a comparison of the vector and direct torque control techniques.

Table 1.1 Performance comparison of DTC and Vector control

	Field oriented control	Direct torque control
Coordinate reference frame	Synchronous rotating d-q	Stationary d-q
Controlled variables	Torque, rotor flux	Torque , stator flux
Control variables	Stator currents	Stator voltage space vector
Sensed variables	Rotor mechanical speed Stator currents	Stator voltages Stator currents
Estimated variables	Slip frequency rotor flux position θe	Torque Stator flux
Regulators	Three stator currents regulators(hysteresis)	Torque regulator(hysteresis) Stator flux regulator(hysteresis)
Torque control	Indirectly controlled by stator currents High dynamics Torque ripple	Directly controlled High dynamics Controlled torque ripple
Flux control	Indirectly controlled by stator currents Slow dynamics	Directly controlled Fast dynamics
Parameter sensitivity	Sensitive to variations of rotor time constant	Sensitive to variations of stator resistance
implementation	High complexity calculations requiring trigonometric functions	Medium complexity

1.3 Literature Survey

The first direct torque controlled induction motor drive was reported by Takahasi and noguchi [1] and this is known to be the conventional DTC. The detailed principle of operation, the modeling and the control aspects of the drive are presented in the reference [2]. Since then many other techniques have been reported to improve the performance of the drive. The literature reviews for some of the evolved techniques of direct torque control are discussed.

1.3.1 Conventional Direct Torque Control Scheme

Takahasi [1] has given the novel technique for the direct torque control of induction motor drive in 1986. This method is based on the selection of an appropriate voltage vector that quickly changes the position of the stator flux linkage vector depending upon the requirement of the flux and torque errors. The proposed scheme is based on limit cycle control of both the flux and the torque using optimum inverter output voltage vectors so as to attain as fast torque response. At present ABB is the only industrial company who has introduced a commercially available direct torque controlled induction motor drive and it is a drive based on the technology of Takahashi. The product is patented by the ABB. The implementation aspects of the direct torque controlled induction motor drive along with its advantages and the considerations for the design of different parameters of the drive have been reported in the reference [3] by john R G Schofield, ABB Industrial Systems Ltd.

The other implementations of the optimum voltage vector selection technique that are reported includes the one by the Texas instruments [4] by utilizing a DSP controller board, DS1102 from Dspace consisting of TMS320C31 AT 60 MHz. To minimize the sampling period of the implemented system, a Xilinx FPGA (XC4005E) is used to perform some of the main tasks of DTC drives. The TMS320C31 was programmed in c-language with the motors terminal variables sampled at 60us.

Bibhu Prasad Panigrahi, Dinkar Prasad, Sabyasachi SenGupta [5] proposed hardware scheme mimics the conventional switching table based DTC scheme and does not require use of any online fast computing device like microprocessor, PC or DSP. The controller uses only commonly used discrete hardware components.

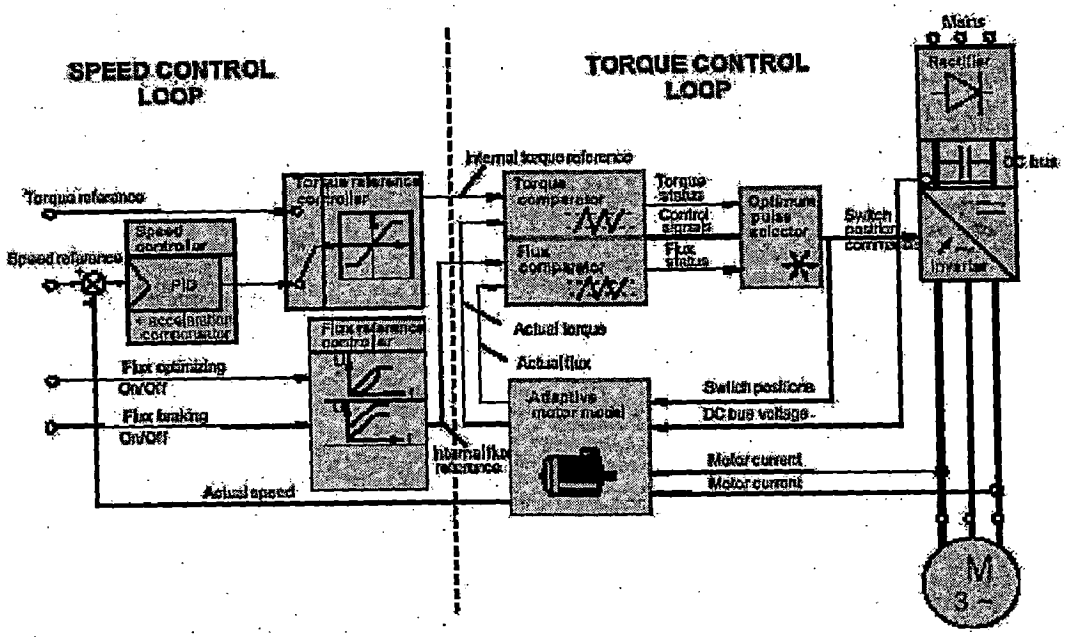

Fig 1.5 ABB Model of the direct torque control drive

1.3.2 Constant Frequency DTC

The switching frequency of the inverter used for the direct torque control in the technique proposed by Takahashi is not fixed due to the presence of the hysteresis controllers. To overcome this limitation a constant inverter switching frequency DTC is proposed by N.R.N. Idris, A.H.M. Yatim, N.D. Muhamad and T.C. Ling [6]. This paper proposed a simple solution to the variable switching frequency and high torque ripples problems encountered in hysteresis-based DTC drives. The method replaces the hysteresis-based controllers with fixed switching controllers, which operate based on the comparison between the error signals and the triangular waveforms. Implementation of these controllers using digital circuits is highly suitable since they only require comparisons of waveforms rather than calculations of duty cycles or voltage vectors.

Nik Rumzi Nik Idris Abdul Halim Mohd Yatim Naziha Ahmad Azli [7] proposed a new torque controller for constant switching frequency and a compensation scheme to eliminate the phase and magnitude errors for the stator flux estimation under steady state condition. Theses simple schemes have significantly improved the performance of the DTC drive system while at the same time maintaining the simple control structure of the DTC drive.

Nik Rumzi Nik Idris, *Senior Member, IEEE,* and Abdul Halim Mohamed Yatim, *Senior Member, IEEE* [8] proposed a new torque controller for constant switching frequency and reduced torque ripple. With the proposed controller, a linear model of the torque loop can be derived and, hence, a proper controller can be designed.The feasibility of the proposed controller is demonstrated by hardware realization using a DSP and a Xilinx FPGA. For a higher torque bandwidth and switching frequency, realization using a hybrid analog–digital circuit can be easily implemented since the controller works based on waveforms comparisons. This simple scheme has significantly improved the performance of the DTC drive system while at the same time maintaining the simple control structures of the DTC drive

Jun-Koo Kang, *Student Member, IEEE,* and Seung-Ki Sul, *Senior Member, IEEE* [9] proposed a new direct torque control strategy for induction machines to achieve both constant switching-frequency regulation and reduced torque-ripple control. In the proposed torque-ripple control algorithm, the optimal switching instant is calculated at each switching cycle to satisfy the ripple minimum condition based on the instantaneous torque slope equations. The differences between the proposed and the conventional DTC have been investigated through experiment. The experimental results verify that the proposed DTC improves the torque control characteristic without deteriorating the flux control capability.

1.3.3 Space Vector Modulation Based DTC

It is well known that the principle of vector control of induction motor drive is to align the flux and torque current along the d-axis and q-axis of the reference frame, respectively. And therefore the torque can be controlled by the associated current component, once the flux is kept constant. Therefore the main theme of direct torque control is to regulate the torque and magnitude of flux directly without invoking any concept of field orientation. In conventional DTC, the torque and stator flux are controlled to follow their references. In the PI regulation method, the errors of torque and stator flux are controlled by two PI regulators [10], and the outputs of regulators give the d, q space voltage vector to control motor directly. As the amplitude and angle phase of voltage vectors are decided by the PI regulation, i.e. an average dynamic control without large fluctuation, which lead to good steady performance in low speed range. It is quite straightforward to implement the PI regulators; however, the coefficients of PI need to be selected properly.

As shown in fig 1.6, two proportional integral (PI) controllers regulate the flux amplitude and torque respectively. Therefore, both the torque and the magnitude of flux are under control, thereby generating the voltage command for inverter control. Noting that no decoupling mechanism is required since the flux magnitude and torque can be regulated by the PI controllers.

The inverter is controlled by the SVM technique using symmetrical regular sampling. Therefore, the inverter switching frequency is significantly increased, and the associated torque ripple and current harmonics can be dramatically reduced. To increase the inverter switching frequency for the same sampling frequency, the symmetrical Regular-Sampled SVM technique is used to control of the new DTC-based drive. The inverter switching frequency is constant and is equal to sampling frequency. SVM modulator, which requires calculating several equations online for the switching time periods.

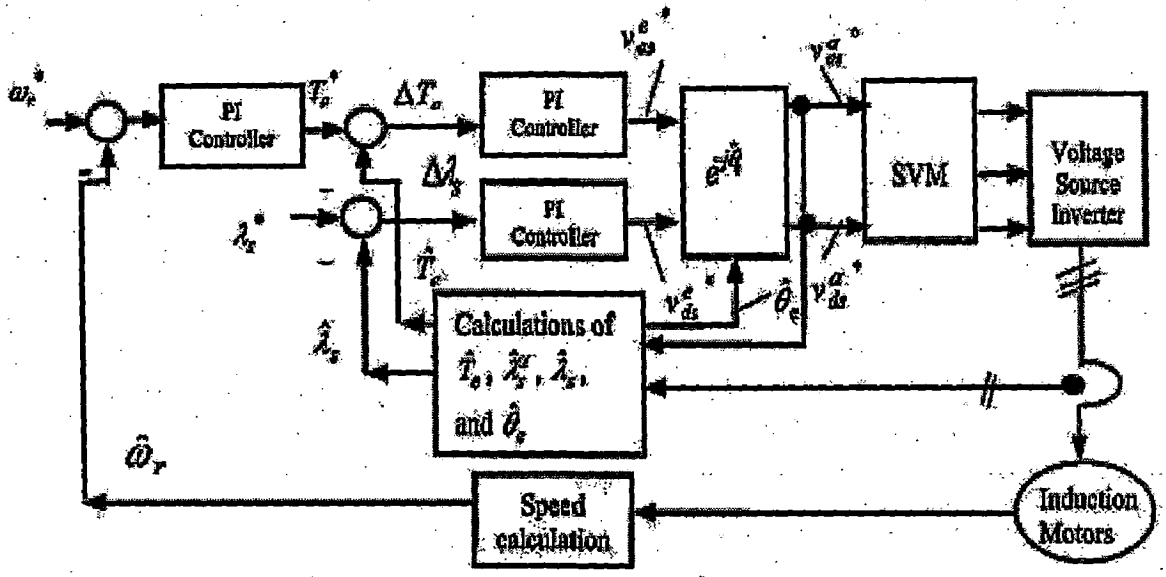

Fig 1.6 Block diagram of SVM based DTC Induction motor drive

Since the above technique requires the use of more number of controllers this is not usually employed since this form of DTC drives hinders the very advantage of direct torque control that has reduced hardware complexity.

J. Rodr.´guez, J. Pontt, C. Silva, R. Huerta and H. Miranda [11] proposed a new method for direct torque control (DTC) based on load angle control is developed. The use of simple equations to obtain the control algorithm makes it easier to understand and implement. Fixed switching frequency and low torque ripple are obtained using space vector modulation, overcoming the most important drawbacks of classic DTC.

P. Marino, M. D'Incecco and N.Visciano [12] presented a paper on comparison of various direct torque control methodologies (Classical DTC, DSVM-DTC and SVM-DTC) have been made in order to evaluate the influence of the motor operating condition on steady state performance. A particular emphasis on stator current distortion and on torque ripple has been made. It can be noted that SVM-DTC has the best performances, but it requires more complex control scheme and the knowledge of some motor parameters. DSVM-DTC is a good compromise between classical and SVM DTC schemes. It shows small torque ripple and requires only the knowledge of stator resistance. The use of this technique is very useful in applications where the maximum sampling frequency is limited by large computational time.

1.3.4 DSVM Based DTC

The discrete space vector modulation is a control system able to generate a number of voltage vectors higher than that used in direct torque control scheme [13]. The increased number of voltage vectors allow the definition of more accurate switching tables in which the selection of the voltage vectors is made according to the rotor speed, the flux error and the torque error. The switching tables are derived from the analysis of the equations linking the applied voltage vector to the corresponding torque and the flux variations. The functional block diagram of the DSVM DTC is shown in fig 1.9.

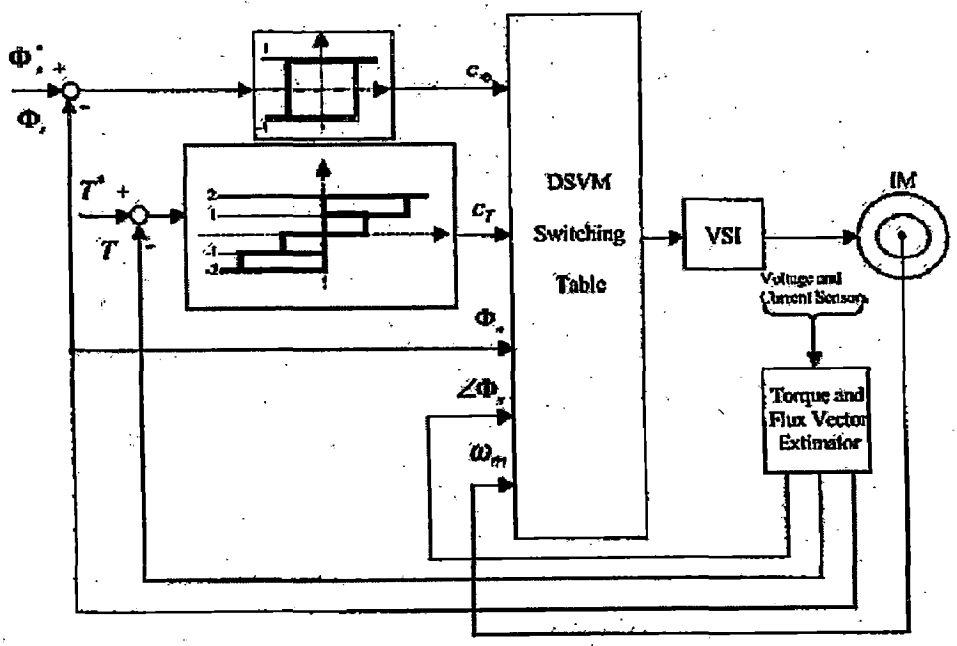

Fig 1.7 Block diagram of DSVM based DTC

Junfeng Xu, Jianping Xu, Yinglei Xu, Fengyan Wang [14] proposed a control strategy of Direct Torque Control (DTC) based on discrete space vector modulation (DSVM) system of induction motor fed with GTO voltage source inverter applied to railway traction is introduced. The switching frequency cannot be high in high power GTO inverter applications. When direct torque control of induction machines is implemented using microprocessor, undesired torque and current ripple happen because of using the six voltage vectors and the time delay due to digital implementation. An improvement of driver performance can be obtained using DSVM without increasing the frequency of the system. Moreover, it doesn't lead to extra complexity of the control system.

1.3.5 Fuzzy Based Direct Torque Control

In the DTC induction motor drive there are torque and flux ripples because none of the VSI states is able to generate the exact voltage value required to make zero both the torque electromagnetic error 'and the stator flux error. The suggested technique is based on applying to the inverter the selected active states just enough time to achieve the torque and flux references values. The rest of the switching period a null state is selected which won't almost change both the torque and the flux. Therefore, a duty ratio (δ) has to be determined each switching time. By means of varying the duty ratio between its extreme values (0 up to 1) it is possible to apply any voltage to the motor.

The optimum duty ratio per sampling period is a non-linear function of the electromagnetic torque error, the stator flux position and the working point, which is determined by the motor speed and the electromagnetic torque. It is obvious that it is extremely difficult to model such an expression since it is a different non linear Function per working point. Thus, it is believed that by using a fuzzy-logic-based DTC system it is possible to perform a fuzzy-logic-based duty-ratio controller, where the optimum duty ratio is determined every switching period.

A fuzzy logic based direct torque controlled induction motor [15] [16] has the advantage that the flux and the torque ripples can be reduced the so called duty ratio control of the inverter switches thus using the fuzzy technique to realize the nonlinear relationship of the duty ratio with the torque and the flux errors and the position of the flux linkage space vector.

1.4 Sensorless Schemes

The advantage of the direct torque control torque technique is the capability of its ready application to the sensor less drives because of its reduced parameter sensitivity. Also the estimation of the stator flux readily helps in the speed estimator being [20-24] incorporated into the system there by enabling robust control to be achieved.

The speed and position controls require the speed or position feedback. For this purpose it is common to use mechanical sensors directly coupled to the rotor shaft. In the last decade many authors have centered their efforts in solving the rotor speed measuring problem without mechanical sensors. Some of the methods perform state estimation using the electric variables, actual values and the machine model parameters. In this technique, precision is reduced due to parameters variation with temperature or saturation. Other speed estimation methods are based on the spectral analysis of the stator current spatial vector. Current harmonics contain information about the rotor speed, produced by the presence of stator and rotor slots, or by the dynamic eccentricities. An oriented field model is used to determine rotor speed during dynamic operation, and the time frequency transformation is used to adjust the rotor time constant during steady state. This allows for real time rotor time constant calculation and reduces rotor speed estimation errors.

1.5 SWITCHING SCHEMES

Over the last decade there has been a significant improvement in the switching techniques for the voltage source inverters used for direct torque control. This section presents the different switching techniques of non PWM techniques applied in the direct torque control of induction motor.

1.5.1 Hysteresis controllers

Takahashi [1] presented a method in which to determine the inverter switching pattern using flux and torque errors, two hysteresis controllers, one for the flux control and other for torque control are employed. The inverter is switched based on these errors and position of the flux within the six region control, in such a way that the inverter output voltage vector minimizes the flux and torque errors and determines the direction of rotation. The output of these controllers S_a, S_b, S_c with values 0 or 1, is used to determine the inverter output voltage vector

1.5.2 Four band flux controller and five band torque controller

This form of the control technique is reported in [15] and this is the technique that uses a non hysteresis controller. The algorithm of the technique is stated in the following set of equations.

If $\Delta T > \varepsilon_T$ then $K_T = 1$

If $0 \le \Delta T \le \varepsilon_T$ and $d\Delta T/dt > 0$ then $K_T = 0$

If $0 \le \Delta T \le \varepsilon_T$ and $d\Delta T/dt < 0$ then $K_T = 1$

If $-\varepsilon_T \le \Delta T < 0$ and $d\Delta T/dt > 0$ then $K_T = -1$

If $-\varepsilon_T \le \Delta T < 0$ and $d\Delta T/dt < 0$ then $K_T = 0$

If $\Delta T < -\varepsilon_T$ then $K_T = -1$

If $\Delta\phi > \varepsilon\phi$ then $K\phi = 1$

If $-\varepsilon\phi \le \Delta\phi \le \varepsilon\phi$ and $d\Delta\phi/dt > 0$ then $K\phi = 0$

If $-\varepsilon\phi \le \Delta\phi \le \varepsilon\phi$ and $d\Delta\phi/dt < 0$ then $K\phi = 1$

If $\Delta\phi < -\varepsilon\phi$ then $K\phi = 0$

If $-\varepsilon\phi \le \Delta\phi \le 0$ then $K\phi = 2$

If $\Delta\phi < -\varepsilon\phi$ then $K\phi = 3$

1.6 Organization of the Report

Chapter 1: It deals with the general aspects of the direct torque control of induction motors and the literature review of the direct torque control and various techniques, control techniques, torque and flux ripple reduction strategies and about sensor less direct torque control.

Chapter2: It deals with the operating principle and control strategy of the direct torque control along with the function of the individual blocks in the closed loop DTC system.

Chapter 3: It deals with the description of the different blocks in direct torque control modeling equations of the different components on the drive system and the simulation of the conventional direct torque control for induction motor drive with speed sensor and with out speed sensor using MATLAB/SIMULINK toolboxes and concludes with results of the simulation along with their discussion.

Chapter 4: It deals with the description of fuzzy controller structure and the features of the presented hybrid fuzzy controller are highlighted by comparing the performance of various control approaches, including PI control, PI-type fuzzy logic control (FLC), proportional-derivative (PD) type FLC, and combination of PD-type FLC and I control, for DTC-based induction motor drives using simulation results and their discussion.

Chapter 5: It deals with the implementation aspects of the conventional direct torque control for induction motor drive. Innovative integration sbc6711 DSP board is used for the implementation of the drive system. The fabrication of power circuit and the necessary sensing circuits is detailed in this chapter.

Chapter 6: Conclusion is drawn from the work done and presented. Future scope for improvements in the same field to improve the performance and to handle the problems associated are briefly studied and presented to carry out in upcoming projects.

Chapter 2

Direct Torque Control of Induction Motor

2.1 Introduction

In the last decade, high performance drives based on the spatial position of the flux and on space vector theory have been developed and industrially applied. Based on the works of blaschke, Hasse, and Leonard, vector controlled drives have become increasingly popular and have become the standard in the drives industry. The advent of this technique has made possible to achieve with an induction motor as fast torque response as that of a DC motor. Direct torque controlled drives were developed ten years ago by Depenbrock and Takahashi. However, at present, ABB is the only industrial company that has introduced a commercially available direct torque controlled induction motor drive. This chapter deals with the description, operating principle and control strategies of the direct torque controlled induction motor drive. The general and the fundamental aspects of the direct torque control of induction machine are examined in great detail; the mathematical and the physical analysis of the processes involved are explained thoroughly.

2.2 DTC Schematic

The block diagram of the direct torque controlled induction motor drive is shown in fig 2.1. The reference speed (W*n) and the rotor speed (Wn) are compared and the error is input to the speed controller. The error is processed in the speed controller that outputs the reference torque (Teref). Based on the rotor speed (Wn), the flux controller provides reference flux ($\psi sref$). The reference flux and the reference torque (Te) along with the estimated values of the torque and stator flux($|\psi s|$) are fed to the flux and torque hysteresis comparators. The output of the comparators is 1, 0, -1 depending on the status of the torque and flux errors. This is then input to the optimum switching vector selection table, which gives an appropriate switching vector (Sa, Sb, Sc) to be applied to the inverter so as to minimize the torque and the flux errors. The function of the estimator is to estimate the stator fluxes in the direct and the quadrature axis, the electromagnetic

torque developed by the induction motor and speed of the motor. The inputs to the estimator are the dc link voltage, and any two motor winding currents and the out puts are the stator fluxes in direct (ψsd)and quadrature axis (ψsq), the modulus of the stator flux, electromagnetic torque developed by the motor and speed of the rotor. The phase voltages of the induction motor are obtained from switching vectors and the dc link voltage.

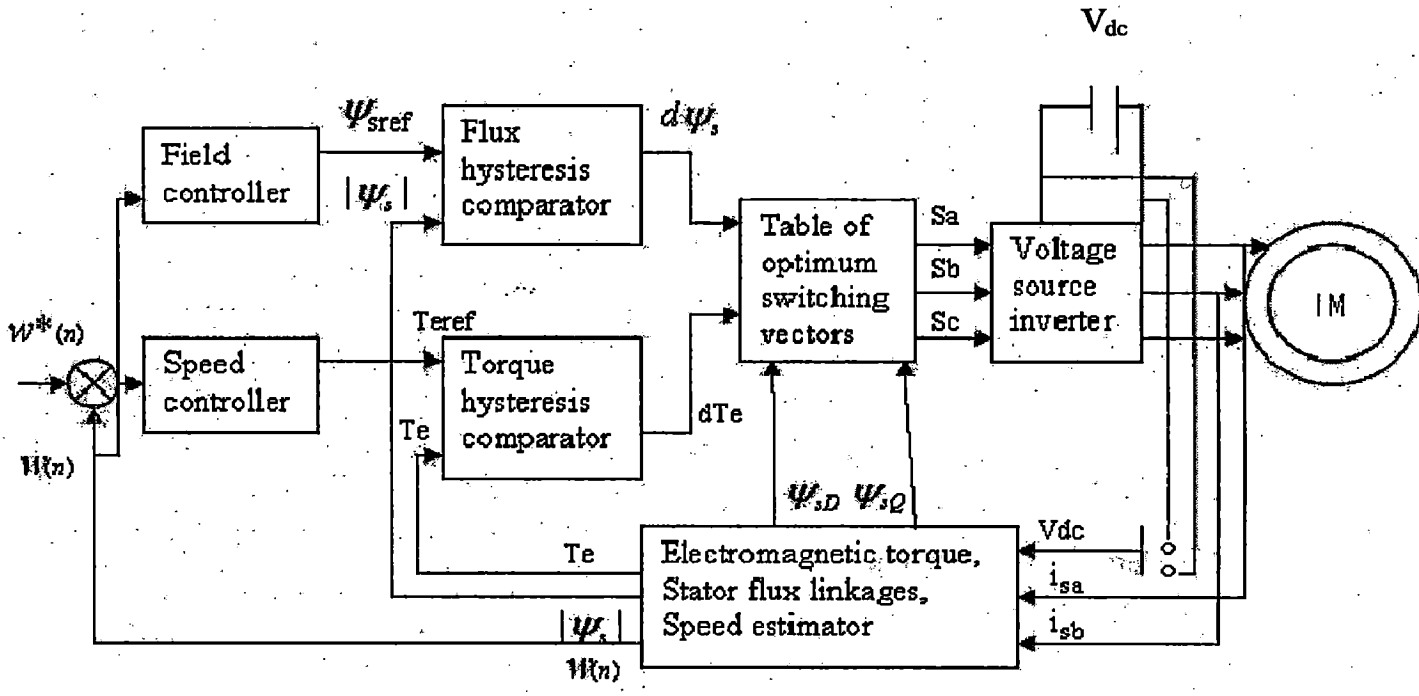

Fig 2.1 Schematic of stator flux based DTC induction motor drive

2.3 Description

The conventional direct torque controlled induction motor drive as shown in fig 2.1 consists of the following main blocks.

- PI speed controller
- Field weakening controller
- Torque hysteresis comparator

- Flux hysteresis comparator
- Optimal inverter switching table
- Voltage source inverter
- Induction motor

2.4 Control Strategy

This section explains the control strategy of the classical direct torque controlled induction motor drive and the selection of the inverter switching vectors depending on the flux and torque errors.

2.4.1 Inverter Control

Consider the six pulse voltage source inverter shown below in fig 2.2. There are six non zero active voltage switching space vectors and two zero space vectors (u1, u2, u3, u4, u5, u6), these are shown in fig 2.3. The switching voltage space vectors are shown in fig 2.4. The six active inverter switching vectors can be expressed as

$$us = uk = 2V_{dc}/3 \exp[j(k-1)\pi/3] \quad k=1, 2, 3, 4, 5, 6. \qquad (2.1)$$

Where V_{dc} is the dc link voltage. How ever for k=7, 8, $u_k = 0$ holds for the inverter switching states where the stator windings are short circuited, $u_s = u_k = 0$.

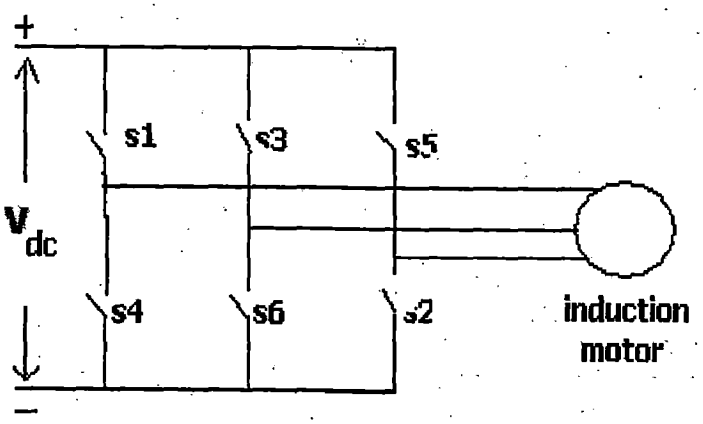

Fig 2.2 Schematic PWM VSI Inverter

U1(100)

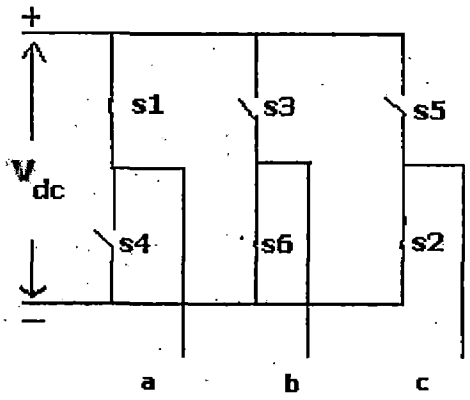

U2(110)

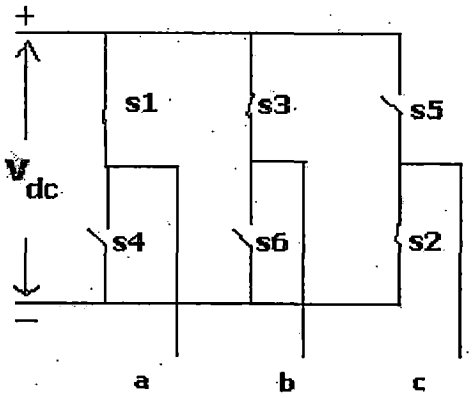

U3(010)

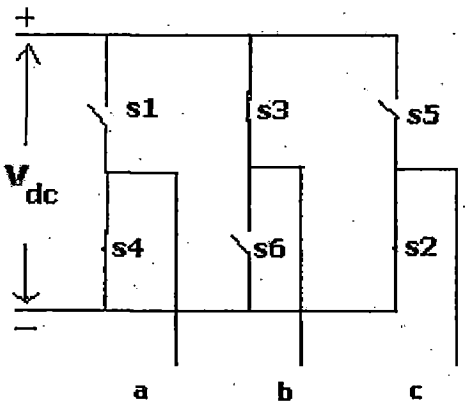

U4(011)

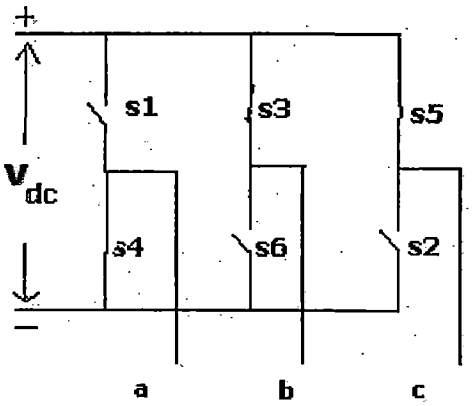

U5(001)

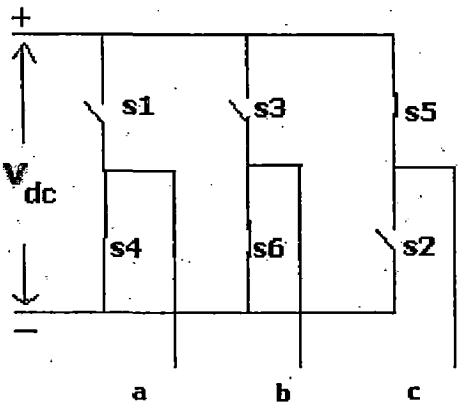

U6(101)

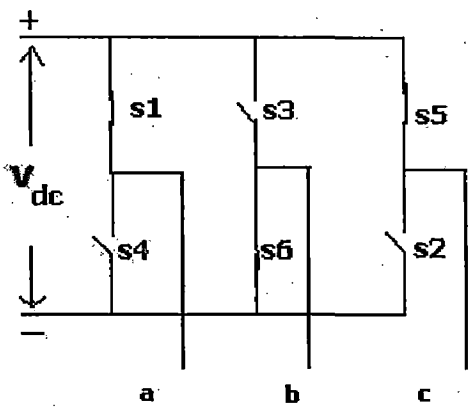

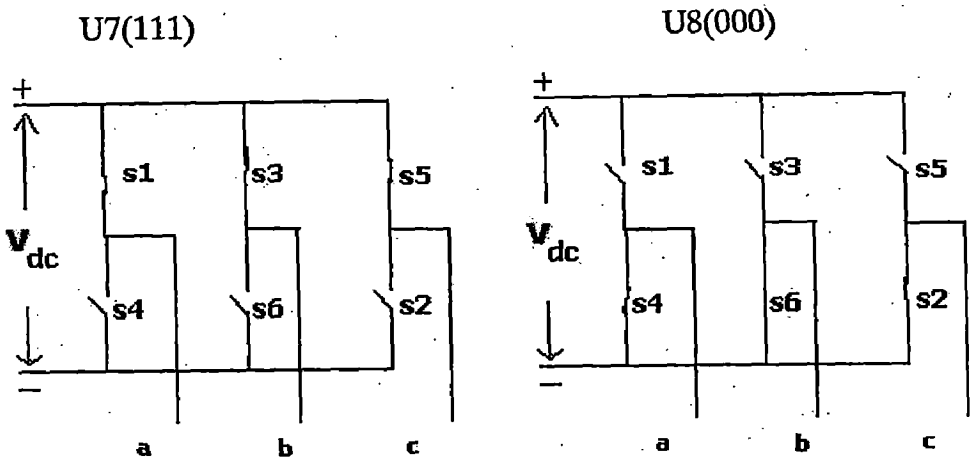

Fig 2.3 Eight Switching states of PWM VSI

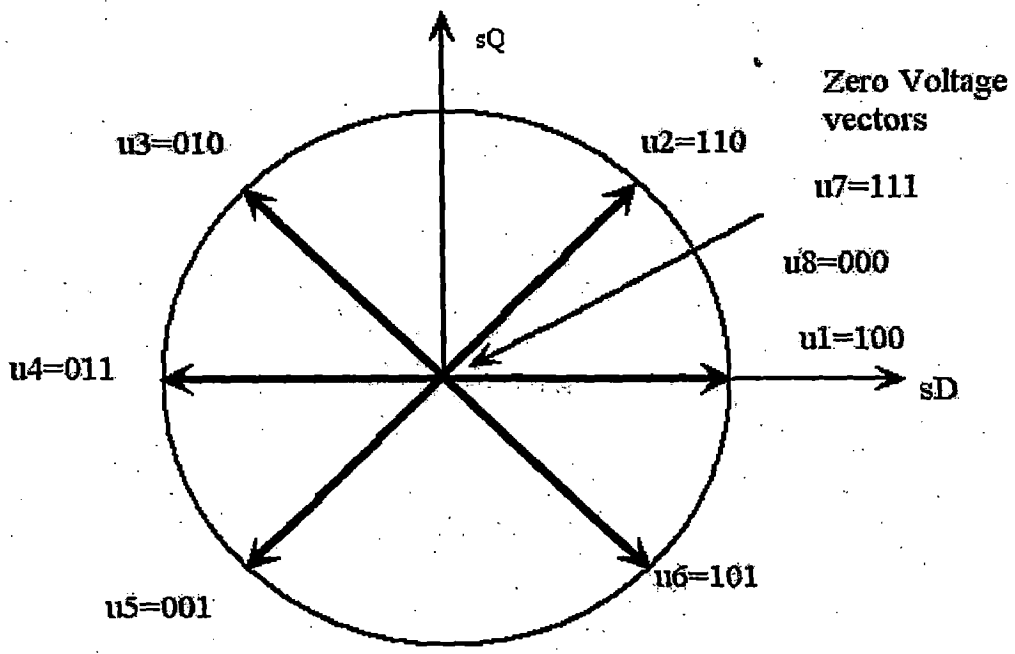

Fig 2.4 Stator voltage space vectors

Since $\Delta\psi s = us\Delta t$, it can be seen that the stator flux linkage space vector will move fast if nonzero switching vectors are applied , for a zero switching vector it will almost stop (it will move slowly due to the small ohmic voltage drop). In the DTC drive at every

sampling period the switching vectors are selected on the basis of keeping the stator flux linkage errors in a required tolerance band and the torque error in the hysteresis band. If the stator flux linkage lies in the k th sector, where k=1,2,3,4,5,6,its magnitude can be increased by using the vectors uk,uk+1,uk-1;however ,its magnitude can be decreased by using the switching vectors uk+2,uk-2 and uk+3.Obviously the selected voltage vectors affect the electromagnetic torque as well. The speed of the space vector is zero if a zero switching vector is selected, and it is possible to change this speed by changing the output ratio between the zero and non zero voltage vectors.

2.4.2 Hysteresis Flux and Torque Control

The ultimate goal of the control is to keep the modulus of the stator flux linkage space vector with in the hysteresis band whose width is $2\Delta\psi s$ as shown in the fig 2.5. The locus of the flux linkage vector is divided into several sectors and due to six step inverter the minimum number steps required is six, six sectors are shown in fig 2.5. Assume that initially the stator flux linkage space vector is at position P0, thus in sector 1.

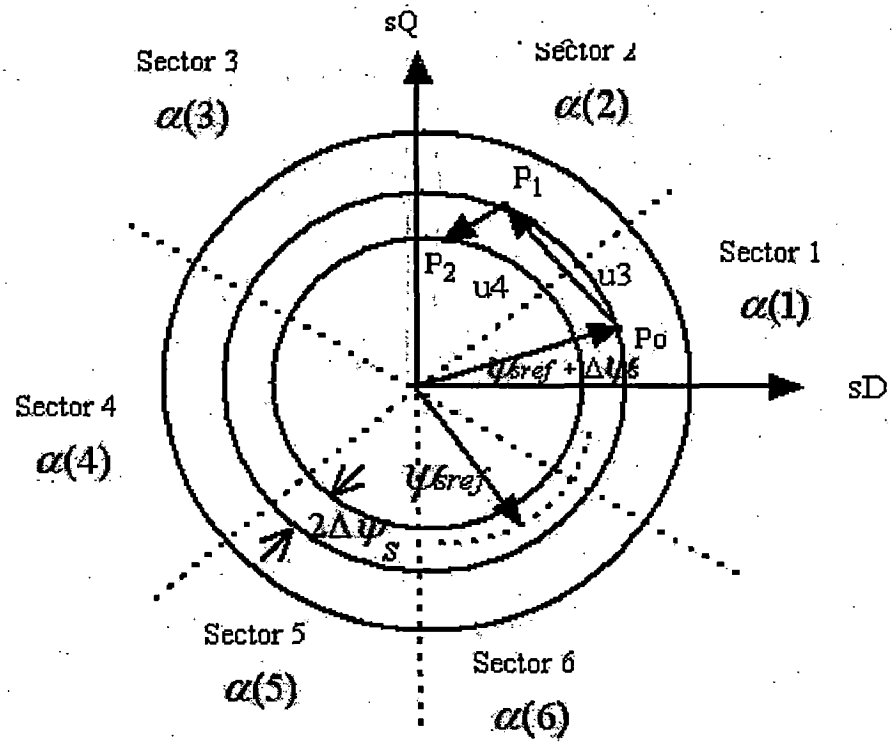

Fig 2.5 Control of stator flux linkage space vector

The procedure in which the stator flux linkage vector position is varied according to the error in the modulus of the stator flux linkage vector is explained in the following steps:

- Assuming that the stator flux linkage space vector is rotating clockwise, since at position P0 the stator flux linkage space vector is at the upper limit ($|\psi sref + \Delta\psi s|$) it must be reduced and this is achieved by selecting the switching vector u3.
- The stator flux linkage space vector is now in the new position P1 in sector 2 and it can be seen that the stator flux linkage space vector is again at its upper limit and hence it has to be reduced and hence for this purpose the switching vector u4 have to be selected. Because of which sis moves from point P1 to P2 , which is also in sector 2.

- Since the sector 2 the stator flux linkage space vector is at the lower limit($|\psi sref - \Delta\psi s|$) it has to be increased and the quick rotation of the vector in this case is achieved by selecting the switching vector u3 and even in this position of the stator flux linkage space vector is still in sector 2.

Stopping the rotation of the stator flux linkage space vector corresponds to the case when the electro magnetic torque does not have to be changed. However when the electromagnetic torque has to be changed then the stator flux linkage space vector has to be rotated depending upon whether the torque need to increased or decreased in the same or opposite direction is explained in the following steps.

- When the stator flux linkage space vector has to be rotated in the appropriate direction and if an increase in the electromagnetic torque is needed, for example if the stator flux linkage space vector lies in the sector 2 at position P1 where the flux has to be decreased then the electromagnetic torque increase can be achieved by applying switching sector u4.

- When the stator flux linkage space vector has to be rotated in the appropriate direction and if an decrease in the electromagnetic torque is needed, for example

if the stator flux linkage space vector lies in the sector 2 then this can be achieved by applying switching sector u1 since this moves the stator flux linkage space vector in the clockwise direction and also increases the stator flux linkage.

- If the stator flux linkage space vector is in the second sector and torque decrease is required, but the stator flux linkage has to be decreased then the switching vector u1 has to be applied.

The fig 2.6 below shows the position of the various flux linkage space vectors and switching vectors that has to be selected to obtain the required increase or decrease of the stator flux linkage and the required increase or decrease of the electromagnetic torque.

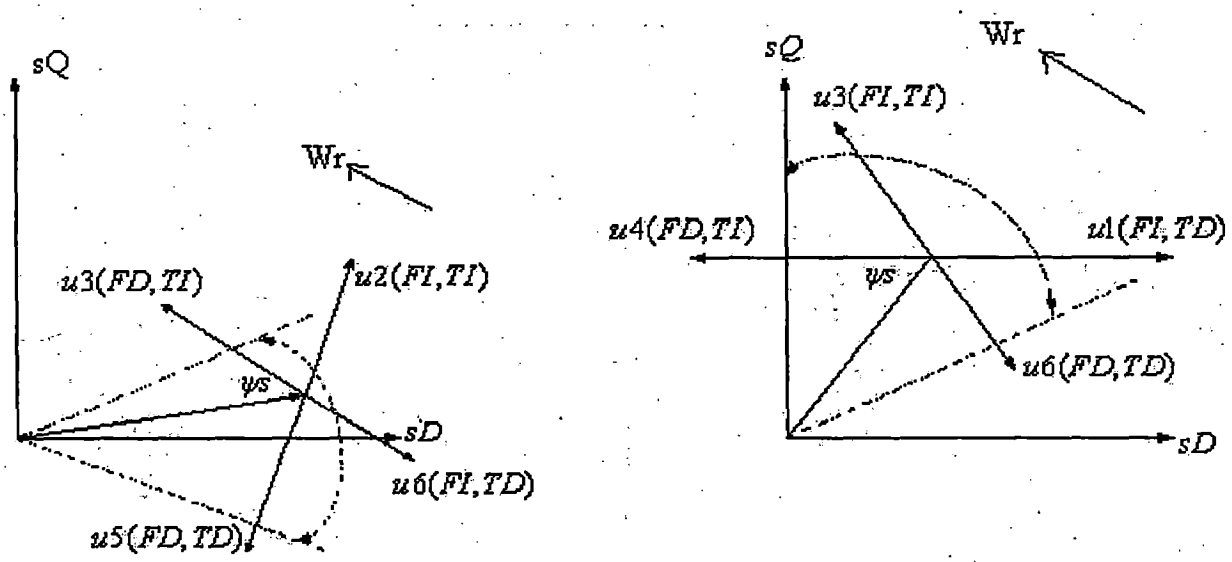

ψs in sector 1 ψs in sector 2

Fig 2.6 Position of various stator flux linkage space vectors and the selection of the optimum switching voltage vectors

Thus in general it can be inferred that:

- If an increase in the torque is required then the torque is controlled by applying voltage vectors that advance the flux linkage space vector in the direction of rotation.
- If a decrease in the torque is required then applying voltage vectors that advance the flux linkage space vector opposite to the direction of the torque.
- If zero torque is required then that zero switching vector is applied, which minimizes the inverter switching.

From the above discussion it can clearely be seen that in the direct torque control the torque demand is simply reduced to a choice of increase (positive torque), decrease (negative torque), or zero. Similarly the stator flux linkage vector modulus is limited to a choice of increase (flux increase) or decrease, or zero. Decoupled control of the stator flux linkage modulus and the torque is obtained by acting on the radial and the tangential components respectively of the stator flux linkage space vector in its locus.

2.4.3 Optimum Switching Vector Selection

The way to impose the required stator flux by means of choosing the most suitable voltage source inverter state. This is achieved using the so called optimum switching vector selection table that is shown in table. This table gives the optimum selection of the switching vectors for all possible stator flux linkage space vector positions depending on the corresponding errors in the stator flux modulus and the electromagnetic torque (dψ &dte).The representation of the digital outputs of the two level flux hysteresis comparator and the three level torque hysteresis comparator is

Flux comparator

$$d\psi = 1 \text{ if } |\psi s| \le |\psi sref| - \Delta\psi s \quad (2.2)$$

$$d\psi = -1 \text{ if } |\psi s| \ge |\psi sref| + \Delta\psi s \quad (2.3)$$

Torque comparator

For anticlockwise direction (forward direction):

$$dte = 1 \text{if } |te| \le |teref| - |\Delta te| \quad (2.4)$$

$dte = 0 \text{ if } |te| \geq |teref| \quad (2.5)$

For clockwise direction (backward direction):

$dte = -1 \text{ if } |te| \geq |teref| + |\Delta te| \quad (2.6)$

$dte = 0 \text{ if } |te| \geq |teref| \quad (2.7)$

The selection of the flux and torque hysteresis bands has important effects, a too small value may have the effect of losing control as the stator flux linkage may exceed the values required by the tolerance band width and the switching frequency also increases. The flux hysteresis band is usually selected to be very small so as to obtain currents as close to sinusoidal as possible thus reducing the harmonics and hence the losses in the motor.

Table 2.1 Optimum voltage switching vector look up table

$d\psi$	dte	Sector 1	Sector 2	Sector 3	Sector 4	Sector 5	Sector 6
1	1	U2	U3	U4	U5	U6	U1
	0	U7	U8	U7	U8	U7	U8
	-1	U6	U1	U2	U3	U4	U5
0	1	U3	U4	U5	U6	U1	U2
	0	U8	U7	U8	U7	U8	U7
	-1	U5	U6	U1	U2	U3	U4

Active switching vectors: U1(100); U2(110); U3(010); U4(011); U5(001); U6(101)

Zero switching vectors: U7(111); U8(000)

2.5 Determination of the Flux Linkage Vector Position

For the instantaneous correction of the flux and the torque errors an appropriate voltage vector needs to be applied to the voltage source inverter and this voltage vector that need to be applied to compensate for the flux and torque errors is obtained from the switching vector look up table. The optimum switching vector look up table requires the knowledge

of the position of the stator flux linkage space vector, since it must be known in which sector the stator flux linkage space vector is located. The discussion below presents the different methods that are commonly employed, for the sector determination, in the drive implementation.

2.5.1 METHOD-1

The stator flux angle can be determined by using the estimated values of the direct and the quadrature axis stator flux linkages expressed in the stationery reference frame (ψsd / ψsq) as

$$\rho s = \text{arc tan}\,(\psi sq / \psi sd) \qquad (2.8)$$

The angle ρs can be used to determine the various angles $\alpha(1)$, $\alpha(2)$ etc. The disadvantage of the method however is the computation of the trigonometric function, which if implemented as a look up table in the processor takes in much memory and the time of computation is also increased. It is however possible to eliminate the need for using trigonometric functions, since it is not the accurate position of the stator flux linkage space vector that's has to be known, but only the sector number in which the stator flux linkage space vector is positioned.

2.5.2 METHOD-2

The information about the location of the stator flux linkage space vector can be simply obtained by considering only the signs of the stator flux linkage components and this allows a simple implementation, which requires only the use of comparators. For this purpose it should be noted that in sector 1, $\psi sd > 0$, but since it sector 1, ψsq can both be positive and negative, the sign of, ψsq will not give any useful information on the position of the stator flux linkage space vector in sector 1.How ever instead of ψsq it is possible to use the stator flux linkage in stator phase B (ψsB), and it can be seen that $\psi sB < 0$ if ψs is in the first sector. Similarly if ψs is in sector 2 then $\psi sd > 0$, $\psi sq > 0$ and $\psi sB > 0$ .The results are summarized in the table shown below.

Table 2.2 Selection of the stator flux linkage space vector sector

Signs of the flux linkages	Sector 1	Sector 2	Sector 3	Sector 4	Sector 5	Sector 6
Sign of ψsd	+	+	-	-	-	+
Sign of ψsq	(nu; - +)	+	+	(nu; + -)	-	-
Sign of ψsB =sign of $[\sqrt{3}\,\psi sd - \psi sq]$	-	+	+	+	-	-

(nu = not useful)

As it can be inferred from the table the sign of ψsq does not give useful information in sectors 1and 4, since in both of these sectors the sign can both be positive and negative. Thus this method of the determination of the sector in which the stator flux linkage space vector positioned is much simpler to be implemented than the earlier method.

2.5.3 METHOD-3

In this technique the signs of the direct and the quadrature axis flux linkages are determined first. These give information on the quadrant where the space vector of the stator flux linkage is located. Since every quandrant contains only one full sector and half of another sector, thus there are two possible sectors (in a quandrant), but the specific sector where Ψs is located can be obtained by using the ratio of $\psi sq / \psi sd$.

2.6 Fundamentals of stator flux-linkage estimation

In the DTC induction motor drive the stator flux-linkage components have to be estimated due to two reasons. First, these components are required in the optimum switching vector selection table discussed in the previous section. Secondly, they are also

required for the estimation of the electromagnetic torque. It should be noted that, in general, it follows directly from the stator voltage equation in the stator reference frame that

$$\psi sd = \int (V_{sD} - i_{sD} R_s)\, dt \qquad (2.9)$$

$$\psi sq = \int (V_{sQ} - i_{sQ} R_s)\, dt \qquad (2.10)$$

and as $$\psi sB = (\sqrt{3}\, \psi sd - \psi sq) / 2 \qquad (2.11)$$

If non-power-invariant forms of the space vectors are used, then

$\Psi s = 2/3\, (\Psi sA + a\, \Psi sB + a^2 \Psi sC) = \Psi sD + j\, \Psi sQ$

$\Psi sD = \Psi sA = \int (V_{sD} - i_{sD} R_s)\, dt$

Where $V_{sD} = V_{sA}$ and $isD = i_{sA}$.

Further more $\Psi sQ = (\Psi sB - \Psi sC) / \sqrt{3} = \int (V_{sQ} - i_{sQ} R_s)\, dt$

Where $V_{sQ} = (V_{sB} - V_{sC}) / \sqrt{3}$ and $isQ = (i_{sB} - i_{sC}) / \sqrt{3}$. However since $\Psi sC = -(\Psi sA + \Psi sB)$, thus $\psi sB = (\sqrt{3}\, \psi sd - \psi sq) / 2$ is obtained. It not necessary to use three stator voltage sensors and three stator current sensors since it is possible to show, by considering $V_{sA} + V_{sB} + V_{sC} = 0$ and $i_{sA} + i_{sB} + i_{sC} = 0$, that V_{sD} and V_{sD} can be obtained by monitoring only two stator currents. Thus,

$V_{sD} = (1/3)(V_{ba} - V_{ac})$

$V_{sQ} = (-1/\sqrt{3})(V_{ac} + V_{ba})$

$i_{sD} = i_{sa}$

$i_{sQ} = (1/\sqrt{3})\, (i_{sa} + 2 i_{sb})$

It follows from eq (2.11) that the sign of ΨsB can be obtained by examining the sign of the flux linkage $(\sqrt{3}\, \psi sd - \psi sq)$ (physically this corresponds to twice the stator flux linking stator phase ΨsB).

It is very important to note that the performance of the DTC drive using Eqns (2.9) and (2.10) will depend greatly on the accuracy of the monitored voltage and currents, and also on and accurate integration technique. However, errors may occur in the monitored stator voltages and stator currents due to the following factors: phase shift in the measured values (due to the sensors used), magnitude errors due to conversion factors and gain, offsets in the measurement system, quantization errors in the digital system, etc. Furthermore, an accurate value has to be used for the stator resistance. For accurate flux

Chapter 3

Modeling and Simulation of DTC drive

3.1 Introduction

Circuit modeling and simulation plays an important role at a preliminary design stage. Without the component models the simulation of the circuit becomes futile. This fundamental approximation provides a quick way to calculate the system parameters. For instance a simulation of the system can be very helpful for tuning the proportional and the integral gains of a PI controller and also other control parameters of the system. These fundamental approximations can be achieved at the initial design stage with the help of the simulation in which the non-linear equations of the system are solved to obtain the system performance for different conditions. The more exact the modeling equations of the system are the more practical are the obtained simulation results. This chapter outlines the modeling procedure and the modeling equations of the various components in the direct torque controlled induction motor drive with a detailed discussion of the results obtained for the simulation model constructed using MATLAB/SIMULINK toolboxes. A detailed analysis of the obtained results and the effect on the system performance of various parameters like the flux and torque hysteresis bands, switching frequency is presented.

3.2 Modeling of the DTC Drive System

This section presents the mathematical modeling of the various blocks in the classical direct torque controlled induction motor drive is shown in fig 3.1. DTC induction motor drive constitutes the following main blocks:

- Field weakening controller
- PI speed controller
- Torque hysteresis controller
- Flux hysteresis controller
- Induction motor
- Voltage source inverter

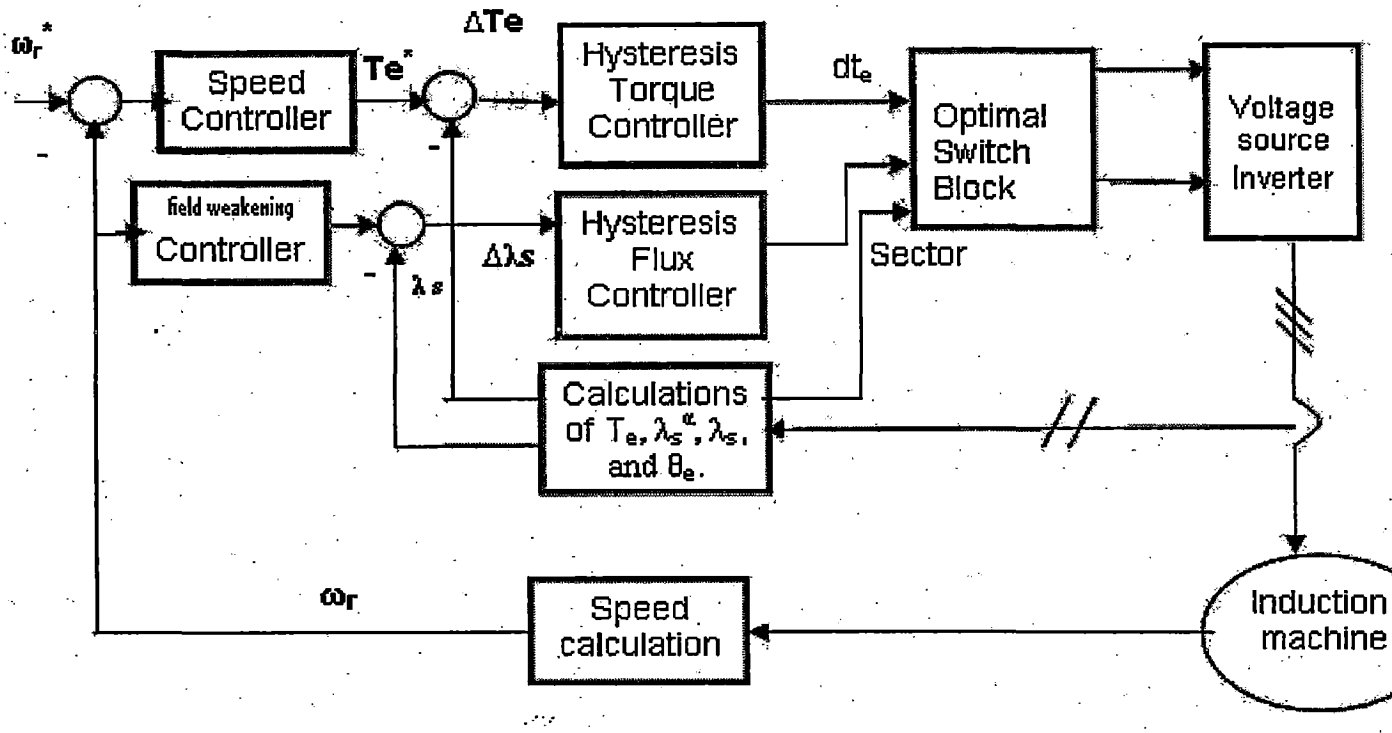

Fig 3.1 Block diagram of classical DTC drive

3.2.1 Modeling of Torque Hysteresis controller

As the name implies this is a hysteresis comparator. The block has its inputs as the reference torque and the actual torque and it gives an output depending on whether the error, which is the difference of the reference and actual torques, lies within the hysteresis band or outside the hysteresis band. Mathematically this can expressed as

- **Two level comparator:**

For anticlockwise direction (forward direction):

$$dte = 1 \text{ if } |te| \le |teref| - |\Delta te| \quad (3.1)$$

For clockwise direction (backward direction):

$$dte = -1 \text{ if } |te| \ge |teref| + |\Delta te| \quad (3.2)$$

- **Three level comparator:**

For anticlockwise direction (forward direction):

$$dte = 1 \text{ if } |te| \le |teref| - |\Delta te| \quad (3.3)$$

$$dte = 0 \text{ if } |te| \ge |teref| \quad (3.4)$$

For clockwise direction (backward direction):

$$dte = -1 \text{ if } |te| \geq |teref| + |\Delta te| \quad (3.5)$$

$$dte = 0 \text{ if } |te| \geq |teref| \quad (3.6)$$

3.2.2 Modeling of Flux Hysteresis controller

This block has the inputs as the reference and the actual values of the stator flux linkage and it gives an output depending on whether the error, which is the difference of the reference and the actual flux linkages, lies within or outside the hysteresis band. Mathematically this can expressed as

- **Two level comparator**

$$d\psi = 1 \text{ if } |\psi s| \leq |\psi sref| - \Delta\psi s \quad (3.7)$$

$$d\psi = -1 \text{ if } |\psi s| \geq |\psi sref| + \Delta\psi s \quad (3.8)$$

- **Three level comparator**

$$d\psi = 1 \text{ if } |\psi s| \leq |\psi sref| - \Delta\psi s \quad (3.9)$$

$$d\psi = -1 \text{ if } |\psi s| \geq |\psi sref| + \Delta\psi s \quad (3.10)$$

$$d\psi = 0 \text{ if } |\psi s| \geq |\psi sref| \quad (3.11)$$

3.2.3 Modeling of PI Speed Controller

The controller used is the discrete PI controller that takes in the reference speed and the actual speed and gives the value of the reference torque depending on the error in the reference and the actual values. The mathematical equations for the discrete PI controller are given as,

The speed error We(n) is given as

$$We(n) = W^*(n) - W(n) \quad (3.12)$$

The output of the speed controller at the nth instant is given as:

$$T(n) = T(n-1) + Kp[We(n) - We(n-1)] + Ki\, We(n) \quad (3.13)$$

3.2.4 Modeling of voltage source inverter

The inverter can be modeled in terms of the switching vector being applied to it. The voltage equation for the inverter for a non-zero voltage space vector being applied to it can be given as:

$$us = uk = 2V_{dc}/3 \exp[j(k-1)\pi/3] \quad k=1, 2, 3, 4, 5, 6. \quad (3.14)$$

Where V_{dc} is the DC link voltage.

The voltage being applied to the motor at any instant can be obtained from the knowledge of the switching vector being applied to the motor, DC link voltage and space phasor of the stator voltages in the stationery reference frame can be given in terms of the switching functions as:

$$Vs(t)=2/3Ud(Sa(t)+aSb(t)+a^2Sc(t)) \quad (3.15)$$

Where $a=e^{j(2\pi/3)}$

3.2.5 Calculation of the direct and qudrature stator voltages

The three phase voltages being applied to the motor at any instant can be calculated using the switching functions S_a, S_b, S_c as

$$V_{as} = (1/3)V_{dc}(2S_a - S_b - S_c) \quad (3.16)$$

$$V_{bs} = (1/3)V_{dc}(-S_a + 2S_b - S_c) \quad (3.17)$$

$$V_{cs} = (1/3)V_{dc}(-S_a - S_b + 2S_c) \quad (3.18)$$

The direct and the quadrature axis stator voltages can be obtained from three phase voltage equations as

$$V_{sD} = (1/3)(V_{ba} - V_{ac}) \quad (3.19)$$

$$V_{sQ} = (-1/\sqrt{3})(V_{ac} + V_{ba}) \quad (3.20)$$

$$V_{ba} = V_{bs} - V_{as} \quad (3.21)$$

$$V_{ac} = V_{as} - V_{cs} \quad (3.22)$$

Thus using the DC link voltage and the switching functions of each inverter legs the direct and the quadrature axis voltages in the stationery reference frame can be obtained from the above equations.

3.2.6 Calculation of direct and quadrature axis currents

In either the field oriented controlled drive or the induction motor drive normally two current sensors are installed and the third can be obtained by numerical summation of the two since, the sum of three-phase current of symmetrical induction machine is zero. The direct and quadrature axis stator current can be obtained from two sensed currents as

$$i_{sD} = i_{sa} \quad (3.23)$$

$$i_{sQ} = (1/\sqrt{3})(i_{sa} + 2i_{sb}) \quad (3.24)$$

Hence with the knowledge of two phase currents i_{sa}, i_{sb} the direct and quadrature axis stator currents in the stationery reference frame can be obtained from the above two equations.

3.2.7 Estimation of the direct and quadrature axis stator flux linkages

The stator flux linkages in the DTC drives have to be estimated for two reasons. First, these components are required in the optimum switching vector selection table. Secondly they are also required for the estimation of electromagnetic torque. The flux linkages can be obtained directly from the stator voltages and currents in the stationery reference frame as

$$\psi sd = \int (V_{sD} - i_{sD} R_s)\, dt \qquad (3.25)$$

$$\psi sq = \int (V_{sQ} - i_{sQ} R_s)\, dt \qquad (3.26)$$

In general to be accurate in the estimation flux linkages the model should also include an online stator resistance estimator. In practice the integrator poses problem of integration drift or sometimes referred as integration wind-up due to the presence of even small offset in the back Electromotive force (emf) of appropriate cut-off frequency. This is commonly overcome by replacing the integrator with a low-pass filter with appropriate cut-off frequency.

3.2.8 Estimation of the torque

The electromagnetic torque developed by the induction motor can be obtained from knowledge of the direct and the quadrature axis stator flux linkages as

$$T_e = 1.5\, P\, (\psi sd\, i_{sQ} - \psi sq\, i_{sD}) \qquad (3.27)$$

3.2.9 Estimation of flux linkage vector position

The various methods commonly employed for the estimation of the sector in which the flux linkage vector is located are explained in 2.5.The method that is most commonly employed is the one in which the signs of the various flux linkages are compared to obtain the sector. The mathematical equations showing the conditions to be satisfied for the stator flux linkage vector to be in a particular sector are given as,

Sector1: $\psi sd \geq \sqrt{3}\psi sq$, $\psi sd \geq 0$ (3.28)

Sector2: $\psi sd < \sqrt{3}\psi sq$, $\psi sd \geq 0$ (3.29)

Sector3: $\text{abs}(\psi sd) < \sqrt{3}\psi sq$, $\psi sd < 0$ (3.30)

Sector4: $\text{abs}(\psi sd) \geq \sqrt{3}\psi sq$, $\psi sd < 0$ (3.31)

Sector5: $\text{abs}(\psi sd) \leq \sqrt{3}\,\text{abs}(\psi sq)$, $\psi sd < 0$, $\psi sq < 0$ (3.32)

Sector6: $\psi sd < \sqrt{3}\,\text{abs}(\psi sq)$, $\psi sd \geq 0$, $\psi sq < 0$ (3.33)

Using the above conditions the sector in which the stator flux linkage vector is located can be obtained and this information along with the torque and the flux errors can be used to obtain the switching vector to be applied to the inverter at that instant.

3.2.10 Field weakening controller

The field-weakening controller sets the reference value of flux depending upon the base speed and actual speed of the motor. If the speed of the motor is below the base or the nominal speed then the flux reference is maintained at a constant nominal value. If speeds above the base speed are to be attained then the flux of the motor is weakened and the mathematical equations governing the relationship between the speed of the motor and the flux linkage reference is given as:

$$| W_{(n)} | \leq W_b \Rightarrow \psi'_{sref} = \psi_{sref} \quad (3.34)$$

$$| W_{(n)} | > W_b \Rightarrow \psi'_{sref} = \psi_{sref} (W_b / | W_{(n)} |) \quad (3.35)$$

Thus the flux field-weakening controller sets the reference flux command depending on the speed of the motor.

3.2.11 Modeling of a Three–Phase Induction Motor

The per phase equivalent circuit of the machine is valid in steady-state condition only. In an adjustable-speed drive, the machine normally constitutes an element within a feedback loop, and therefore its transient behavior has to be taken into consideration. The dynamic performance of an ac machine is somewhat complex because the three-phase rotor windings move with respect to the three-phase stator winding. The machine model can be described by differential equations with time-varying mutual inductances but such a model tends to be very complex. R.H. Park in 1920s, proposed a new theory of electric machine analysis to solve this problem. He transformed or referred the stator variables to a synchronously rotating reference frame fixed in the rotor. With such a transformation (called Park's transformation), he showed that all the time varying inductances that occur due to an electric circuit in relative motion and electric circuits with varying magnetic reluctances can be eliminated. Later in the 1930s, H.C. Stanley showed that time-varying inductances in the voltage equation of an inductance machine due to electric circuits in relative motion can be eliminated by transforming the rotor variables to variables associated with fictitious stationary windings. Later, G. Kron proposed a transformation of both stator and rotor variable to synchronously rotating reference frame that moves with the rotating magnetic field.

D.S. Brereton proposed a transformation of stator variables to a rotating reference frame that is fixed on the rotor. It was shown later by Krause and Thomas that time-varying inductances can be eliminated by referring the stator and rotor variables to a common reference frame which may rotate at any speed (arbitrary reference frame).

Stator circuit equations:

$$V_{qs}^{\ s} = R_s i_{qs}^{\ s} + p\psi_{qs}^{\ s} \tag{3.36}$$

$$V_{ds}^{\ s} = R_s i_{ds}^{\ s} + p\psi_{ds}^{\ s} \tag{3.37}$$

$\psi_{qs}^{\ s}$ is stator q axis flux linkage.

$\psi_{ds}^{\ s}$ is stator d axis flux linkage.

When these equations are converted to $d^e - q^e$ frame, the following equations can be written as:

$$V_{qs}^{\ s} = R_s i_{qs}^{\ s} + p\psi_{qs}^{\ s} + \omega_e \psi_{ds} \tag{3.38}$$

$$V_{ds}^{\ s} = R_s i_{ds}^{\ s} + p\psi_{ds}^{\ s} - \omega_e \psi_{qs} \tag{3.39}$$

The rotor actually moves at speed ω_r, the d-q axis fixed on the rotor moves at a speed $\omega_e - \omega_r$ relative to the synchronously rotating reference frame. The rotor equations are as given below.

$$V_{qr} = R_r i_{qr} + p\psi_{qr} + (\omega_e - \omega_r)\psi_{dr} \tag{3.40}$$

$$V_{dr} = R_r i_{dr} + p\psi_{dr} - (\omega_e - \omega_r)\psi_{qr} \tag{3.41}$$

The flux linkage expressions in terms of the currents can be written as follows:

$$\psi_{qs} = L_{ls} i_{qs} + L_m (i_{qs} + i_{qr}) \tag{3.42}$$

$$\psi_{qr} = L_{lr} i_{qr} + L_m (i_{qs} + i_{qr}) \tag{3.43}$$

$$\psi_{qm} = L_m (i_{qs} + i_{qr}) \tag{3.44}$$

$$\psi_{ds} = L_{ls} i_{ds} + L_m (i_{ds} + i_{dr}) \tag{3.45}$$

$$\psi_{dr} = L_{lr} i_{dr} + L_m (i_{ds} + i_{dr}) \tag{3.46}$$

$$\psi_{dm} = L_m (i_{ds} + i_{dr}) \tag{3.47}$$

Combining the above equations the electrical transient model in terms of voltages and currents can be given in matrix form as

$$\begin{pmatrix} V_{qs} \\ V_{ds} \\ V_{qr} \\ V_{dr} \end{pmatrix} = \begin{pmatrix} R_s + sL_s & \omega_e L_s & sL_m & \omega_e L_m \\ -\omega_e L_s & R_s + sL_s & -\omega_e L_m & sL_m \\ sL_m & (\omega_e - \omega_r)L_m & R_r + sL_r & (\omega_e - \omega_r)L_r \\ -(\omega_e - \omega_r)L_m & sL_m & -(\omega_e - \omega_r)L_r & R_r + sL_r \end{pmatrix} \begin{pmatrix} i_{qs} \\ i_{ds} \\ i_{qr} \\ i_{dr} \end{pmatrix} \quad (3.48)$$

For cage type induction motor, $V_{qr} = V_{dr} = 0$.

If the speed ω_r is considered constant (infinite inertia load), the electrical dynamics of the machine are given by a fourth-order linear system. Then knowing the inputs V_{qs}, V_{ds}, and ω_e, the currents i_{qs}, i_{ds}, i_{qr}, and i_{dr} can be solved from equation (3.48).

The torque expression can be given as

$$Te = \frac{3}{2}\left(\frac{p}{2}\right)(\psi_{dm} i_{qr} - \psi_{qm} i_{dr}) \quad (3.49)$$

3.3 SIMULATION

The mathematical equations that are listed in the previous section are used for simulating the closed loop performance of the direct torque controlled induction motor drive using MATLAB/SIMULINK toolbox.

3.3.1 Selection of the Flux and Torque Hysteresis bands

The flux and the torque hysteresis bands are the only gains to be adjusted in direct torque control. The torque ripple and harmonic loss of motor and switching loss of inverter greatly influence them. Hence these variables must be observed in the control process to maximize the performance of the system. A small value of the flux hysteresis band leads to sinusoidal currents while small torque hysteresis bands allow smoothed torque to be generated. On the other hand, small flux and torque hysteresis bands usually determine high switching frequency thereby increasing the switching losses in the inverter.

The flux and the torque hysteresis bands are so selected as to reduce the torque ripple and at the same time maintain currents as close to sinusoidal as possible. The flux hysteresis band is kept low and the torque hysteresis band to be about 2 to 3% of the rated or the nominal torque of the motor. The flux and torque hysteresis bands are initially chosen and the system is run in open loop without a speed controller for

different values of flux hysteresis band values starting from a high value (about 10% of the nominal value of the flux). The width of the flux hysteresis band is then gradually reduced till the winding currents are sinusoidal and at the same time ensuring required performance of the drive.

3.3.2 Selection of the Stator Flux Reference

The reference value of the motor flux greatly influences the motor behavior. It is initially chosen as the nominal value in many applications. Many motors work in an operating cycle that includes load intervals of less than their nominal power. In these situations, it is not necessary to set the flux reference value as the nominal value. Thus the nominal flux of the motor is not an optimum operating point when the motor load is less than the nominal value. Hence a careful choice of the motor flux is essential so as to obtain a reduction in the flux from the nominal value can help to improve the performance of the motor. Using an optimum value of the flux reference can reduce the torque ripple.

3.3.3 Tuning of the PI speed controller

The proportional and the integral gain parameters of the PI speed controller are obtained by the trial and error and the system is tuned for the best response.

3.3.4 Simulink Model

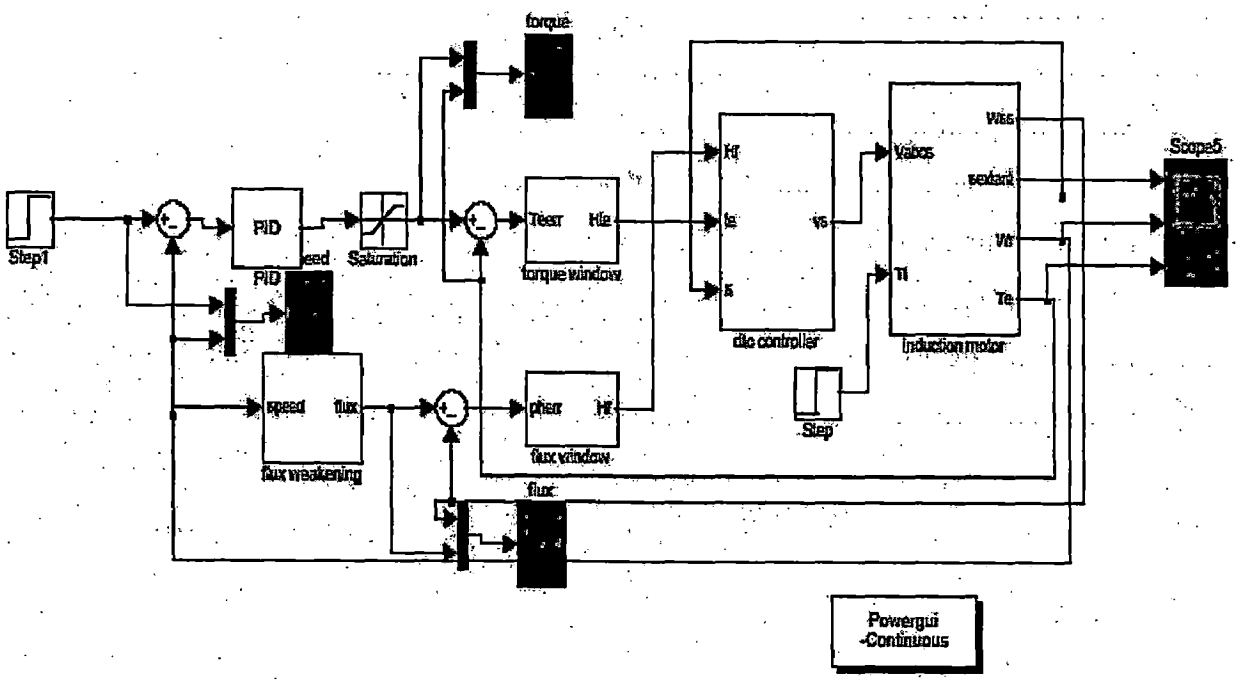

Fig 3.2 simulink model of DTC drive

3.3.5 Results and Discussion

The simulation results of the direct torque controlled induction motor drive built using the MATLAB/SIMULINK toolbox are presented below for the 1Hp induction motor along with discussion.

Performance of the 1Hp Direct torque Controlled Induction Motor Drive with Speed Sensor

The simulation results of the 1Hp induction motor are presented in the figures from 3.3 to 3.10 for the operation of the drive below the base speed and also for the operation above the base speed by field weakening. The torque reference is set at twice the rated torque. The simulated model uses a three level torque hysteresis comparator and a two level flux hysteresis comparator. The waveforms showing the variation of all the parameters namely, the reference and actual speed, stator winding currents, reference load torque and actual torque developed, estimated torque, actual and estimated direct and quadrature axis fluxes, stator flux modulus is given in fig 3.3.for speed below the base speed and in fig 3.8 for speed above the base speed.

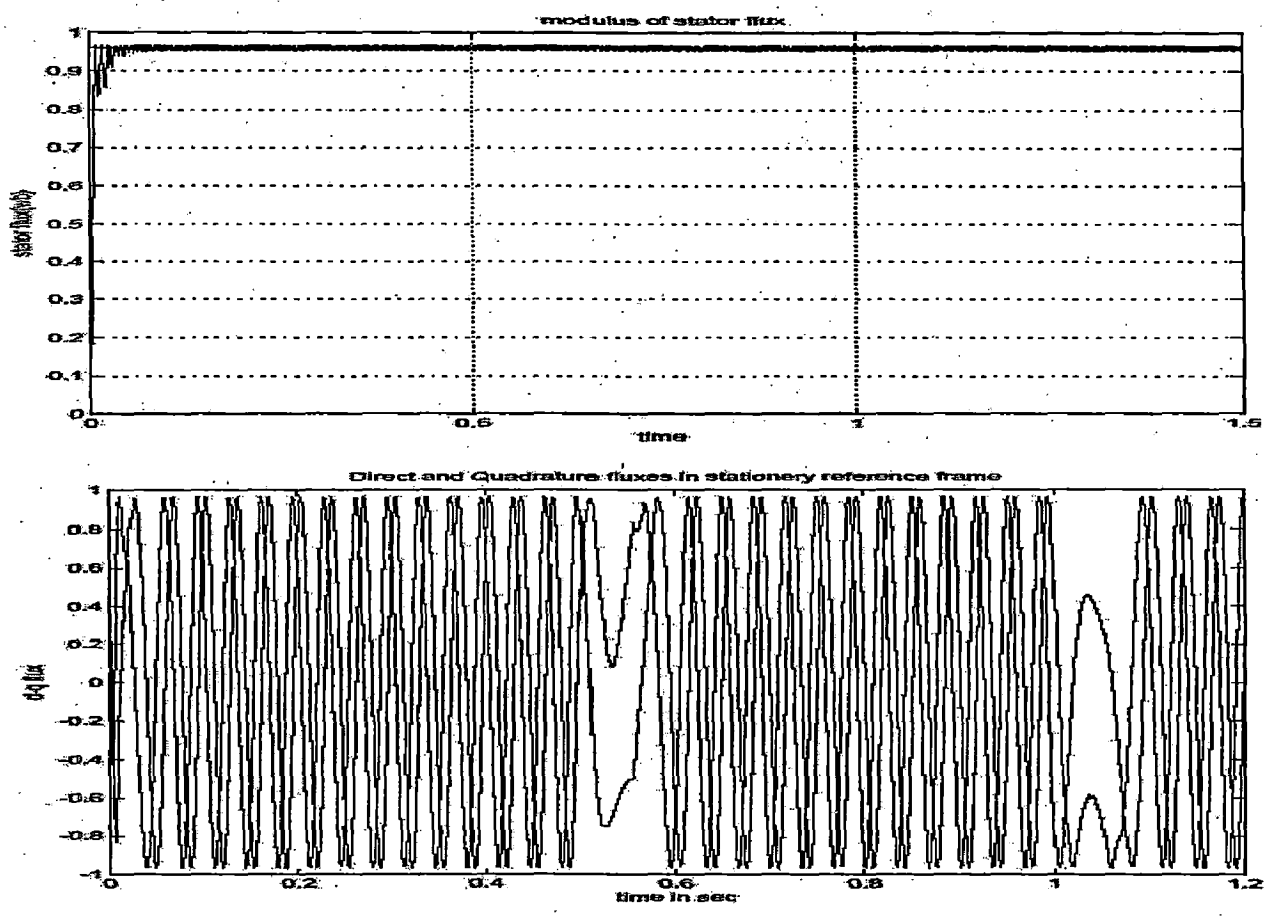

Fig 3.3Modulus of stator flux, direct and quadrature fluxes

Fig 3.3 shows the plots of the modulus of the stator flux linkage vector, and the direct, quadrature axis stator fluxes of the induction motor in the stationery reference frame. As can be seen from the figure the stator flux value is maintained constant through out the running condition. Also can be observed is the change in the direction of the two stator flux linkages following speed reversal commands at 0.5 seconds (900 rpm to -900 rpm) and 1 seconds (-900 rpm to 900 rpm).

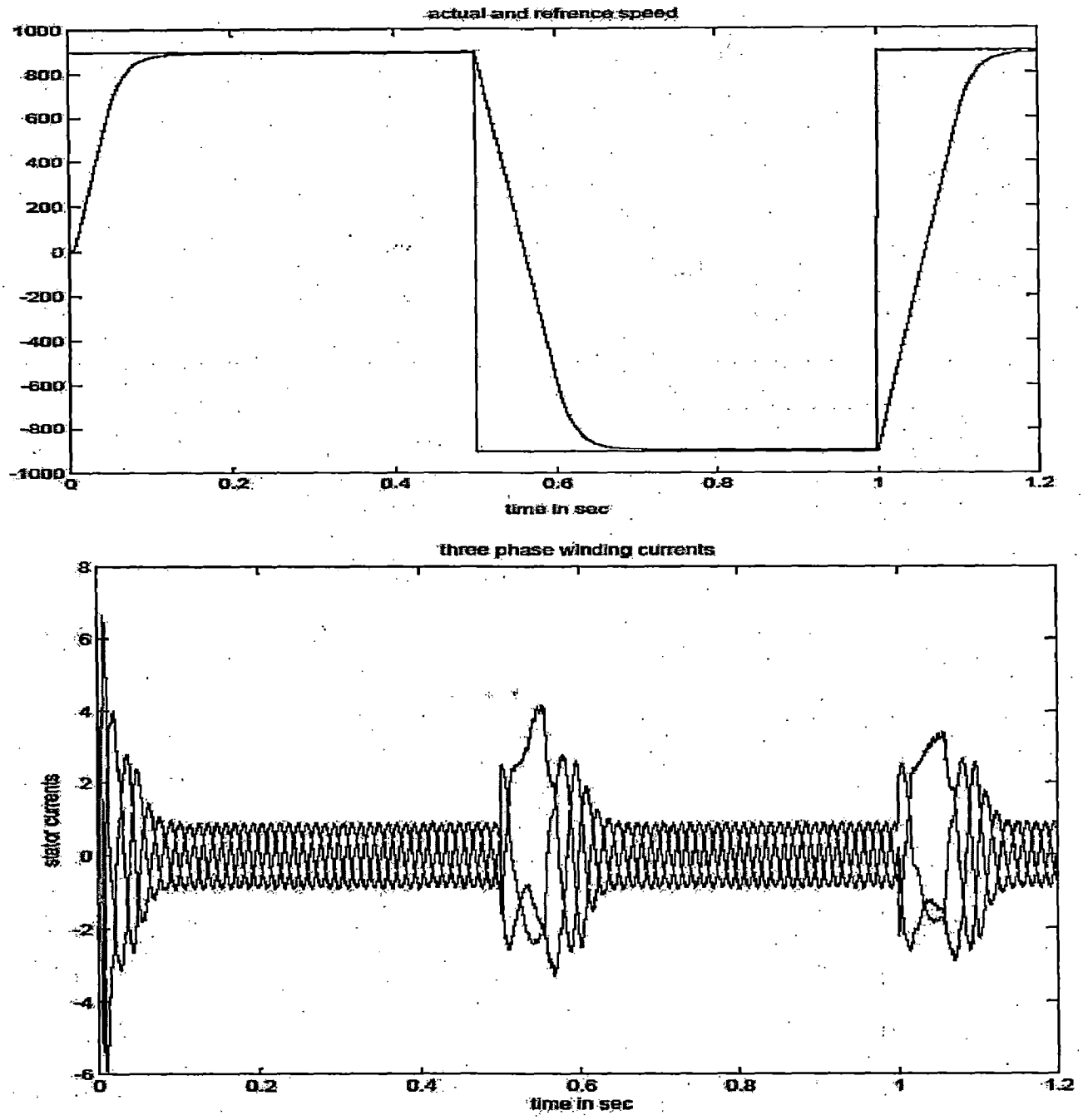

Fig 3.4 Plots of reference speed, actual speed and stator winding currents

Fig 3.4 shows the plots of the reference speed set by the step source externally, the actual speed of the motor and three winding currents of the induction motor. The three phase winding currents are approximately sinusoidal and one can observe the variation of the frequency of the currents of the drive speed changes and also the reversal of a phase current when the speed of the drive is reversed.

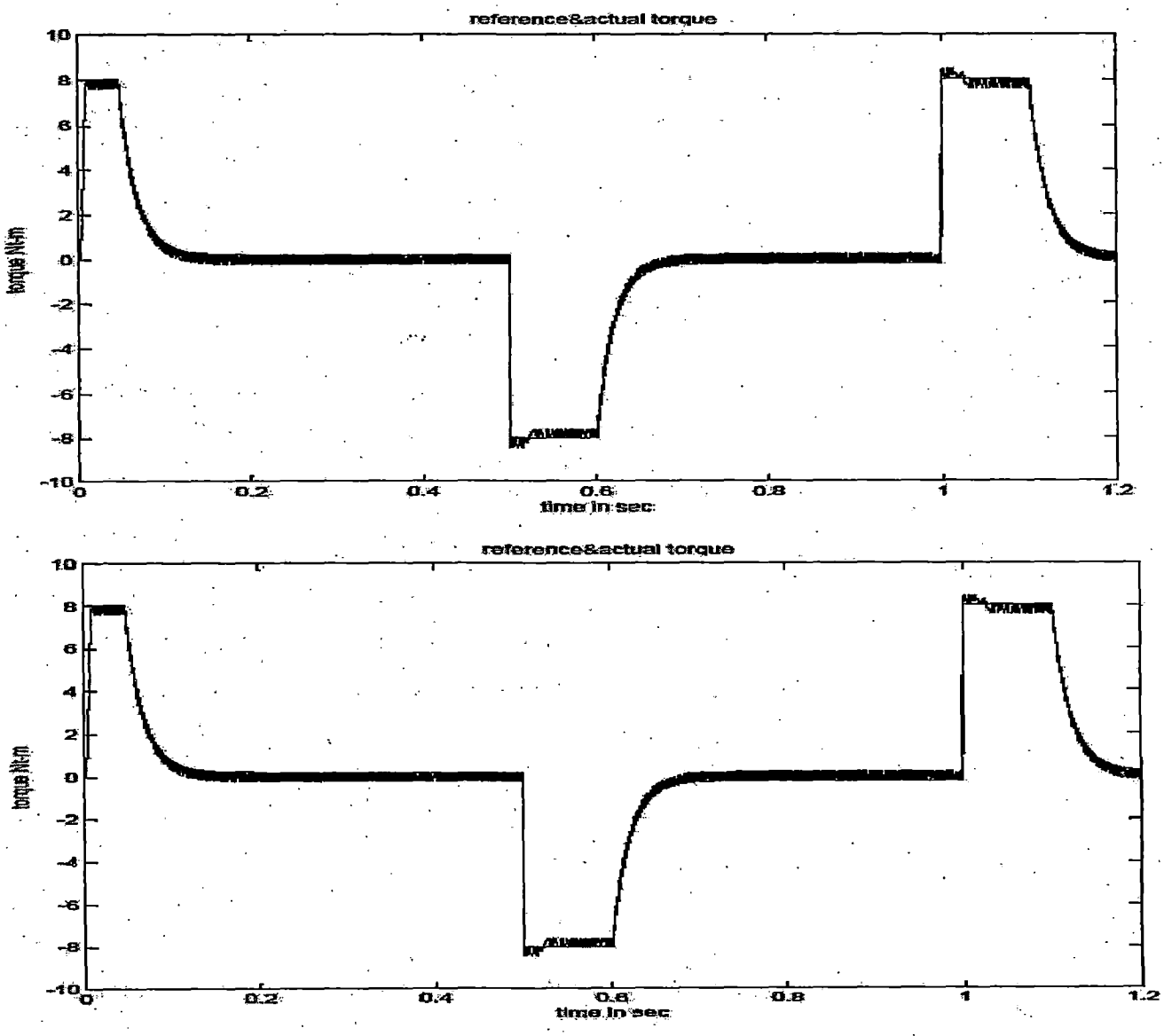

Fig 3.5 plots of reference torque, actual torque developed and the estimated torque

Fig 3.5 shows the plots of the refernce torque, electromagnetic torque developed by the motor and estimated torque.. As can be observed from the reference torque and the developed torque almost follows the set reference and hence this form of control is extremely fast. It can be observed that during the acceleration and the deceleration of the drive reference torque is set to be 8 N-m by the speed controller thereby enabling

the acceleration and the deceleration to occur at the twice the nominal torque of the motor.

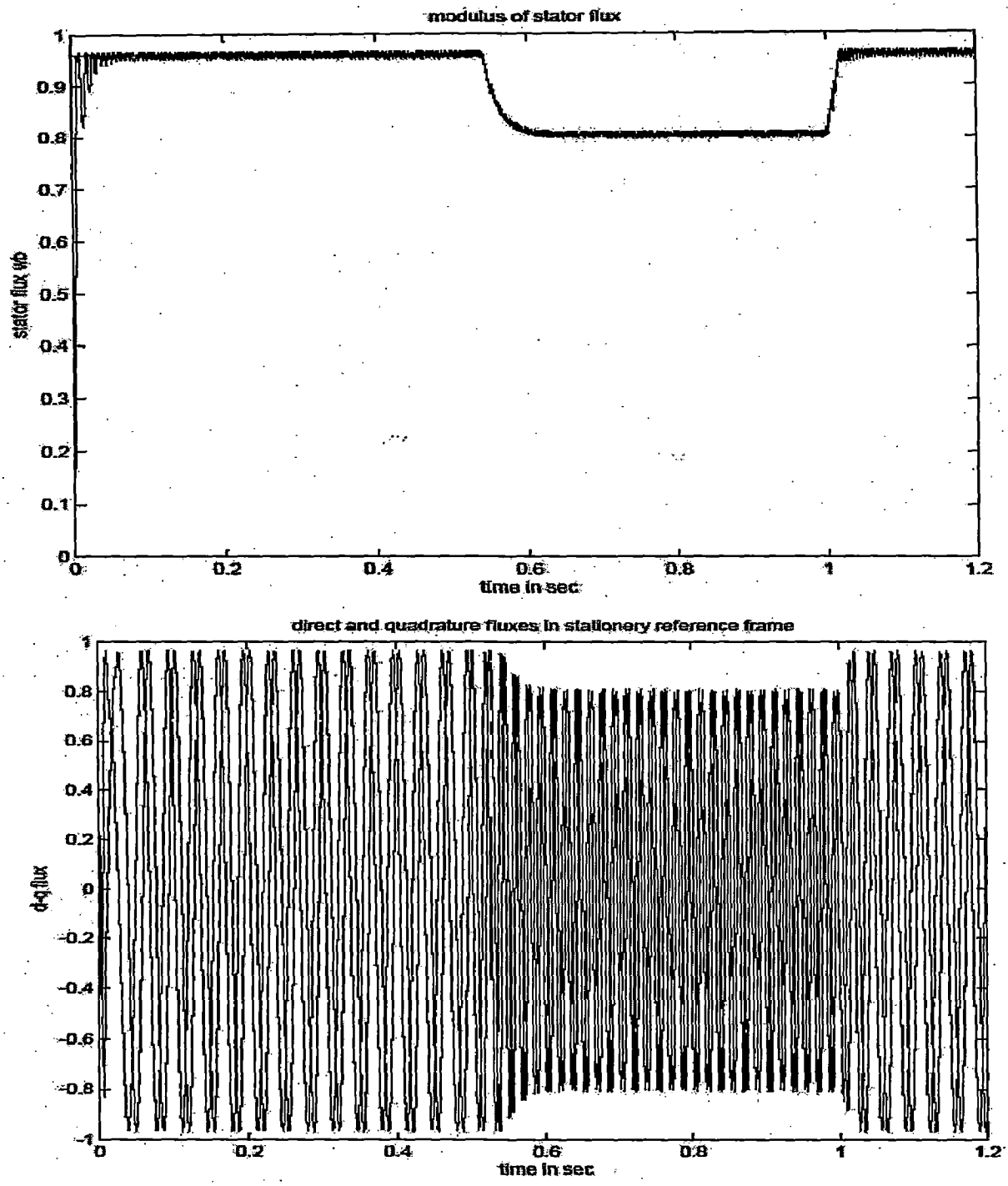

Fig 3.6 Modulus of stator flux, direct and quadrature fluxes

Fig 3.6 to 3.8 shows the different plots with the field weakening employed simulating the drive for speeds above the base speed. As can be seen from the flux plots, the modulus and hence the direct and quadrature axis stator flux magnitudes are reduced

while their frequency increased when the speed command from the step source is above the base speed. This change in the speed can also be observed from the winding current waveform as the frequency of the currents increases with an increase in the speed of the motor. Also from the winding current wave form it can be observed that the drive current is more while operating in field weakening region. This is due the requirement of the maximum torque with the reduced flux and the only way this can be achieved is with the increase in the stator current. This increase in the winding current is clear from fig 3.7 that shows the different plots. To ensure stable operation of the drive in the field weakening region the reference torque is reduced.

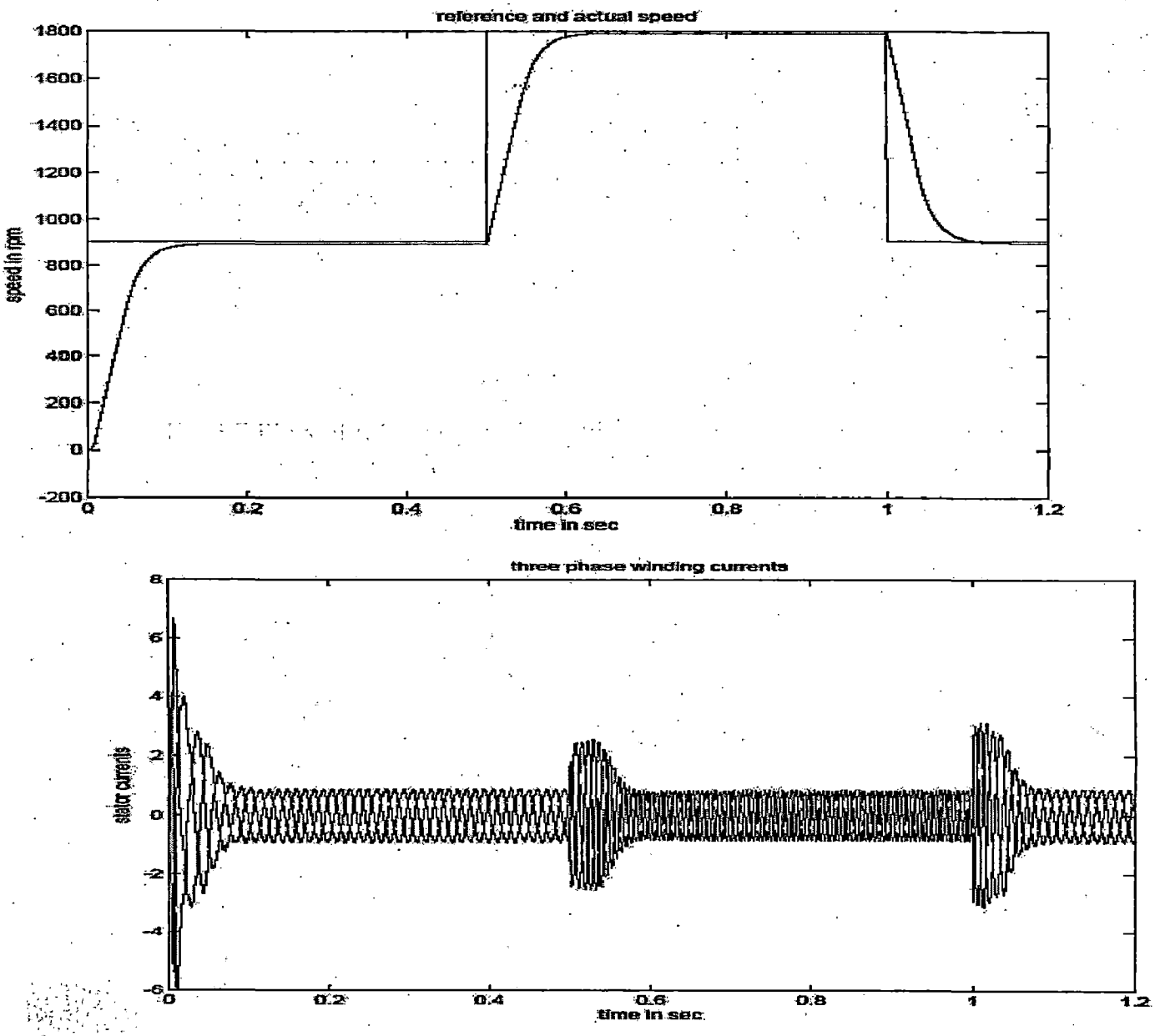

Fig 3.7 Plots of reference speed, actual speed and stator winding currents

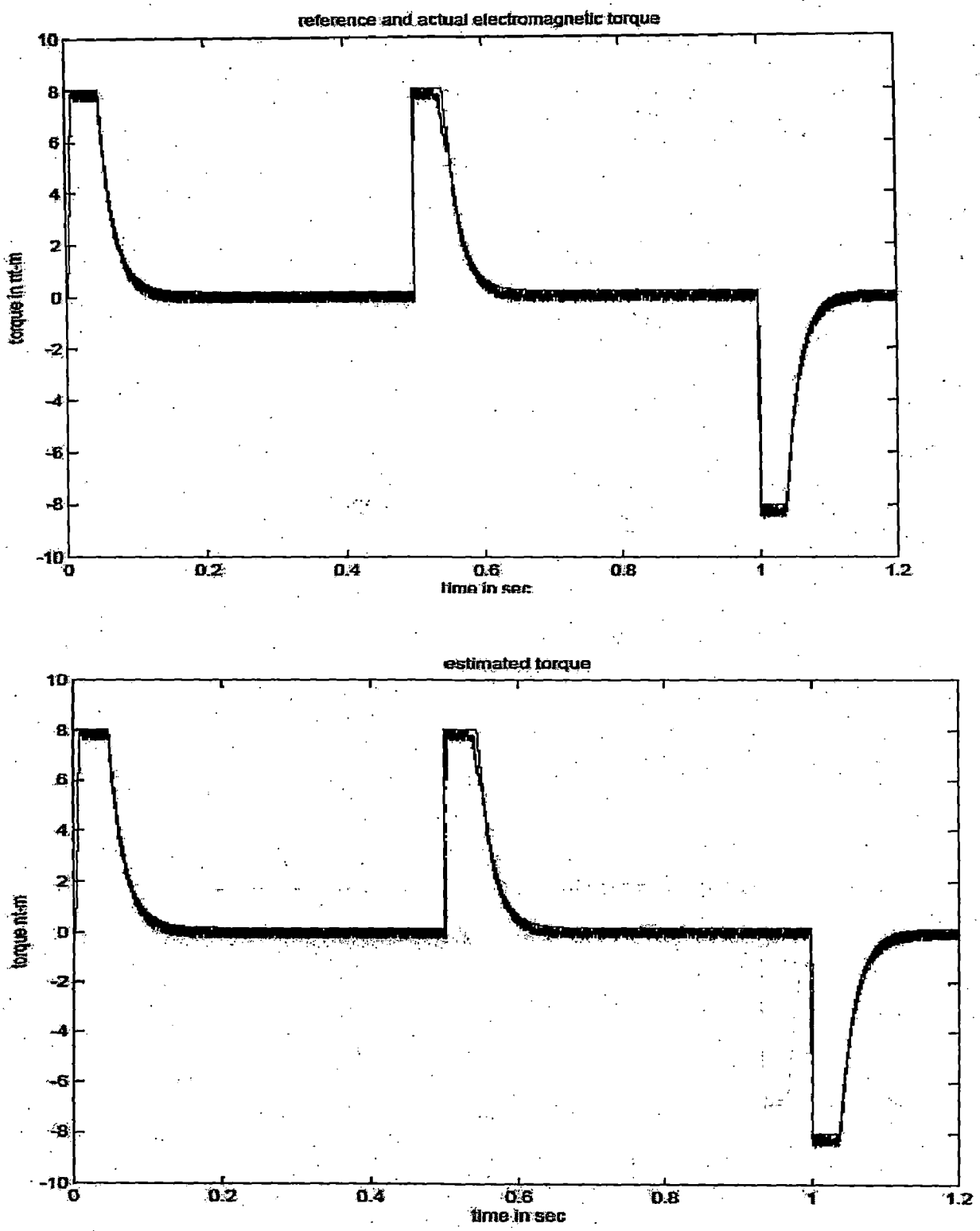

Fig 3.8 plots of reference torque, actual torque developed and the estimated torque

Fig 3.9 shows the simulation results for the step change in speed and constant load is impacted. This change in the speed observed from the d-q fluxes waveform as the

frequency of the currents increases with an increase in the speed of the motor. The speed reaches to its reference speed at 0.12 sec and it remained constant at reference value. At time t=0.5 sec reference speed is changed, the actual speed traces the reference speed accurately. This shows the effective implementation of DTC.

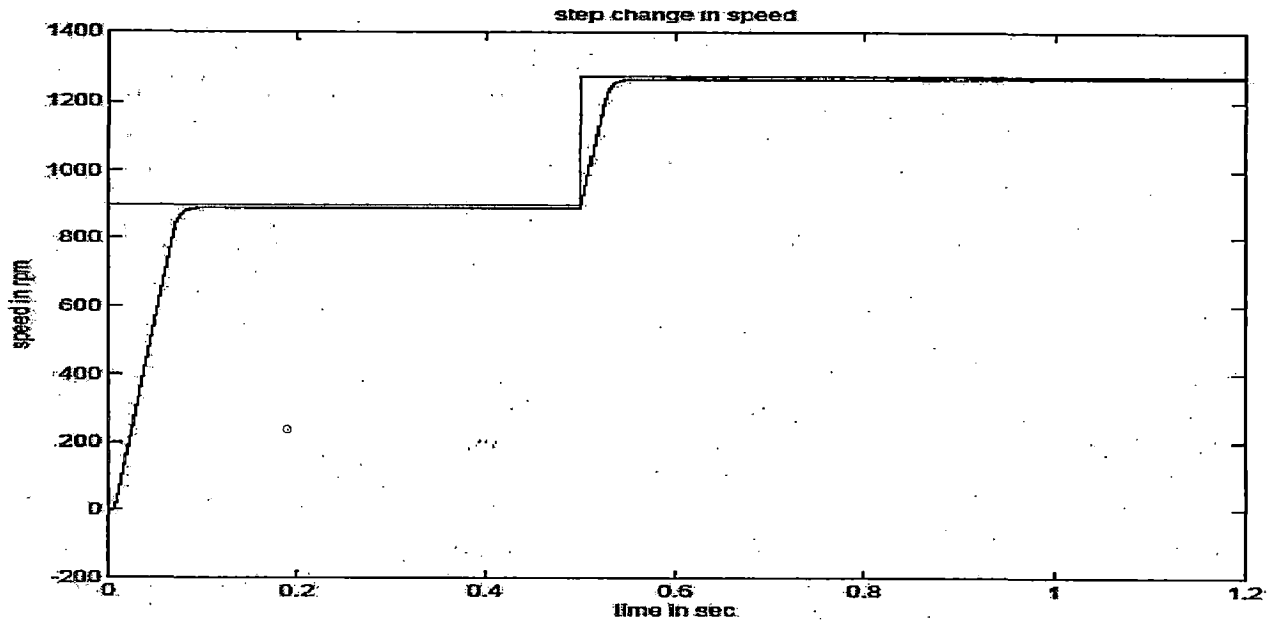

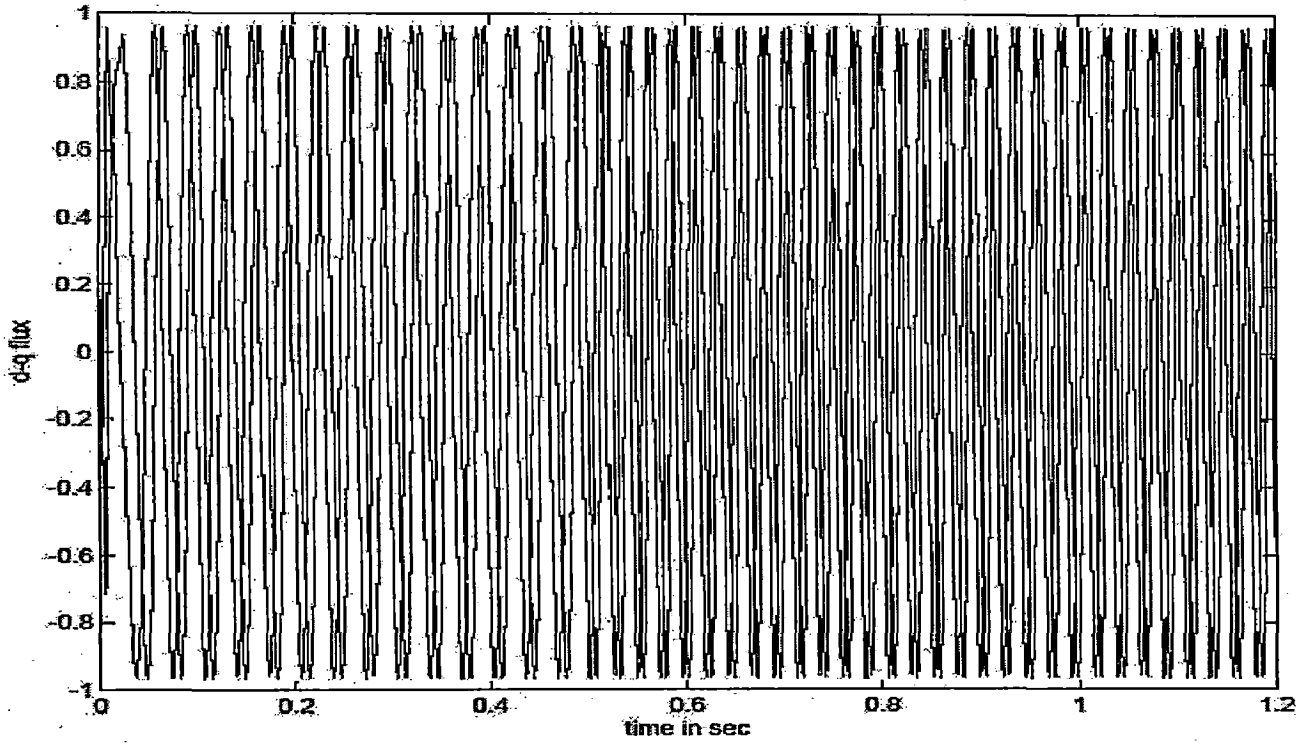

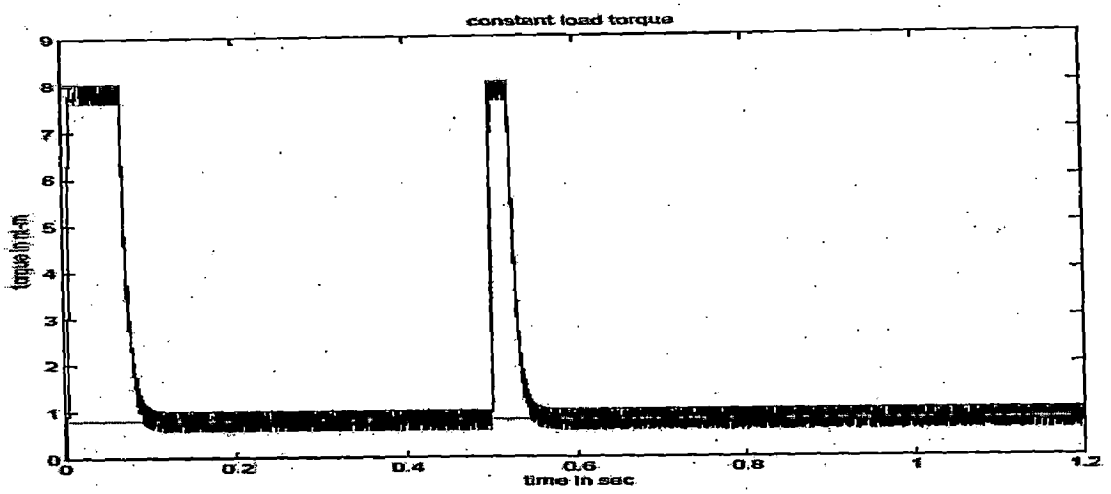

Fig 3.9 plots of reference and actual speed, d-q fluxes, reference load torque, actual torque developed and the estimated torque

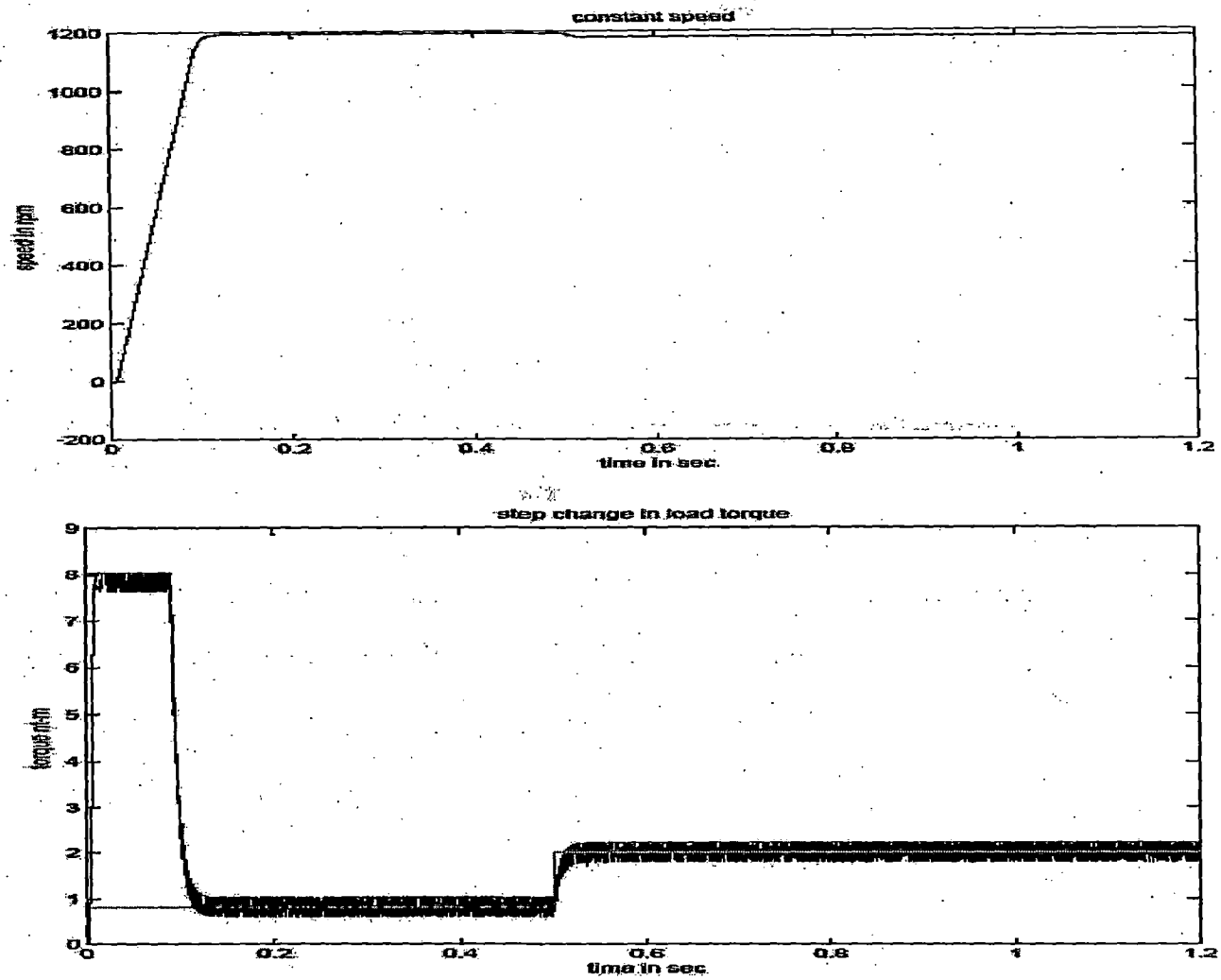

Fig 3.10 plots of reference and actual speed, reference load torque, actual torque developed and the estimated torque

Fig 3.10 shows the simulation results for the step change in load torque and constant speed. From the results the drive speed is maintained constant even for a change in the load torque applied set by external step source. As can be observed from the reference load torque there is a change in the set torque at 0.5 seconds and the developed torque almost follows the set reference and hence this form of control is extremely fast.

3.4 Sensorless Direct torque Controlled Induction Motor Drive

3.4.1 Introduction

Sensorless vector drives have become the norm for the industry and almost every manufacturer has introduced a sensorless induction motor drive. However it is a main feature of almost all of these industrial drives that they cannot operate at very low frequencies without speed or position sensors. Only one large manufacturer (ABB) has developed one form of direct torque controlled induction motor drive, which can work very close to zero frequency and no speed or position feedback is used.

3.4.2 State of Art

The mechanical speed sensor used for speed regulation often presents a source of error and demands additional expense. Especially in the case of robust asynchronous machines, there is a desire to apply speed regulation with out speed measurement.

In the past few years great efforts have been made to introduce speed and/or shaft position sensorless torque controlled (vector and direct torque controlled) drives. However, the first attempts have been restricted to techniques which are only valid in the steady state. These can be used in low-cost drive applications, not requiring high dynamic performance and other techniques are also described which are applicable for high performance applications in vector-direct torque controlled drives. These drives are usually referred to as 'sensorless' drives. Although the terminology 'sensorless' refers to only the speed and shaft sensors; there are still other sensors in the drive system, since closed loop operation cannot be performed without them. There are also techniques that have been reported which can be estimate the three phase stator currents of the induction motor and the dc link voltage from the switching functions and other machine parameters but these methods involve complex calculations and pose problems in their implementation.

Conventionally the speed of the electrical machine can be measured by dc tacho generators, which are nowadays brushless dc tacho generators. Rotor position can be measured by using electromagnetic resolvers or digitally by using incremental absolute encoders. Electromagnetic resolvers are popular for measuring the rotor position because of their rugged construction and higher operating temperature. Obviously if the rotor position is monitored the speed can be estimated directly from the position, but the speed resolution is limited by the resolution of the position transducer and also the sampling time.

3.4.2.1 Objectives

The main objectives of sensorless induction motor drives are

- Reduction of hardware complexity
- Increased mechanical robustness and overall ruggedness
- Operation in hostile environment
- Higher reliability
- Decreased maintenance requirements
- Increased noise community
- Unaffected machine inertia
- Applicability to off-the shelf motors

3.4.2.2 Speed Estimation Methods

The main techniques of sensorless speed estimation of induction motor drives are:

- Open loop estimators using monitored voltages/currents and improved schemes
- Estimators using spatial saturation stator phase third harmonic voltages
- Estimators using saliency effects
- Model reference adaptive systems (MRAS)
- Observers (Kalman, Luenberger)
- Estimators using artificial intelligence (neural network, fuzzy-logic based systems, fuzzy-neural networks).

3.4.3 Simulation of the Sensorless DTC

A closed loop model of the direct torque controlled induction motor drive is built using the MATLAB/SIMULINK toolboxes. The sensorless technique is incorporated into the model by using the speed estimated from the parameters of the induction

motor and the sensed parameters. The mathematical equations governing the model of the speed estimator are explained below.

3.4.3.1 Speed Estimation Method

Estimated speed is calculated using the equation (3.50) shown below.

$$Wm=[(\psi_{ds}-L11i_{ds})\, p\psi'_{qr}-(\psi_{qs}-L11i_{qs})\, p\psi'_{dr}]/[(\psi_{ds}-L11i_{ds})\psi'_{qr}+(\psi_{qs}-L11i_{qs})\psi'_{dr}] \quad (3.50)$$

3.4.4 Results and Discussion

Performance of the 1Hp Sensorless Direct torque Controlled Induction Motor Drive

The simulation results of the 1Hp speed sensorless induction motor are presented in the figures from 3.11 to 3.14 for the operation of the drive below the base speed and also for the operation above the base speed by field weakening.

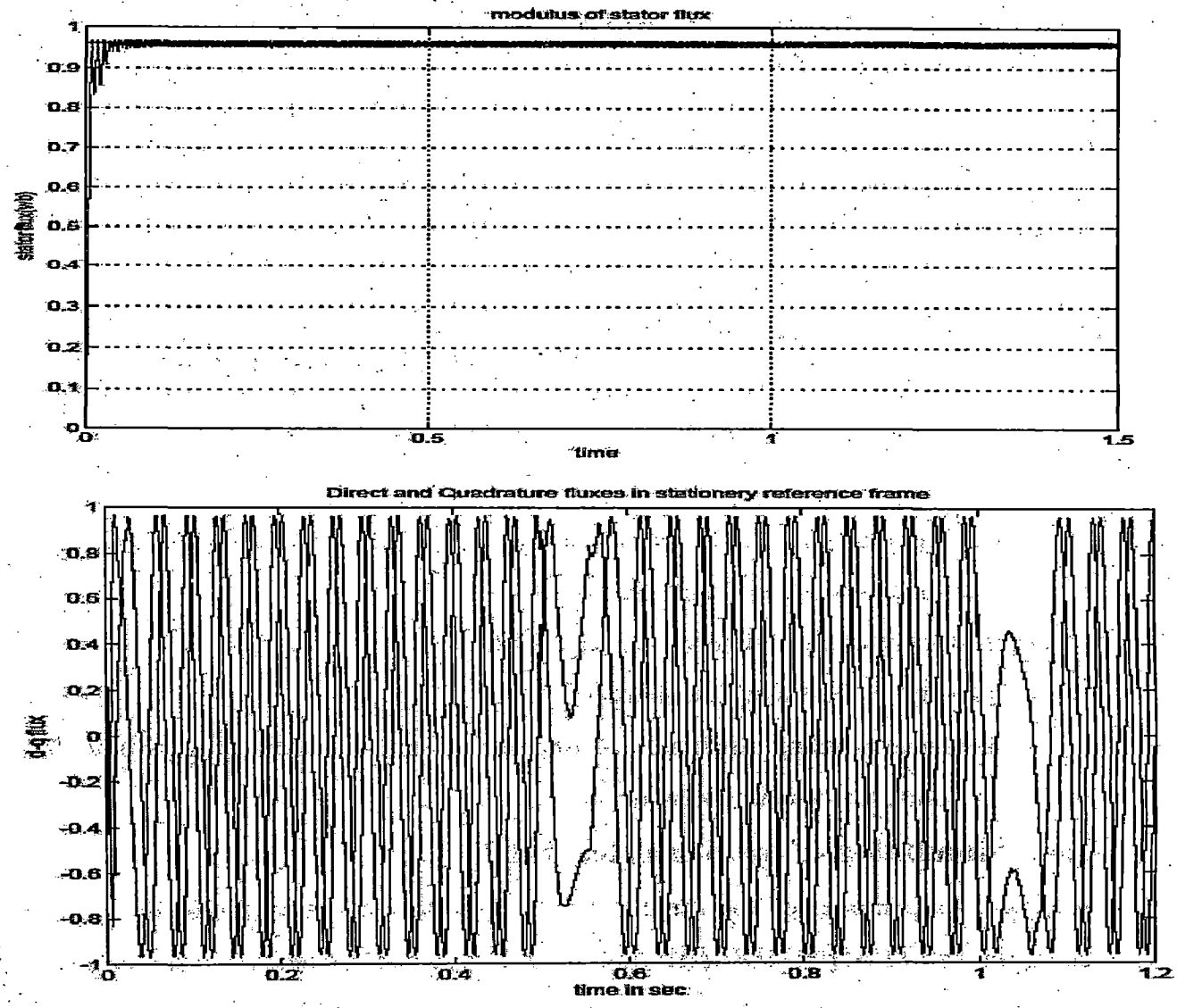

Fig 3.11Modulus of stator flux, direct and quadrature fluxes

Fig 3.11 shows the plots of the modulus of the stator flux linkage vector, and the direct, quadrature axis stator fluxes of the induction motor in the stationery reference frame. As can be seen from the figure the stator flux value is maintained constant through out the running condition. Also can be observed is the change in the direction of the two stator flux linkages following speed reversal commands at 0.5 seconds (900 rpm to -900 rpm) and 1 seconds (-900 rpm to 900 rpm).

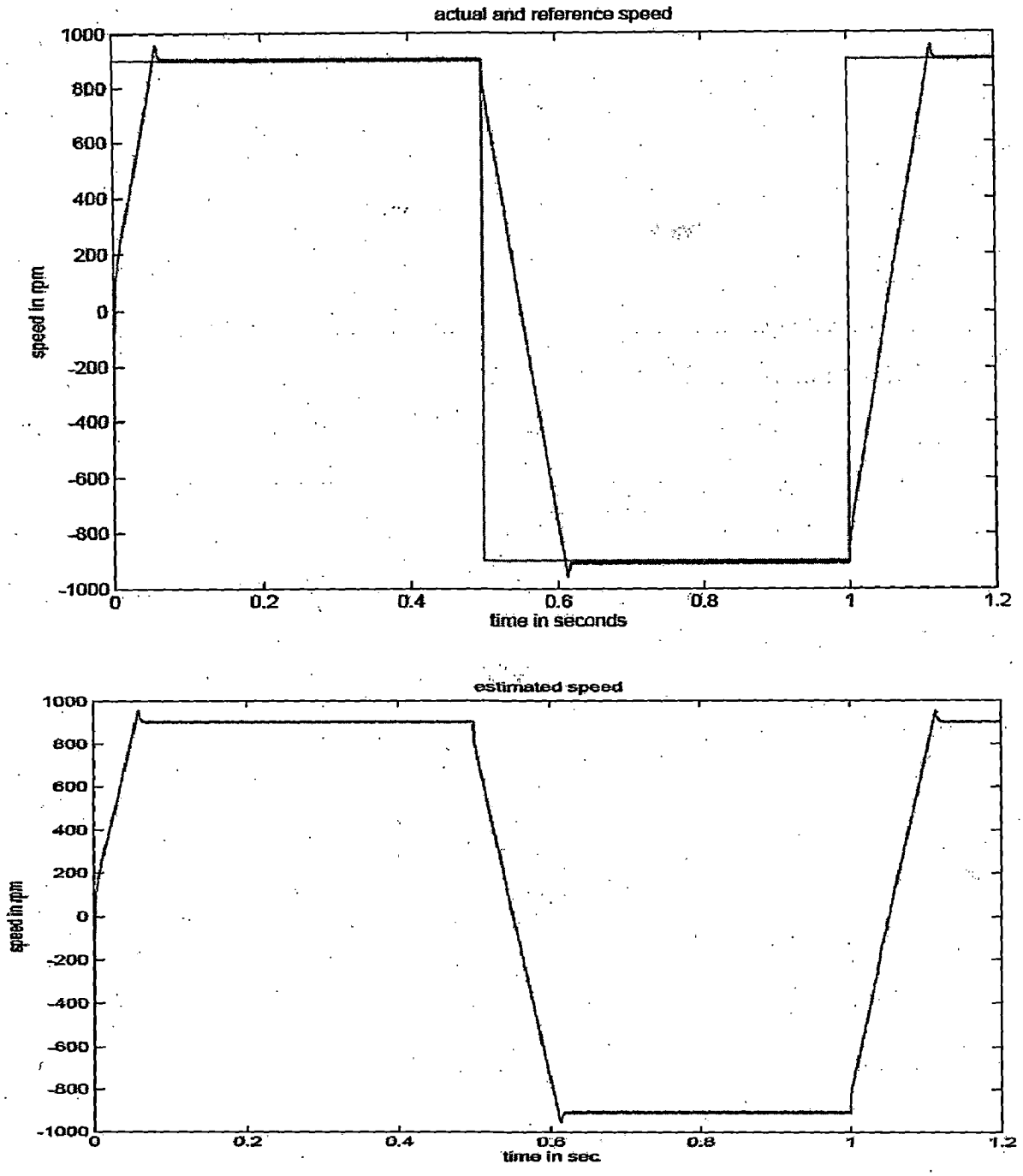

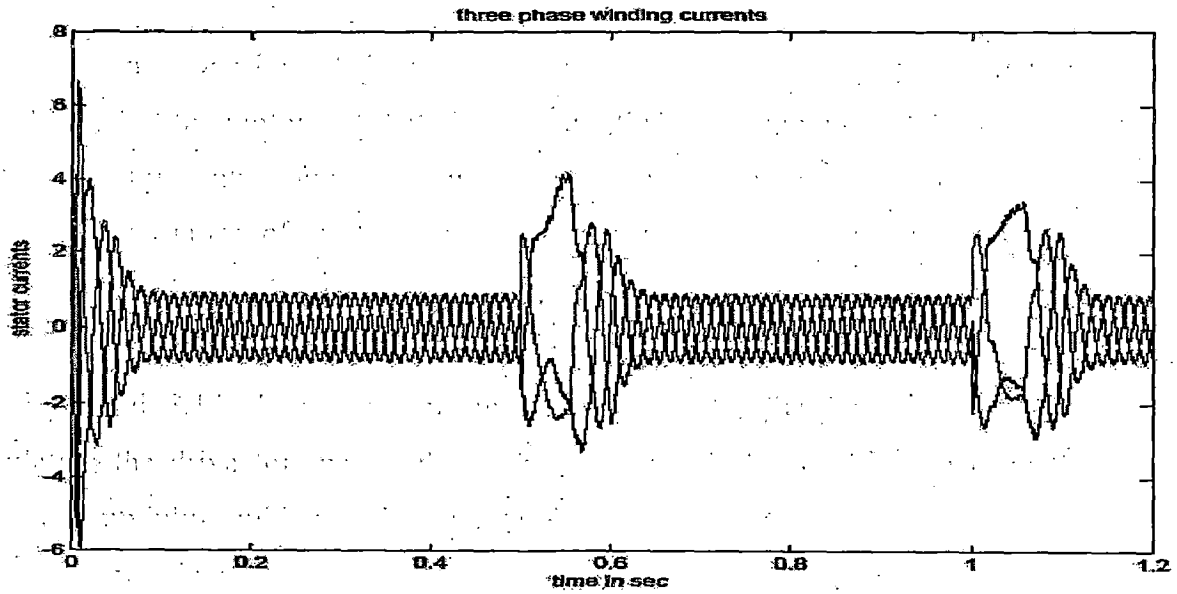

Fig 3.12 Plots of reference speed, actual speed, estimated speed and stator winding currents

Fig 3.12 shows the plots of the reference speed set by the step source externally, the actual speed of the motor, estimated speed and three winding currents of the induction motor. The three phase winding currents are approximately sinusoidal and one can observe the variation of the frequency of the currents of the drive speed changes and also the reversal of a phase current when the speed of the drive is reversed.

Fig 3.13 and 3.14 shows the different plots with the field weakening employed simulating the drive for speeds above the base speed. As can be seen from the flux plots, the modulus and hence the direct and quadrature axis stator flux magnitudes are reduced while their frequency increased when the speed command from the step source is above the base speed. This change in the speed can also be observed from the winding current waveform as the frequency of the currents increases with an increase in the speed of the motor. Also from the winding current wave form it can be observed that the drive current is more while operating in field weakening region. This is due the requirement of the maximum torque with the reduced flux and the only way this can be achieved is with the increase in the stator current. This increase in the winding current is clear from fig 3.14 that shows the different plots.

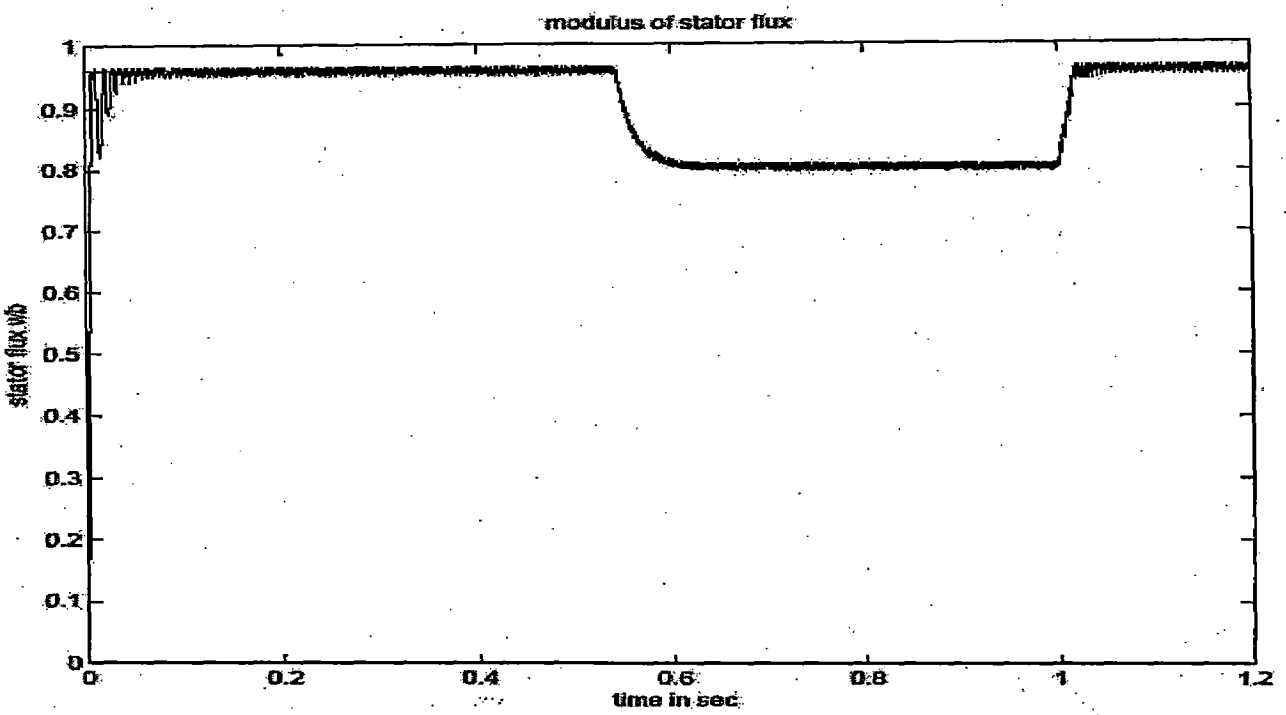

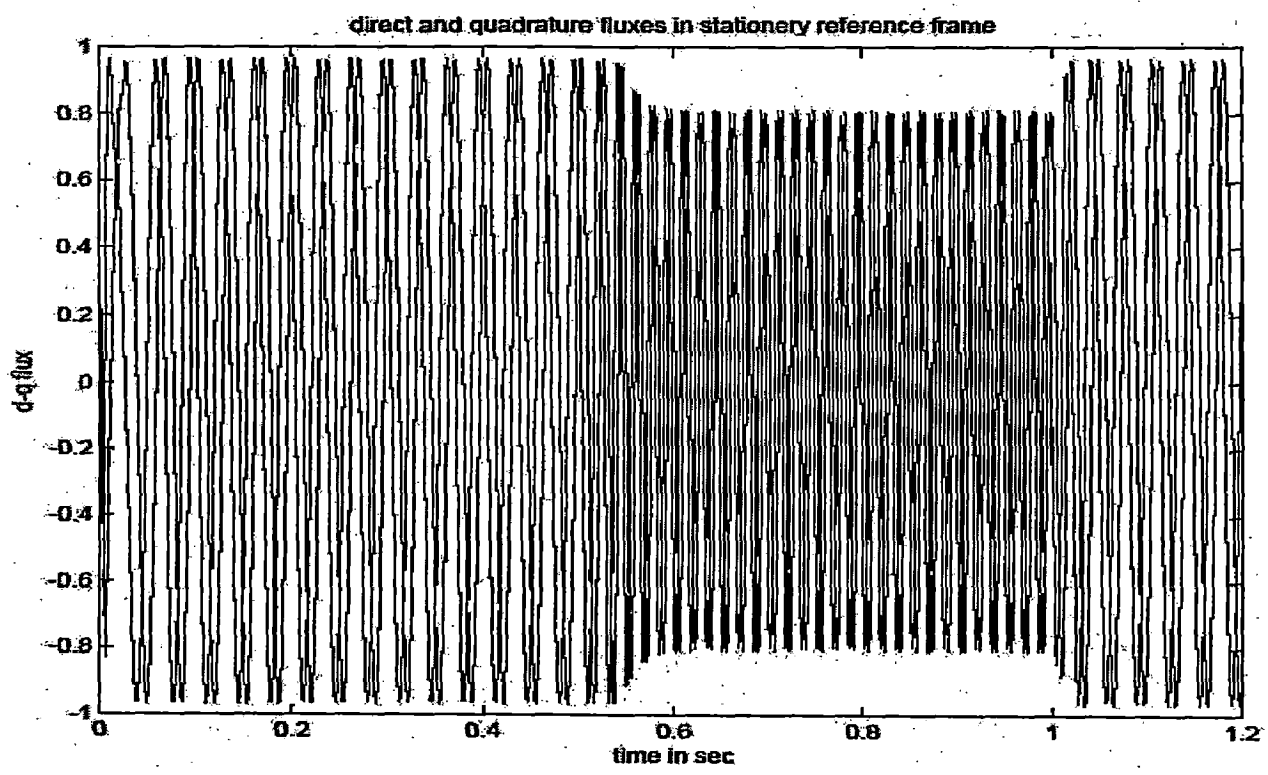

Fig 3.13 Modulus of stator flux, direct and quadrature fluxes

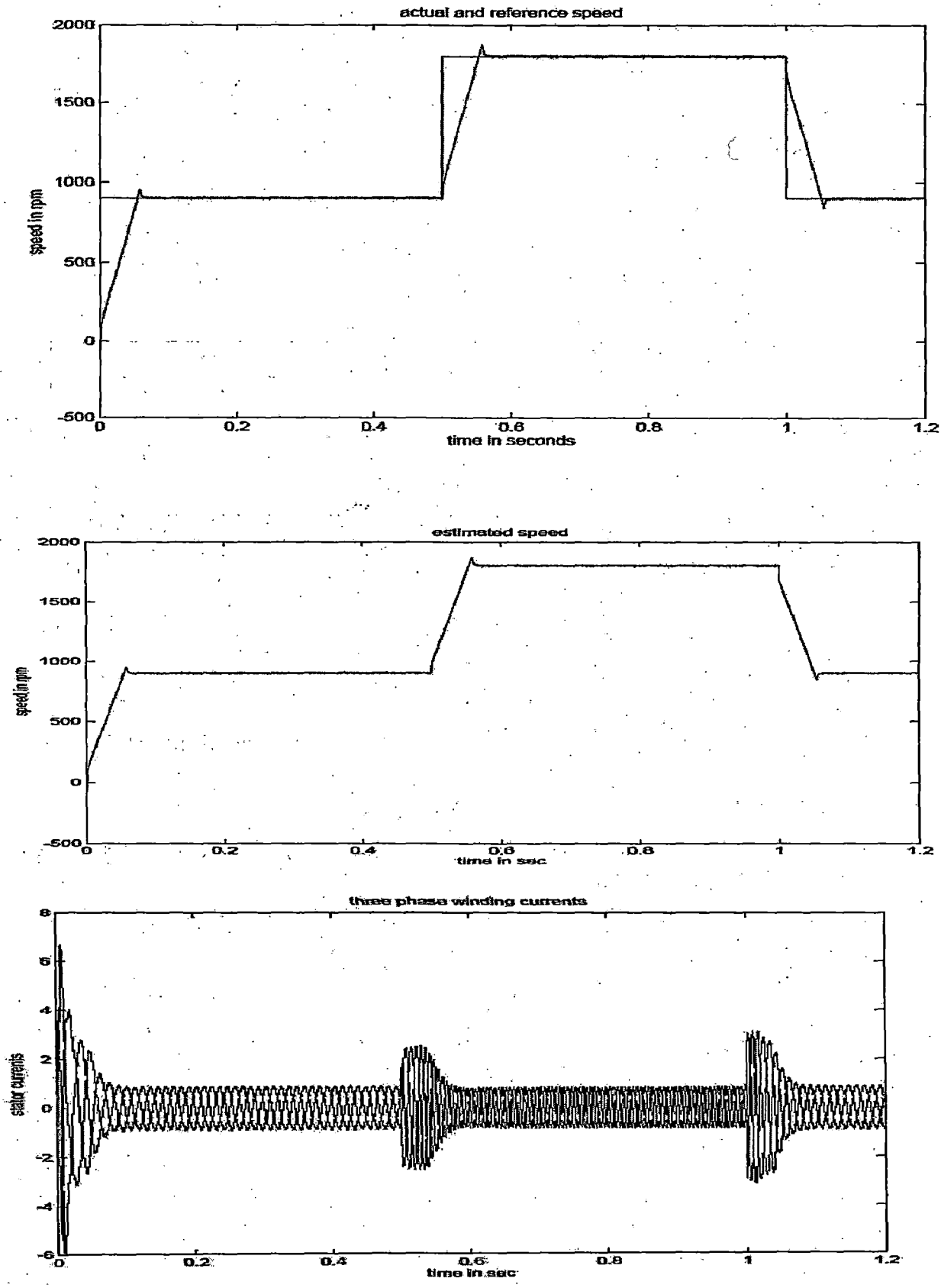

Fig 3.14 Plots of reference speed, actual speed, estimated speed and stator winding currents

3.6 Conclusion

The modeling of the different components of the direct torque controlled induction motor drive is presented. A simulation model is built using MATLAB/SIMULINK toolbox and the results of the simulation are presented with their detailed discussion. The detailed results are presented for the cases of direct torque control with speed sensor and without speed sensor.

Chapter 4

Fuzzy Controllers for Direct Torque Control Induction Motor Drive

4.1 Introduction

Due to continuously developing automation systems and more demanding Control performance requirements, conventional control methods are not always adequate. On the other hand, practical control problems are usually imprecise. The input output relations of the system may be uncertain and they can be changed by unknown external disturbances. New schemes are needed to solve such problems. One such an approach is to utilize fuzzy control. Fuzzy control is based on fuzzy logic, which provides an efficient method to handle in exact information as basis reasoning. With fuzzy logic it is possible to convert knowledge, which is expressed in an uncertain form, to an exact algorithm. In fuzzy control, the controller can be represented with linguistic if-then rules. The interpretation of the controller is the fuzzy but controller is processing exact input-data and is producing exact output-data in a deterministic way. This chapter deals with the description of fuzzy controller structure and the features of the presented hybrid fuzzy controller will be highlighted by comparing the performance of various control approaches, including PI control, PI-type fuzzy logic control (FLC), proportional-derivative (PD) type FLC, and combination of PD-type FLC and I control, for DTC-based induction motor drives.

4.2 Historical Background

Since the introduction of the theory of fuzzy sets by L. A. Zadeh in 1965, and the industrial application of the first fuzzy controller by E.H. Mamadani in 1974, fuzzy systems have obtained a major role in engineering systems and consumer's products in 1980s and 1990s. New applications are presented continuously.

A reason for this significant role is that fuzzy computing provides a flexible and powerful alternative to contract controllers, supervisory blocks, computing units and compensation systems in different application areas. With fuzzy sets very nonlinear control actions can be formed easily. The transparency of fuzzy rules and the locality of parameters are

helpful in the design and maintenances of the systems. Therefore, preliminary results can be obtained within a short development period.

However, fuzzy control does have some weaknesses. One is that fuzzy control is still lacking generally accepted theoretical design tools. Although preliminary results are easily, further improvements need a lot of especially when the number of inputs increases, the maintenances of the multi-dimensional rule base is time consuming

4.3 Structure of a fuzzy controller

Fuzzy control is a control method based on fuzzy logic. Just as fuzzy logic can be described simply as ''computing with words rather than numbers''; fuzzy control can be described simply as ''control with sentences rather than equations''. There are specific components characteristic of a fuzzy controller to support a design procedure. In the block diagram in Fig 4.1, the controller is between a preprocessing block and a post-processing block. The following explains the diagram block by block.

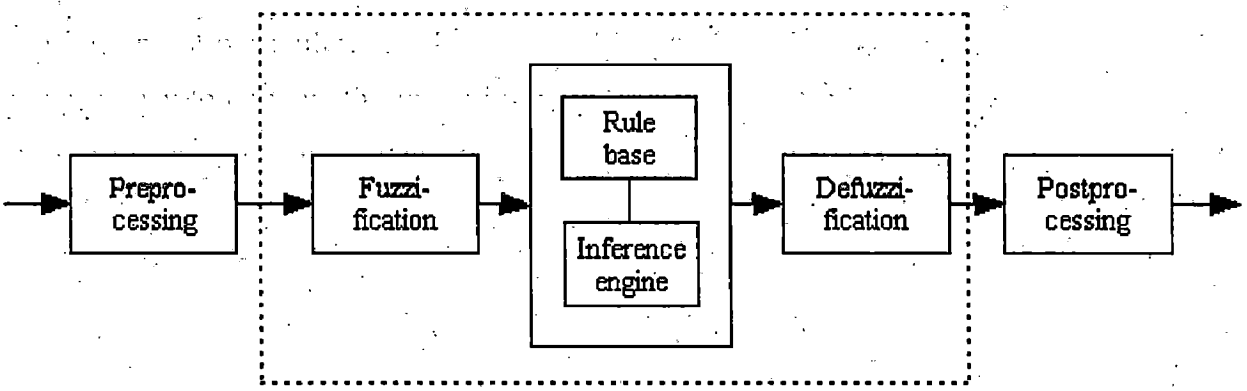

Figure 4.1: Blocks of a fuzzy controller

4.3.1 Preprocessing

The inputs are most often hard or crisp measurements from some measuring equipment, rather than linguistic. A preprocessor, the first block in Fig 4.1, conditions the measurements before they enter the controller. Examples of preprocessing are: Quantization in connection with sampling or rounding to integers; normalization or scaling onto a particular, standard range; filtering in order to remove noise; A quantiser is necessary to convert the incoming values in order to find the best level in a discrete universe. Assume, for instance, that the variable error has the value 4.5, but the universe is U= (-5, -4, 0, 4, 5). The quantiser rounds to 5 to fit it to the nearest level. Quantisation

is a means to reduce data, but if the quantization is too coarse the controller may oscillate around the reference or even become unstable. When the input to the controller is error, the control strategy is a static mapping between input and control signal. A dynamic controller would have additional inputs, for example derivatives, integrals, or previous values of measurements backwards in time. These are created in the preprocessor thus making the controller multi-dimensional, which requires many rules and makes it more difficult to design. The preprocessor then passes the data on to the controller.

4.3.2 Fuzzification

The first block inside the controller is fuzzification, which converts each piece of input data to degrees of membership by a lookup in one or several membership functions. The fuzzification block thus matches the input data with the conditions of the rules to determine how well the condition of each rule matches that particular input instance. There is a degree of membership for each linguistic term that applies to that input variable

4.3.3 Rule base The rule base is to do with the fuzzy inference rules. The step response of the system can be roughly divided into four areas A_I ~A_4 and two sets of points: cross-over $\{b_1, b_2\}$ and peak-valley $\{c_1, c_2\}$ as shown in Fig.4.2. The system equilibrium point is the origin of the phase plane

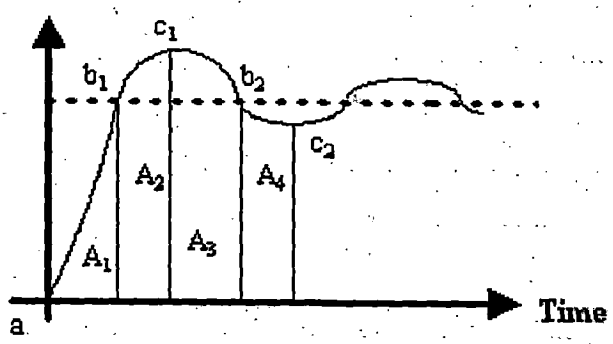

Fig. 4.2 General step response

a) The sign of rules: The sign of the rule base can be determined by following meta-rules

1) If both e and $\dot{e}$ are zero, then maintain present control setting.

2) If conditions are such that *e* will go to zero at a satisfactory rate, then maintain present control setting.

3) If e is not self-correcting, then the sign of the rule can be determined by five sub-criterions.

a) Rules for cross-over $\{b_1, b_2\}$ should prevent the overshoot in A_2/A_4.

b) Rules for peak-valley $\{c_1, c_2\}$ should speed up the response.

c) Rules for area A_1/A_3 should speed up the response when e is large and prevent the overshoot in A_2/A_4 when e is close to zero.

d) Rules for area A_2 should decrease the overshoot around the peak.

e) Rules for area A_4 should decrease the overshoot around the valley.

The above heuristic method can build general rule base

4.3.4 Inference Engine

Figures 4.3 and 4.4 are both a graphical construction of the algorithm in the core of the controller. In Fig. 4.3, each of the nine rows refers to one rule. For example, the first row says that if the error is negative (row 1, column 1) and the change in error is negative (row 1, column 2) then the output should be negative big (row 1, column 3). The picture corresponds to the rule base in (2). The rules reflect the strategy that the control signal should be a combination of the reference error and the change in error, a fuzzy proportional-derivative controller. We shall refer to that figure in the following. The instances of the error and the change in error are indicated by the vertical lines on the first and second columns of the chart. For each rule, the inference engine looks up the membership values in the condition of the rule.

Aggregation: The aggregation operation is used when calculating the degree of fulfillment or firing strength α_k of the condition of a rule k. A rule, say rule 1, will generate a fuzzy membership value μ_{e1} coming from the error and a membership value μ_{ce1} coming from the change in error measurement. The aggregation is their combination,

$$\mu_{e1} \textbf{ and } \mu_{ce1}$$

Similarly for the other rules, Aggregation is equivalent to fuzzification, when there is only one input to the controller. Aggregation is sometimes also called fulfillment of the rule or firing strength.

Activation: The activation of a rule is the deduction of the conclusion, possibly reduced by its firing strength. Thickened lines in the third column indicate the firing strength of each rule. Only the thickened part of the singletons are activated, and **min** or product (*) is used as the activation operator. It makes no difference in this case, since the output membership functions are singletons, but in the general case of s- , . - and z- functions in the third column, the multiplication scales the membership curves, thus preserving the initial shape, rather than clipping them as the **min** operation does. Both methods work well in general, although the multiplication results in a slightly smoother control signal. In Fig. 4.3, only rules four and five are active.

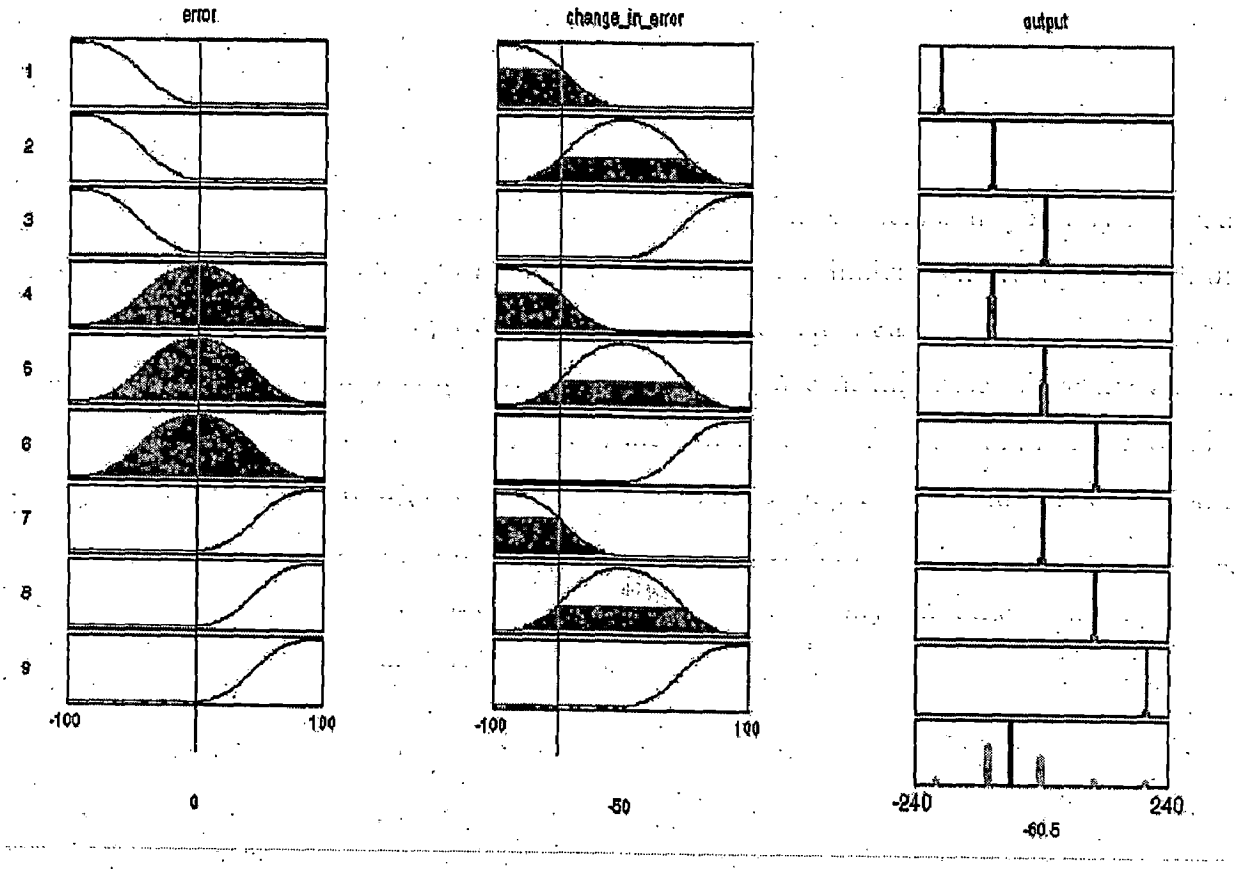

Figure 4.3: Graphical construction of the control signal in a fuzzy PD controller (generated in the Matlab Fuzzy Logic Toolbox).

A rule k can be weighted a priori by a weighting factor $w_k \in [0, 1]$, which is its degree of confidence In that case the firing strength is modified to

$$\alpha^*_k = w_k * \alpha_k$$

The degree of confidence is determined by the designer or a learning program trying to adapt the rules to some input-output relationship.

Accumulation: All activated conclusions are accumulated, using the **max** operation, to the final graph on the bottom right (Fig. 4.3). Alternatively, **sum** accumulation counts overlapping areas more than once (Fig. 4.4). Singleton output (Fig. 4.3) and **sum** accumulation results in the simple output.

$$\alpha_1 * s_1 + \alpha_2 * s_2 + \ldots + \alpha_n * s_n$$

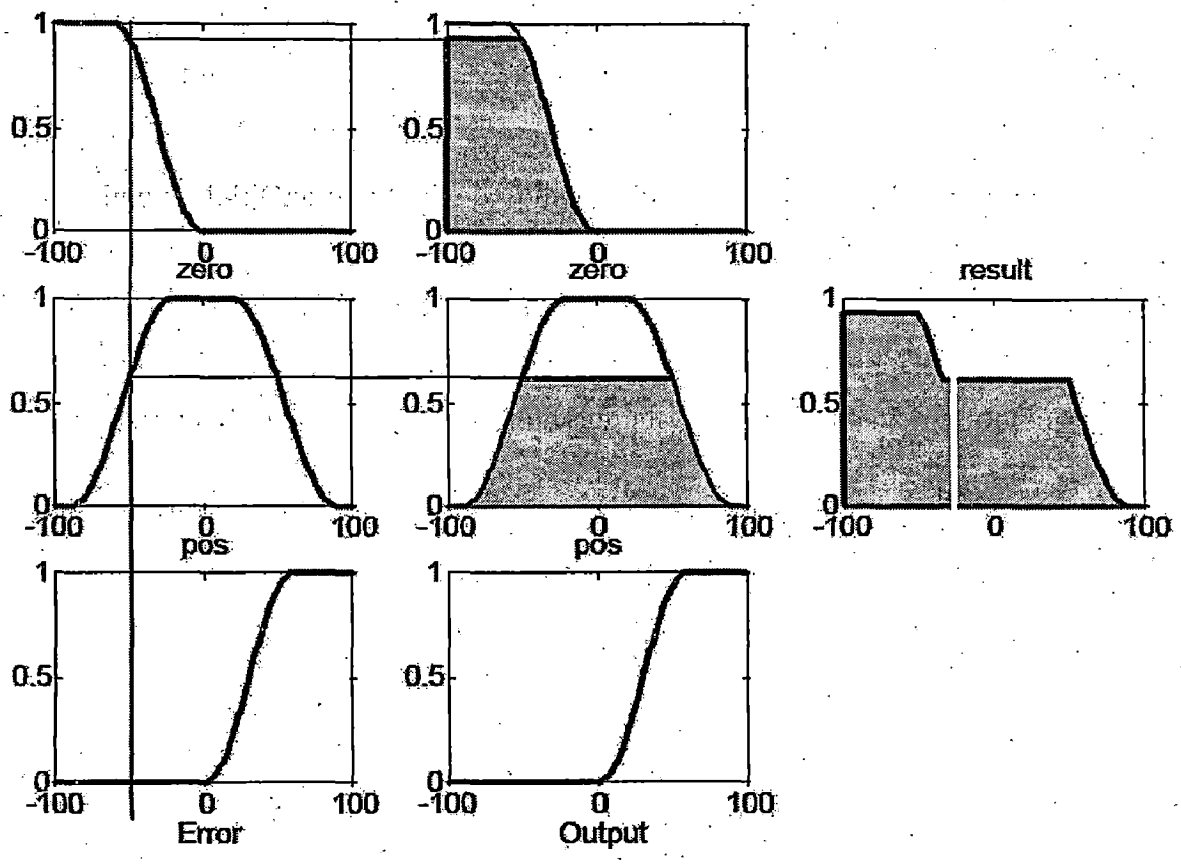

Figure 4.4: One input, one output rule base with non-singleton output sets.

The alphas are the firing strengths from the k rules and s1 ... sn are the output singletons. Since this can be computed as a vector product, this type of inference is relatively fast in a matrix oriented language. There could actually have been several conclusion sets. An

example of a one-input two- outputs rule is ''If e_a is **a** then o_1 is **x** and o_2 is **y**'. The inference engine can treat two (or several) columns on the conclusion side in parallel by applying the firing strength to both conclusion sets. In practice, one would often implement this situation as two rules rather than one, that is, ''If e_a is **a** then o_1 is **x**", ''If ea is **a** then o_2 is **y**".

4.3.5 Defuzzification

The resulting fuzzy set (Fig. 4.3, bottom right; Fig. 4.4, extreme right) must be converted to a number that can be sent to the process as a control signal. This operation is called defuzzification, and in Fig. 4.4 the x-coordinate marked by a white, vertical dividing line becomes the control signal. The resulting fuzzy set is thus defuzzified into a crisp control signal. There are several defuzzification methods.

Centre of gravity (COG): The crisp output value u (white line in Fig. 4.4) is the abscissa under the centre of gravity of the fuzzy set,

$$u = \frac{\sum_i \mu(x_i)\, x_i}{\sum_i \mu(x_i)}$$

Here x_i is a running point in a discrete universe, and $\mu(x_i)$, is its membership value in the membership function. The expression can be interpreted as the weighted average of the elements in the support set. For the continuous case, replace the summations by integrals. It is a much used method although its computational complexity is relatively high. This method is also called centroid of area.

Centre of gravity method for singleton (COGS): If the membership functions of the conclusions are singletons (Fig.4.3), the output value is

$$u = \frac{\sum_i \mu(s_i)\, s_i}{\sum_i \mu(s_i)}$$

Here s_i is the position of singleton i in the universe, and $\mu(s_i)$, is equal to the firing strength α_i of rule i. This method has a relatively good computational complexity, and u is differentiable with respect to the singletons s_i, which is useful in neuro fuzzy systems.

Bisector of area (BOA): This method picks the abscissa of the vertical line that divides the area under the curve in two equal halves. In the continuous case,

$$u=\{x \mid \int_{Min}^{x} \mu(x)\,dx = \int_{x}^{Max} \mu(x)\,dx\}$$

Here x is the running point in the universe $\mu(x)$, is its membership, Min is the leftmost value of the universe, and Max is the rightmost value. Its computational complexity is relatively high, and it can be ambiguous. For example, if the fuzzy set consists of two singletons any point between the two would divide the area in two halves; consequently it is safer to say that in the discrete case, BOA is not defined.

Mean of maximum (MOM): An intuitive approach is to choose the point with the strongest possibility, i.e. maximal membership. It may happen, though, that several such points exist, and a common practice is to take the mean of maximum (MOM). This method disregards the shape of the fuzzy set, but the computational complexity is relatively good.

Left maximum (LM), and Right maximum (RM): Another possibility is to choose the leftmost maximum (LM), or the rightmost maximum (RM). In the case of a robot, for instance, it must choose between left and right to avoid an obstacle in front of it. The defuzzifier must then choose one or the other, not something in between. These methods are indifferent to the shape of the fuzzy set, but the computational complexity is relatively small.

4.3.6 Post processing

Output scaling is also relevant. In case the output is defined on a standard universe this must be scaled to engineering units for instance, volts, meters, or tons per hour. An example is the scaling from the standard universe [-1, 1] to the physical units [-10, 10] volts. The post processing block often contains an output gain that can be tuned, and sometimes also an integrator.

4.4 Fuzzy Controllers

It is well known that fuzzy logic control consists of fuzzification process, linguistic rule base, and defuzzification process. The input variables for the illustrated fuzzy logic controller as shown in Fig. 4.5 using PI-type and PD-type fuzzy logic control are speed error and change of speed error. Fig. 4.6 shows membership function of input variables, E (t) and . E (t), which are with conventional triangular shapes and with 50% overlapping. As shown in Fig. 4.6, each membership function is assigned with seven fuzzy sets, which are negative big (NB), negative medium (NM), negative small (NS), zero (ZE), positive small (PS), positive medium (PM), and positive big (PB). Linguistic rules, which depend on the type of fuzzy logic control, are set up for fuzzy inference. Table 4.1 and 4.2 show the linguistic rule bases for PI-type and PD-type fuzzy logic controllers, respectively. The most distinguishing difference between these two linguistic rules is the switching boundary at which the sign of rule change. As shown in Table 4.1 for PI-type FLC, the switching boundary is diagonal. In contrast the switching boundary for PD-type FLC as shown in Table 4.2 is a horizontal line along speed, "*E*," equals to zero.

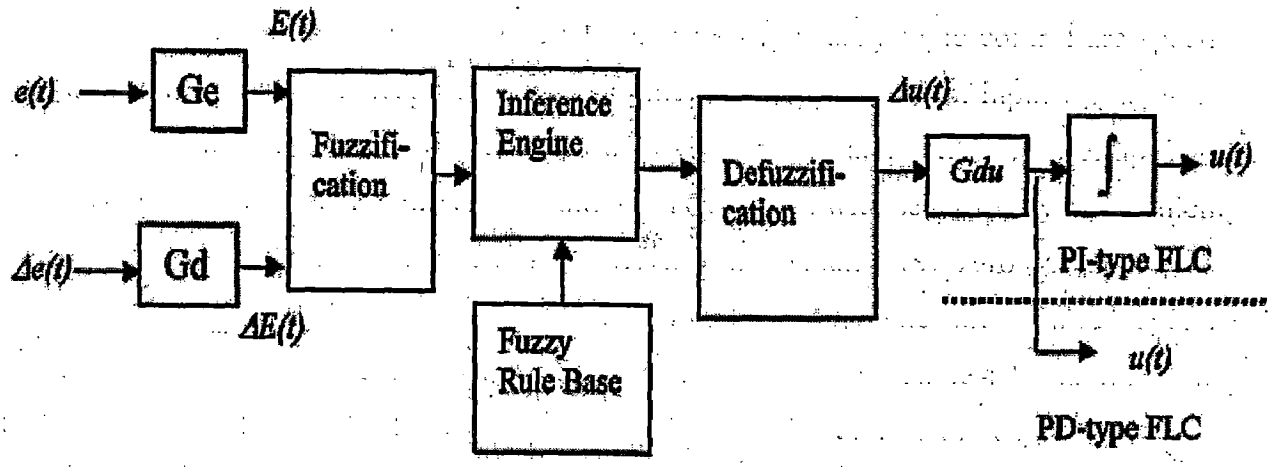

Fig. 4.5. Block diagram of a PI-type and PD-type fuzzy logic controllers.

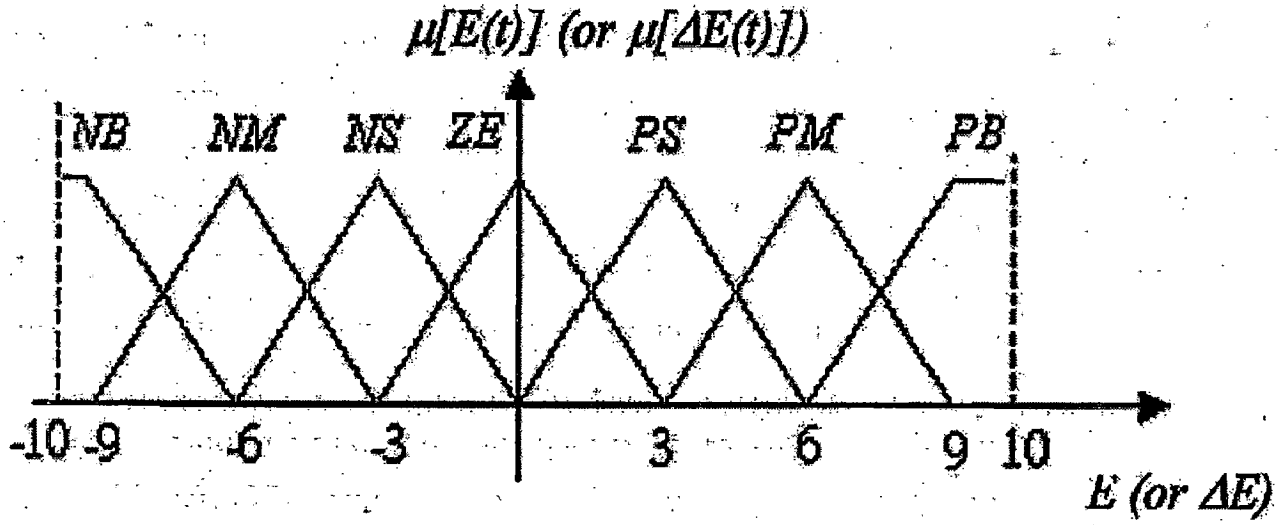

Fig.4.6 Membership function for input variables.

Table 4.1 Linguistic rule for PI type fuzzy logic controller

ce\e	NB	NM	NS	ZE	PS	PM	PB
NB	NB	NB	NB	NB	NM	NS	ZE
NM	NB	NB	NB	NM	NS	ZE	PS
NS	NB	NB	NM	NS	ZE	PS	PM
ZE	NB	NM	NS	ZE	PS	PM	PB
PS	NM	NS	ZE	PS	PM	PB	PB
PM	NS	ZE	PS	PM	PB	PB	PB
PB	ZE	PS	PM	PB	PB	PB	PB

Table 4.2 Linguistic rule for PD type fuzzy logic controller

ce\e	NB	NM	NS	ZE	PS	PM	PB
NB	NB	NB	NB	NB	NM	NS	ZE
NM	NB	NB	NB	NM	NS	ZE	PS
NS	NB	NB	NM	NS	ZE	PS	PM
ZE	NB	NM	NS	ZE	PS	PS	PS
PS	NM	NS	ZE	PS	PM	PB	PB
PM	NS	ZE	PS	PM	PB	PB	PB
PB	ZE	PS	PM	PB	PB	PB	PB

4.4.1 Hybrid fuzzy controller

Although fuzzy logic controller is robust to load disturbance, it has significant steady state error as compared with that for conventional proportional-integral controller. A new hybrid fuzz controller is presented to cope with this issue. Fig. 4.7 shows the block diagram of the presented hybrid fuzzy controller.

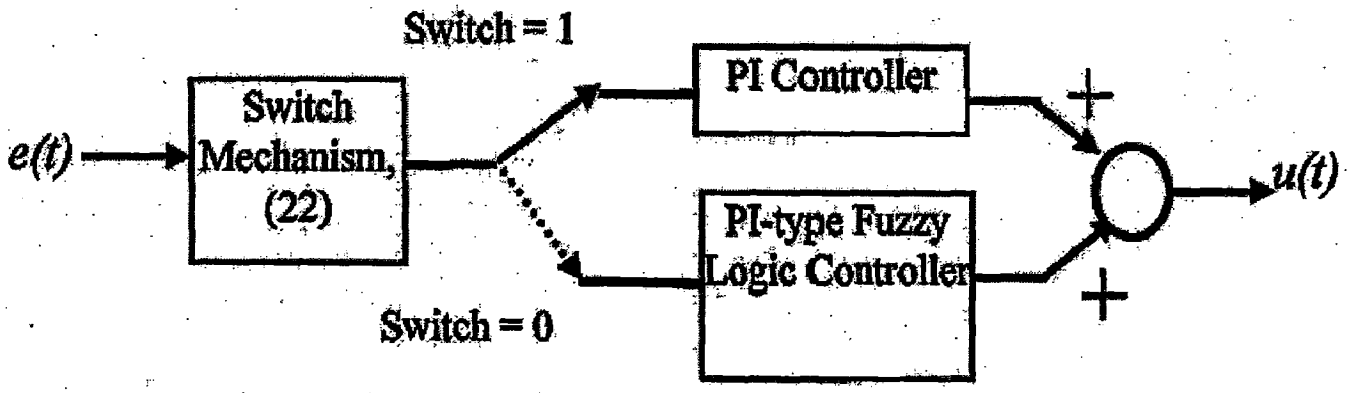

Fig. 4.7. Block diagram of hybrid fuzzy controller.

As shown in Fig. 4.7, the controller consists of PI control law, PI-type fuzzy control law and a simple switching mechanism. The switching mechanism changes the control law adaptively and thereby achieving high performance control under both transient and steady states.

The threshold value for switching control, 10 rpm, is selected to be slightly greater than the maximum value of steady state error for PI-type fuzzy logic controller alone. The threshold value depends upon the PI-type fuzzy logic controller as well as sampling frequency of controller. As the sampling frequency increases, this value decreases since the steady error of PI-type fuzzy logic controller decreases.

To highlight the merits of the presented hybrid fuzzy logic controller, a controller consists of PD-type fuzzy logic control and integral control is also presented. Fig. 4.8 shows the block diagram of the controller.As shown in Fig. 4.8, I-controller actuates

under steady state to reduce the steady state error, and only PD-type fuzzy logic control is active under transient state.

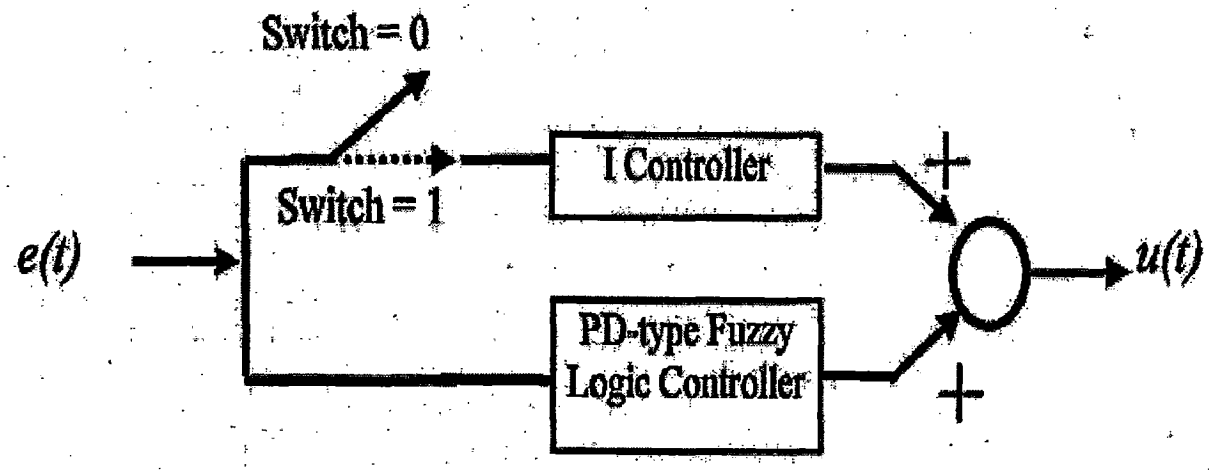

Fig. 4.8. Block diagram of a PD + I controller, PD-type fuzzy logic control plus Integral control.

4.5 Simulink Model

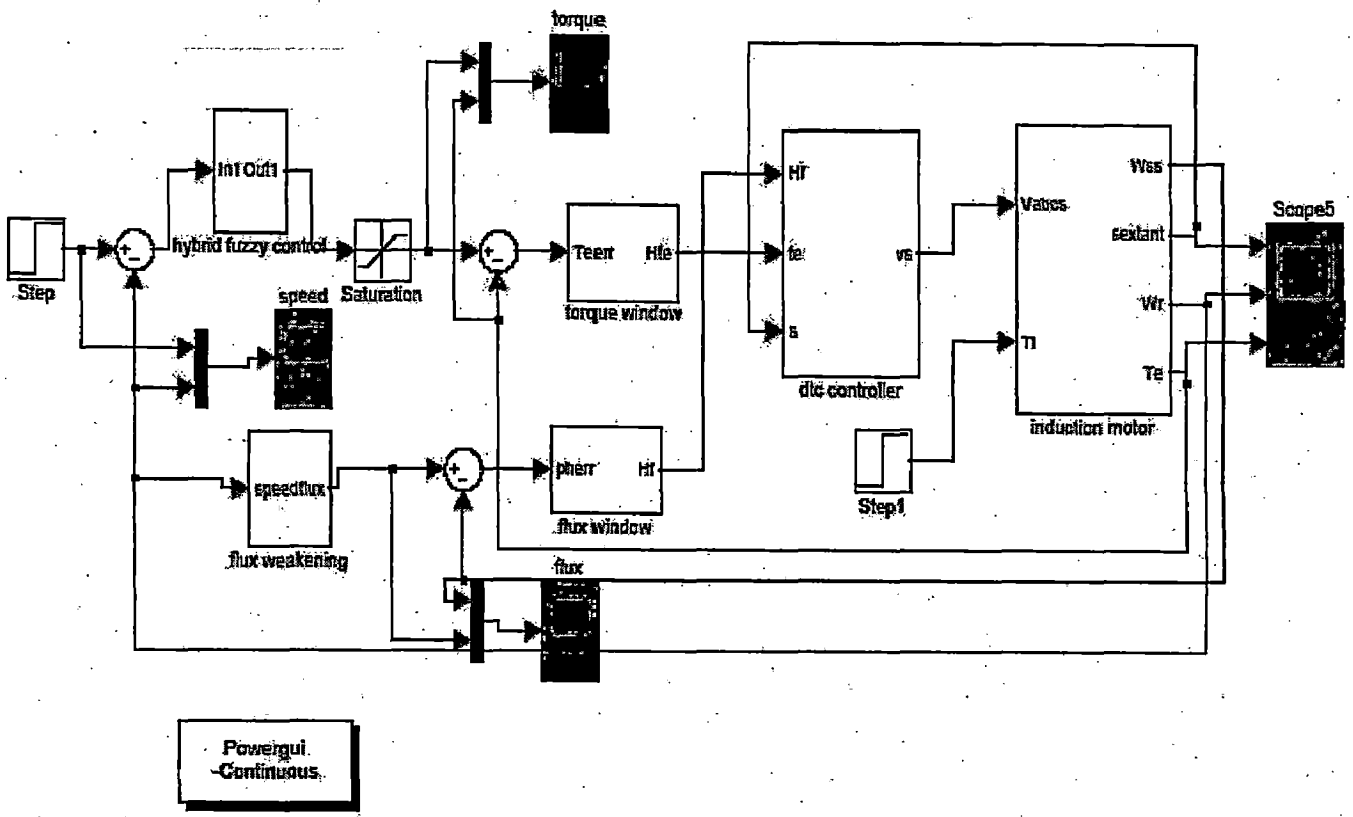

Fig 4.9 Simulink model of Hybrid fuzzy controller for DTC

4.6 Simulation results and discussion

A new hybrid fuzzy controller for direct torque control (DTC) induction motor drives is simulated. The newly developed hybrid fuzzy control law consists of proportional-integral (PI) control at steady state, PI-type fuzzy logic control at transient state, and a simple switching mechanism between steady and transient states, to achieve satisfied performance under steady and transient conditions. The features of the presented new hybrid fuzzy controller will be highlighted by comparing the performance of various control approaches, including PI control, PI-type fuzzy logic control (FLC), proportional-derivative (PD) type FLC, and combination of PD-type FLC and I control, for DTC-based induction motor drives. The problems and conclusions of these controllers will be demonstrated by simulation results are shown below. It will be shown that the presented induction motor drive is with fast tracking capability, less steady state error, and robust to load disturbance while not resorting to complicated control method or adaptive tuning mechanism.

The specification of induction motor is shown in the Appendix-A. The parameters of PI controller are determined by simulation such that there is no overshoot at 900 rpm for step response, no load. Therefore these parameters are selected to achieve fast response. Similarly, the parameters for PI-type FLC, PD-type FLC, PD-type FLC+I control, and hybrid FLC, are derived by simulation.

The below simulation results are obtained for speed reference 1200 rpm and 30% load impacted at t= 1 sec.

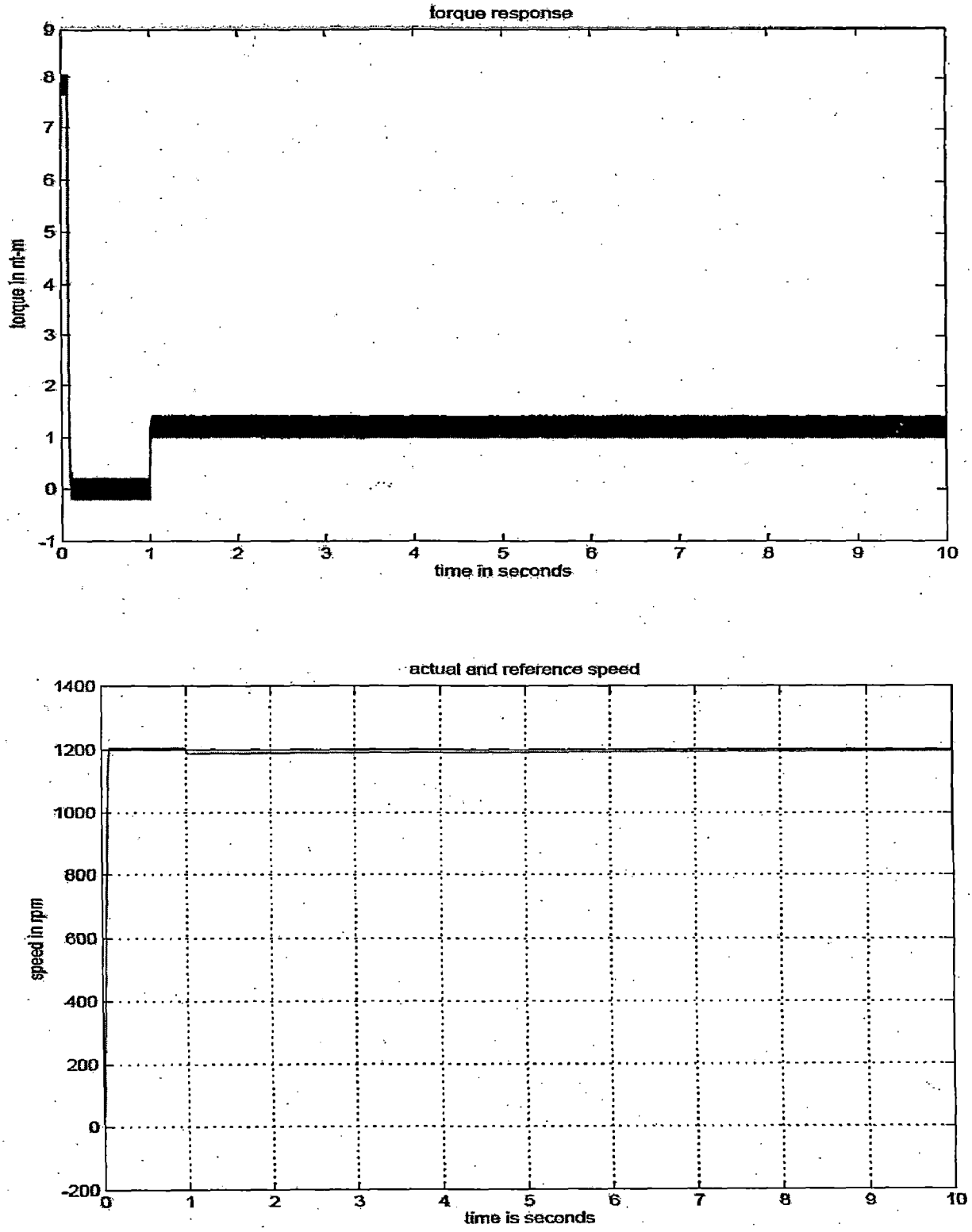

Fig 4.10 Torque and Speed response for PI control

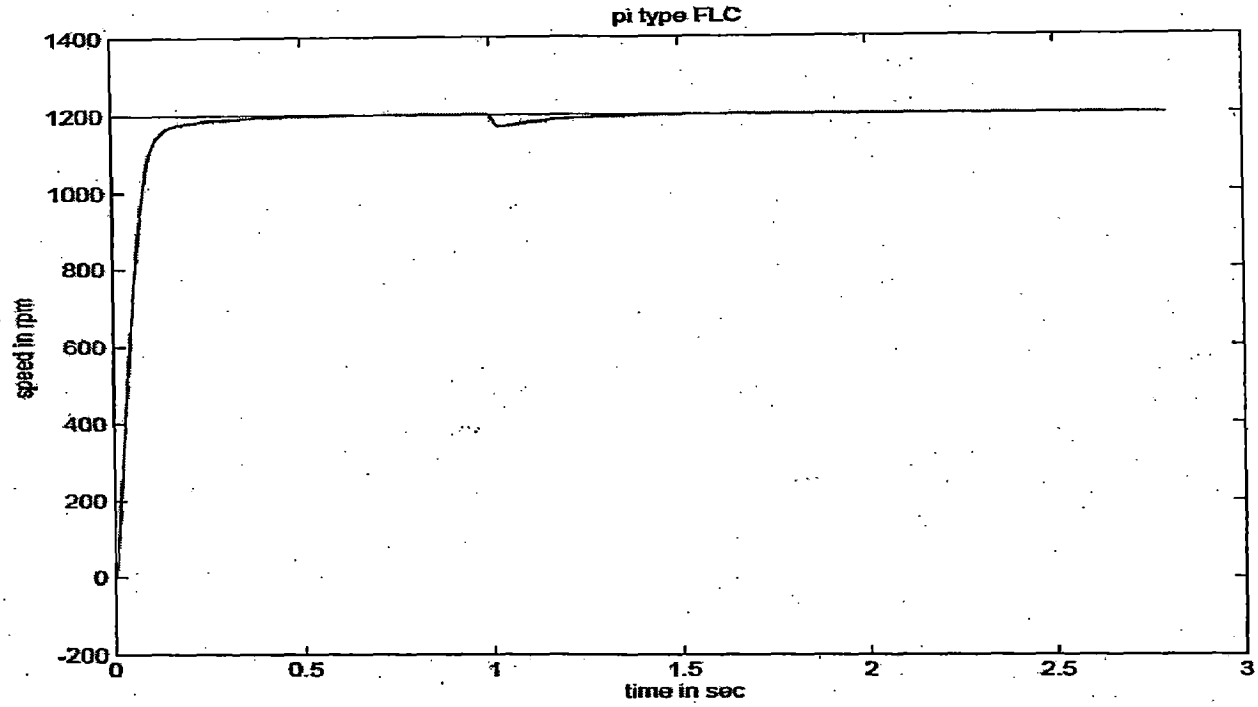

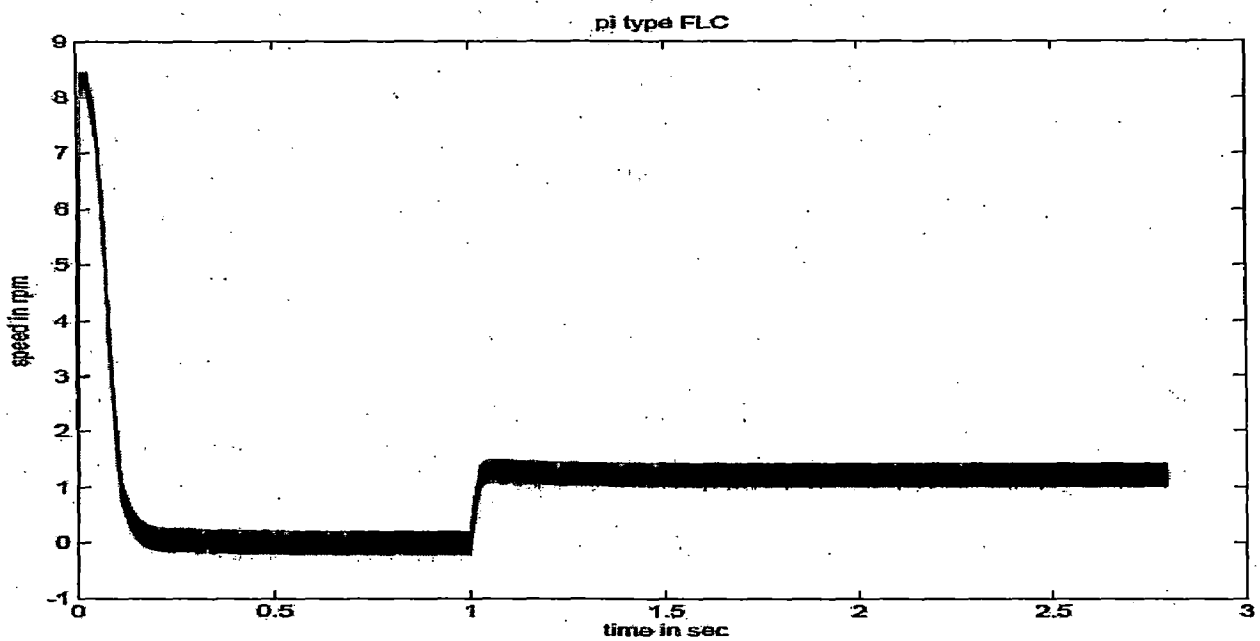

Fig 4.11 Torque and Speed response for PI type fuzzy control

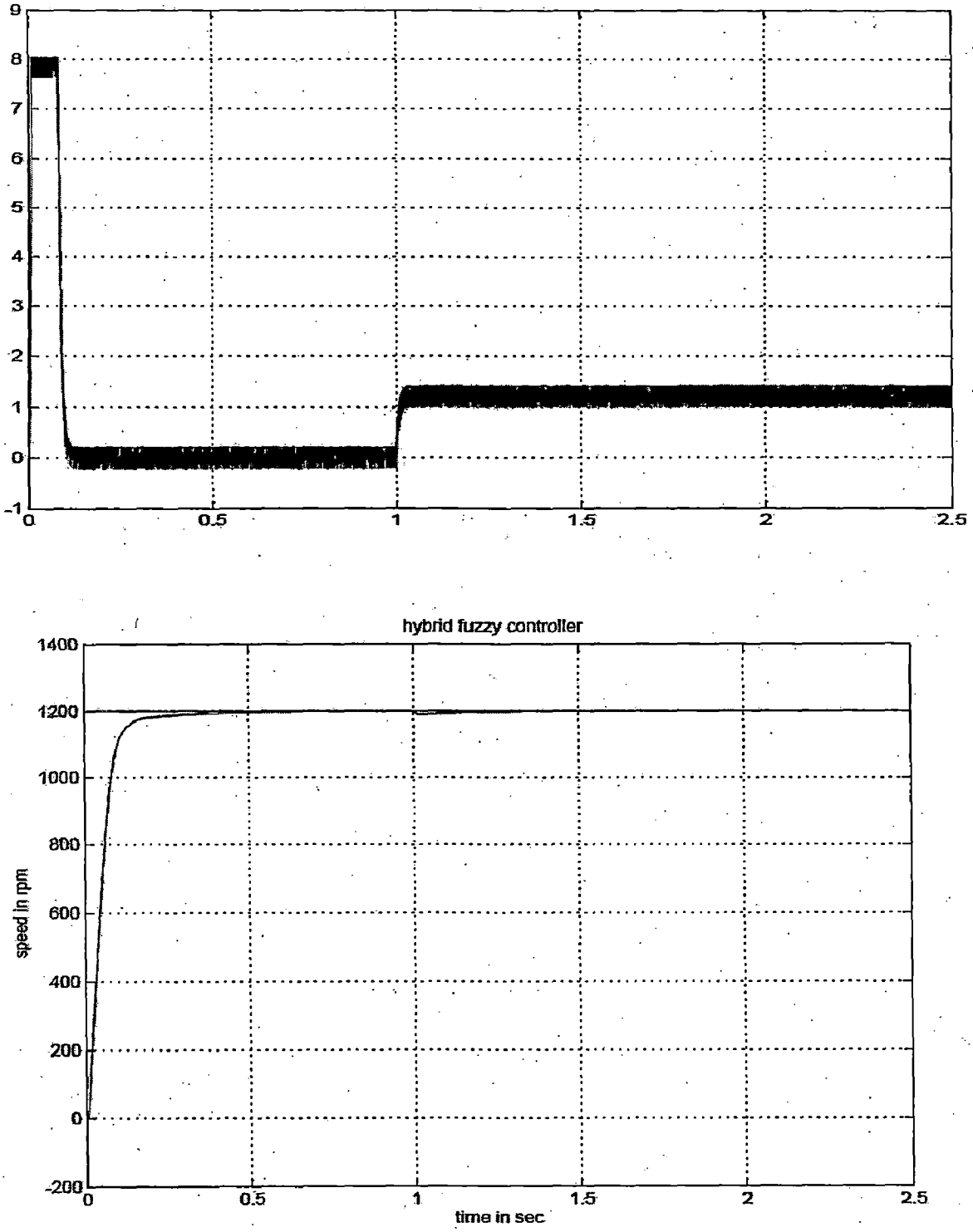

Fig 4.12 Torque and Speed response for hybrid fuzzy logic control

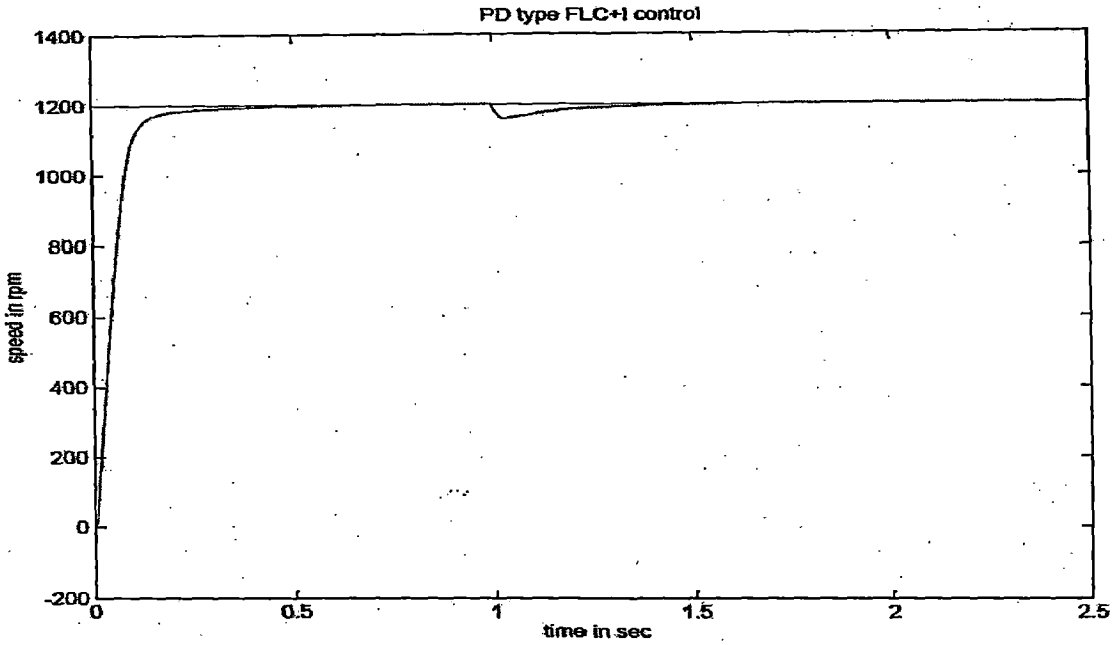

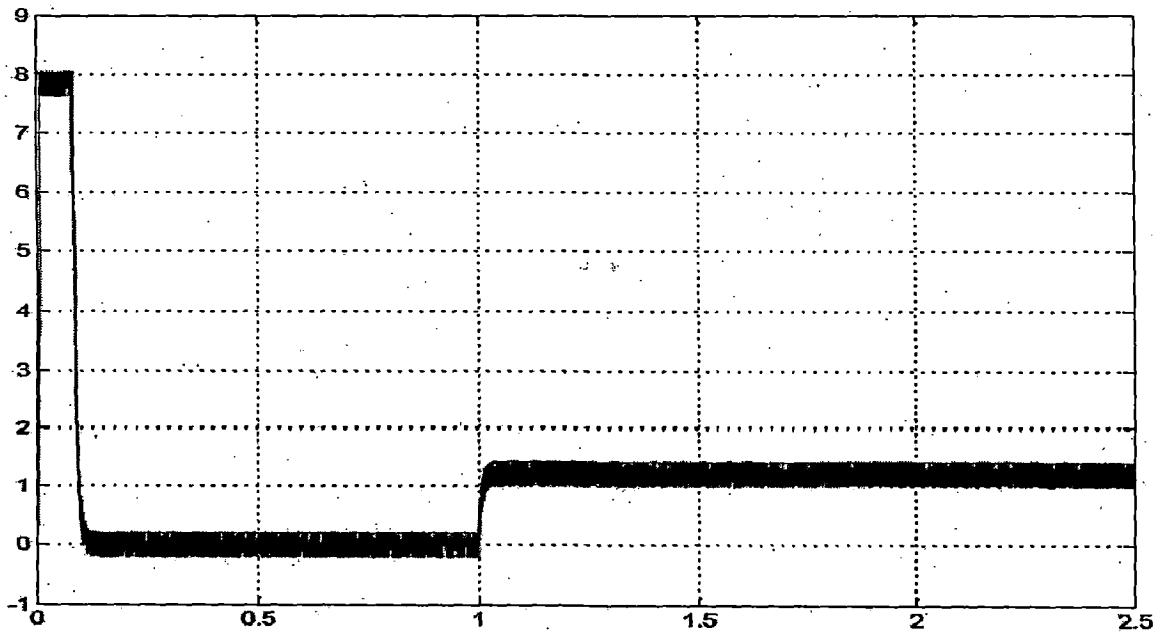

Fig 4.13 Speed response for PD type fuzzy logic control + I control

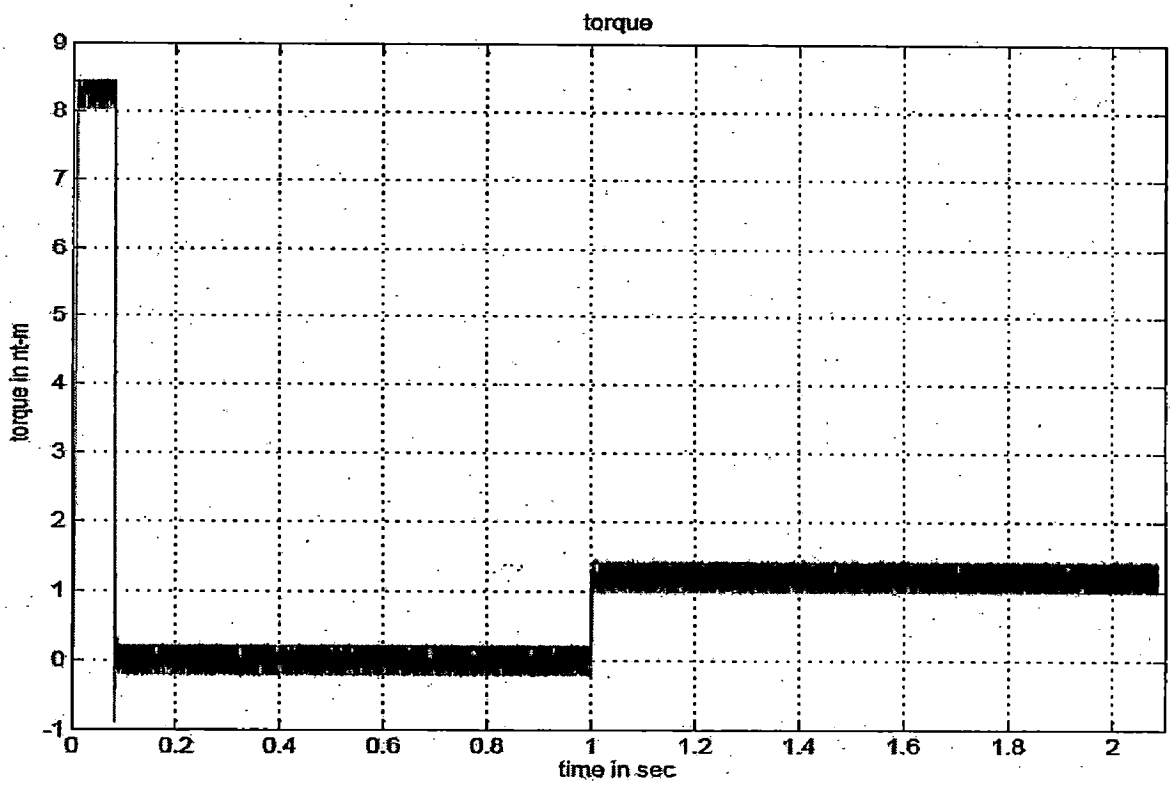

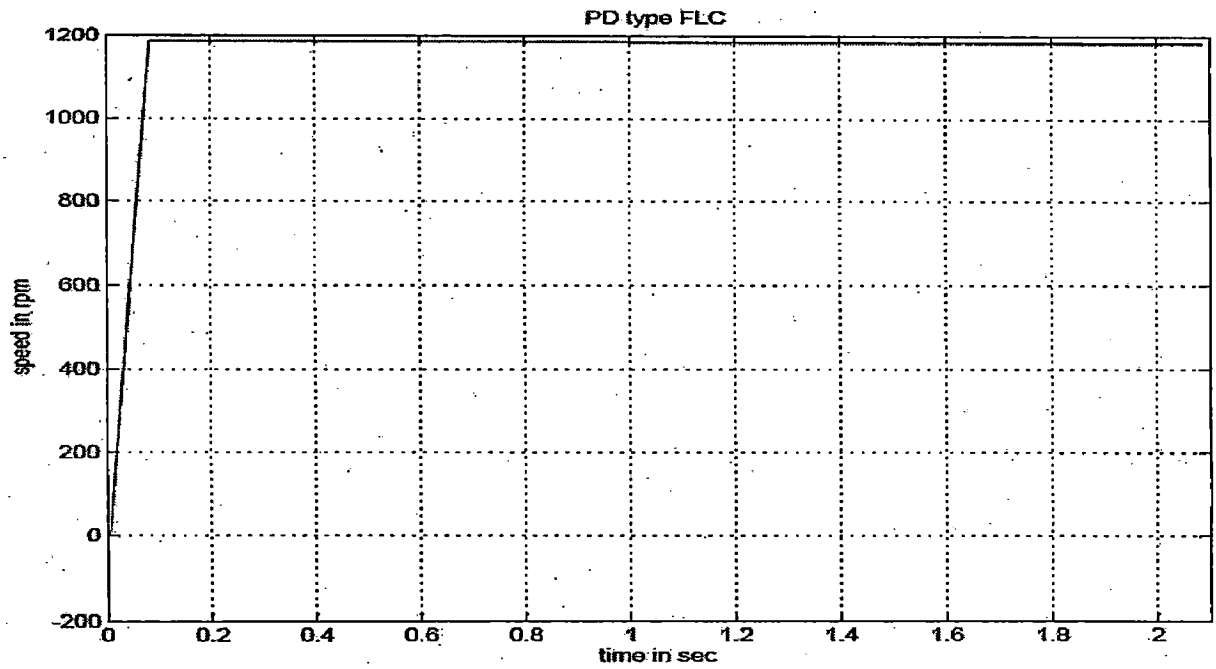

Fig 4.14 Speed response for PD type fuzzy logic control

A few remarks can be derived from the simulation results and are as follows.

1) Since conventional PI control is with one degree of freedom for control, the associated system achieves fast response; however it is not robust to load disturbance; see Fig. 4.10 and 4.13.

2) PD-type fuzzy control does not have integral mechanism, the associated system is with significant steady state error; see Fig. 4.14.

3) In contrast, for the PD-type FLC with I control, the associated steady state error converges as shown in Fig. 4.13.

4) PI-type fuzzy control and new hybrid fuzzy control are nonlinear control laws and with the integral mechanism the associated system is both robust to load disturbance and also with less steady state error, see Fig. 4.11 and 4.12.

Comparison results derived from the simulation can be summarized in Table 4.3, which shows that the hybrid fuzzy logic controller is superior to the others regarding to the steady state error, tracking performance, and load disturbance rejection.

Table 4.3

Comparison results of various types of controllers

Rank	Steady state error	Tracking performance	Disturbance rejection
1	Hybrid FLC	Hybrid FLC PI type FLC	PI type FLC Hybrid FLC
2	PD type FLC+ I control	PD type FLC+ I control	PD type FLC+ I control
3	PI type FLC	PI controller	PI controller
4	PI controller	PD type FLC	PD type FLC
5	PD type FLC		

4.7 Conclusion

This chapter contributes to the description of fuzzy controller structure and the presentation of a hybrid fuzzy controller for a DTC-based induction motor drive. The hybrid fuzzy controller reduces the steady state error as compared with PI-type fuzzy logic controller (FLC), while keeping the merits of PI-type FLC. Simulation results confirm that the presented controller for a DTC-based induction motor drive provides fast tracking capability, less steady state error, and robust to load disturbance, in very wide speed range.

Chapter 5

DSP Implementation of Direct Torque Control

5.1 Introduction

The applications of VLSI in motor control are getting more and more important and popular. In 1980s and 1990s, microprocessors, such as Intel's 8080, 8031, 8098, 80196 and Motorola's 68000, were mostly used in motor control. Recently, microcontroller are widely used in industry and the application of DSP and FPGA emerged in recent a couple of years. Both microcontrollers and DSPs are presently used in motor control; however, because of the real-time control algorithms that must be processed, the majority of these applications are driven by microcontrollers. This is partially due to engineers' comfort with microcontrollers and lack of familiarity with programming DSPs; however, DSPs are expected to surpass microcontrollers in the precision control of motors by 2003.

Embedded motor control applications are expected to reach 7.3 billion units by 2001 (*source: Motion Tech Trends*). Motor control is a significant, but often ignored, segment of embedded applications. Motor control applications span everything from washing machines to fans, hand-held power tools, and automotive window lift and traction control systems. In most of these applications there is a move away from analog motor control to precision digital control of motors. Digital control of motors permits a much more efficient operation of the motor, resulting in longer life, lower power dissipation, and a lower overall system cost.

In motor control area, the applications of DSP and microcontroller is for control of DC motor, brushless DC motor, brushless permanent magnet servo motor, AC induction motor (IM), and switched reluctance motors. In this thesis, a three phase IM (SQIM) is used for adjustable speed control because it is widely used in industrial applications.

The theoretical study of the direct torque control for induction motor drive and simulation results are presented along with their discussion in previous chapters. It can be observed that the simulation results are well in agreement with theoretical studies. This chapter deals with the implementation aspects of the conventional direct torque control technique. Innovative integration sbc6711 DSP board is used for the implementation of the drive system.

5.2 DTC Induction Motor Drive Architecture

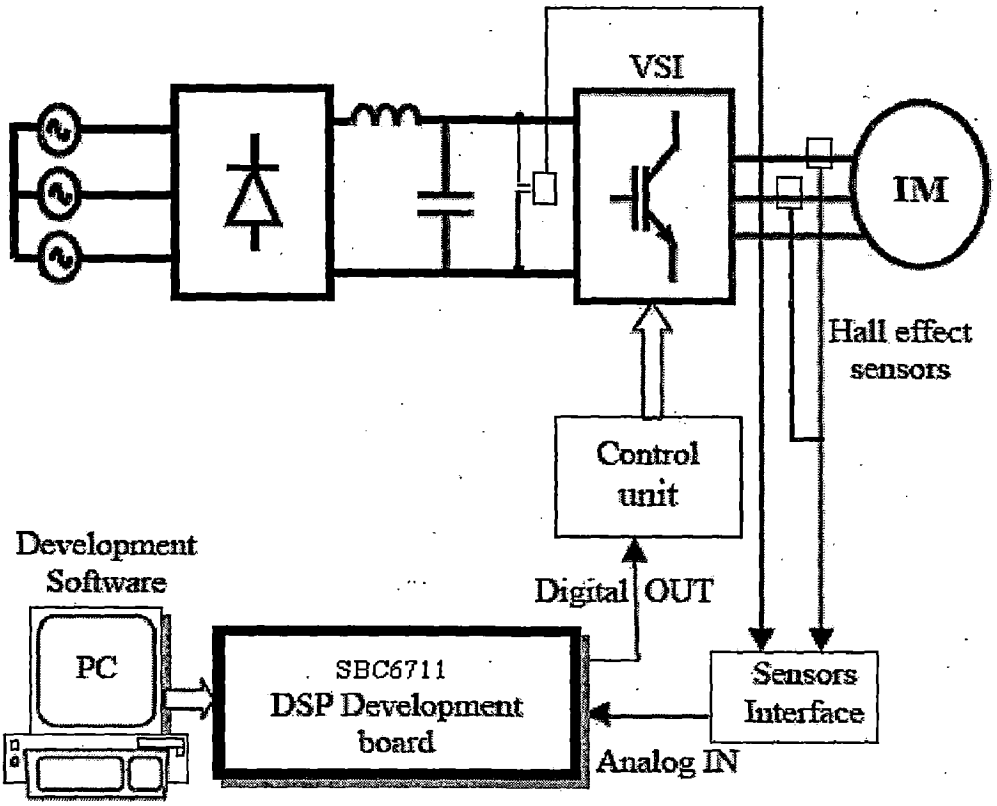

Fig 5.1 Experimental set-up of DTC induction motor drive

The realization of a direct torque controlled induction motor drive can be divided into two parts

- Hardware development
- Software development using SBC6711 DSP Development board

5.3 Hardware development

The system hardware can be divided in the following blocks.

- Power circuit
- Pulse amplification and isolation circuit
- AC current measurement circuit
- DC voltage measurement circuit
- Power supplies
- Circuit protection
- Delay circuit

5.3.1 Power Circuit

Figure5.2 shows the power circuit of the PWM VSI inverter. It consists of six IGBT switches. Each IGBT switch is used in the circuit consists of an inbuilt anti parallel free wheeling diode. No forced commutation circuits are required for IGBT's because these are self commutated devices (they turn on when the gate signal is high and turn of when the gate signal is low). An RCD (resistor, capacitor and diode) turn-off circuit is connected to protect the circuit against high dv/dt and is protected against power voltage by connecting MOV (Metal Oxide Varistor).

Insulated gate bipolar transistors (IGBT's) are widely used in switching power conversion applications because of their distinctive advantages, such as easiness in drive and high frequency switching capability. The performance of IGBT's has been continuously improved, and the latest IGBT's can be operated at 10–20 KHz without including any snubber circuit. Moreover, IGBT's are replacing MOSFET's for the several or several tens of kilowatts power range applications since IGBT's can handle higher voltage and power with higher power density and lower cost compared to MOSFET's. The maximum operating frequency of IGBT's, however, is limited to 20–30 KHz because of their tail-current characteristic. To operate IGBT's at high switching frequencies, it is required to reduce the turn-off switching loss. Zero-voltage switching (ZVS) with a substantial external snubber capacitor or zero current switching (ZCS) can be a solution. The ZCS, however, is deemed more effective since the minority carrier is swept out before turning off.

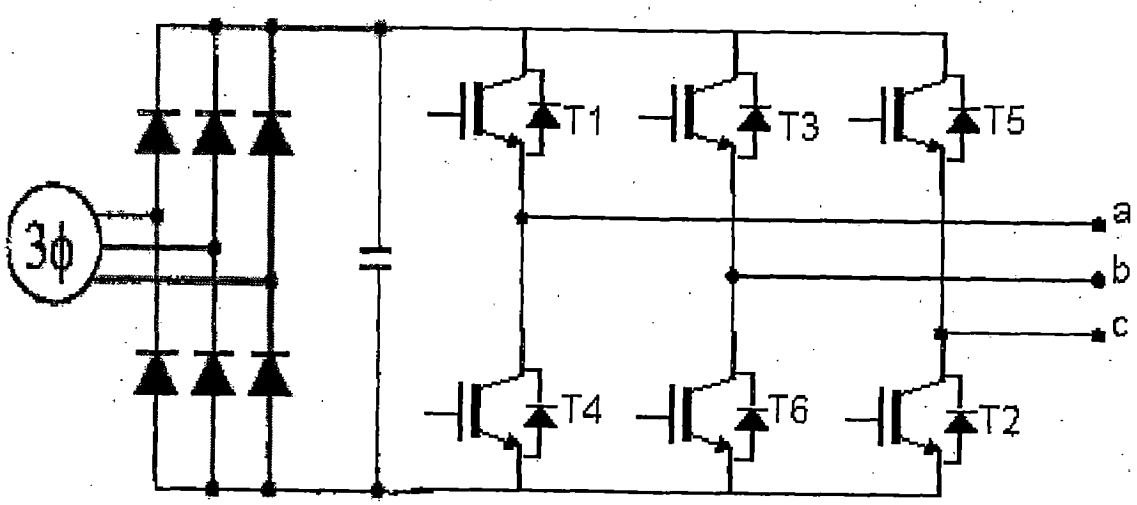

Figure 5.2: PWM VSI inverter.

5.3.2 Pulse Amplification and Isolation Circuit

The pulse amplification and isolation circuit for IGBT is shown in figure 5.3. The opto-coupler (MCT-2E) provides the necessary isolation between the low voltage isolation circuit and high voltage power circuit .The pulse amplification is provided by the output amplifier transistor 2N222.

When the input gating pulse is at +5V level, the transistor saturates, the LED conducts and the light emitted by it falls on the base of phototransistor, thus forming its base drive. The output transistor thus receive no base drive and, therefore remains in cut-off state and a +12 v pulse (amplified) appears across it's collector terminal (w.r.t.ground). When the input gating pulse reaches the ground level (0V), the input switching transistor goes into the cut-off state and LED remains off, thus emitting no light and therefore a photo transistor of the opto-coupler receives no base drive and, therefore remains in cut-off state .A sufficient base drive now applies across the base of the output amplifier transistor .it goes into the saturation state and hence the output falls to ground level. Therefore circuit provides proper amplification and isolation. Further, since slightest spike above 20v can damage the IGBT, a 12 V zener diode IC connected across the output of isolation circuit .It clamps the triggering voltage at 12 V.

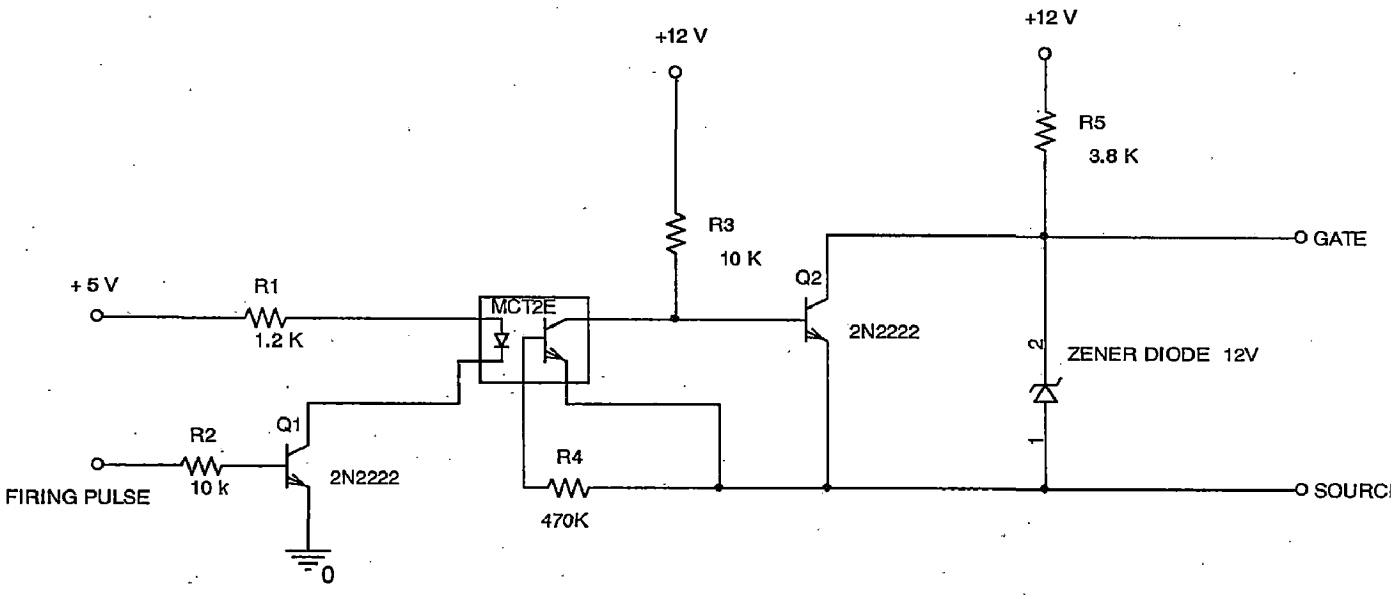

Figure 5.3: Pulse Amplification and Isolation Circuit

5.3.3 Power Supplies

DC regulated power supplies (+12v, -12v, +5v) are required for providing biasing to various transistors, IC's etc. The circuit diagram for various dc regulated power supplies are shown in *fig 5.4*; in it the single phase ac voltage is stepped down to 12V and then rectified using a diode bridge rectifier. A capacitor of 1000μf, 50volts is connected at the output of the bridge rectifier for smoothening out the ripples in the rectified DC regulated voltages. IC voltage regulators are used for regulating the voltages on load also. Different IC voltage regulator that are used are; 7812 for +12V, 7912 for -12V and 7805 for +5V. A capacitor of 100μf, 25V capacitor is connected at the output of the IC voltage regulator of each supply for obtaining the constant and ripple free DC voltage.

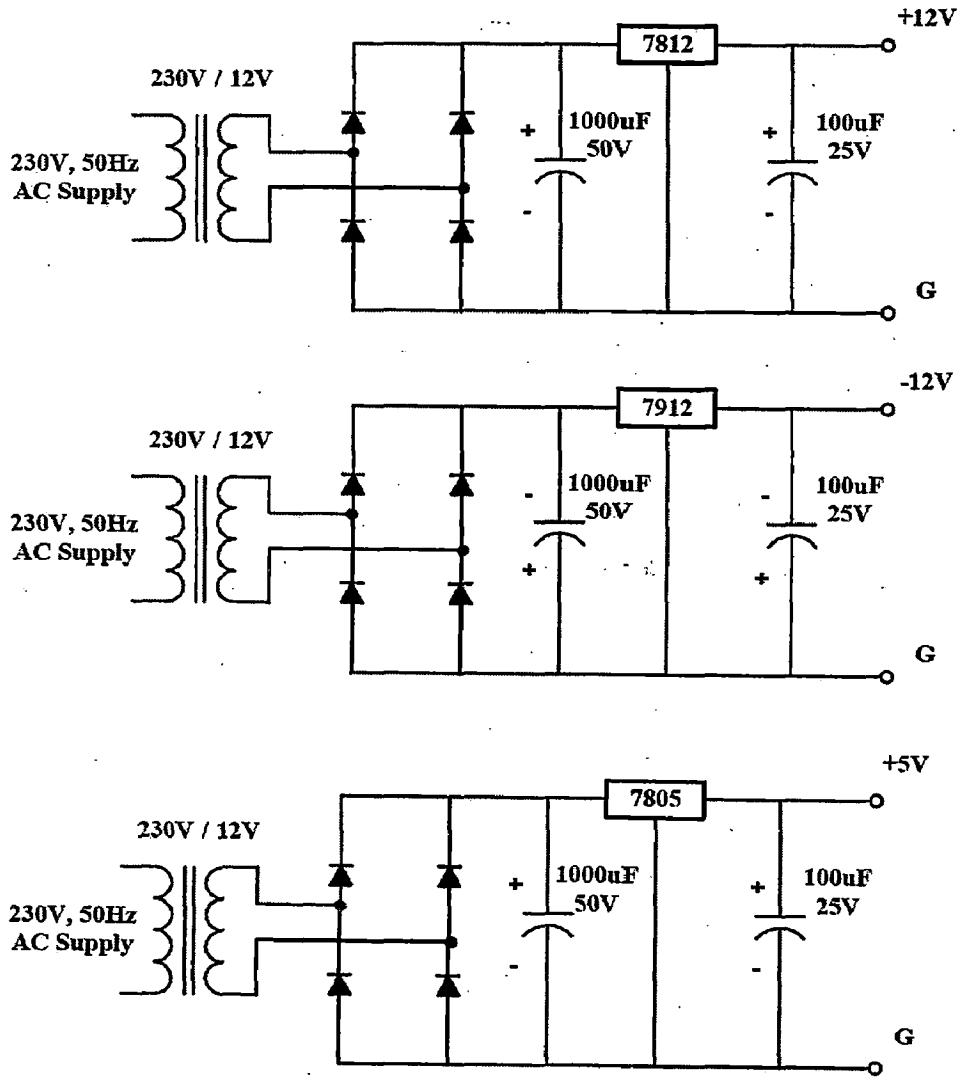

Figure 5.4: Circuit Diagrams for IC regulated Power Supplies

5.3.4 Circuit Protection

(A) Snubber Circuit for IGBT protection

IGBTs are increasingly the switch of the choice for pwm inverters for used in power electronics application, because of hard switching applications and lower conduction losses. Most of the IGBTs are used in hard switching applications up to 20 kHz, beyond that switching losses in IGBTs becomes very significant.

Switching such high currents in short time gives rise to voltage transients that could exceed the rating of IGBT especially if the bus voltage is close to the IGBT's rating. Snubbers are therefore needed to protect the switch from transients. Snubber circuit for IGBT as shown in Figure

Snubbers are employed to:

- Limit di/dt or dv/dt.
- Transfer power dissipation from the switch to a resistor.
- Reduce total switched losses.

RCD snubbers are typically used in high current application. The operation of RCD snubber is as fallows: The turn-off makes the voltage zero at the instant the IGBT turn-off. At turn-off, the device current is transfer through the diode D_s and the voltage across the device builds up. At the turn-on, the capacitor C_s discharges through the resistor R_s. The capacitor energy is dissipated in the resistor R_s at turn-on.

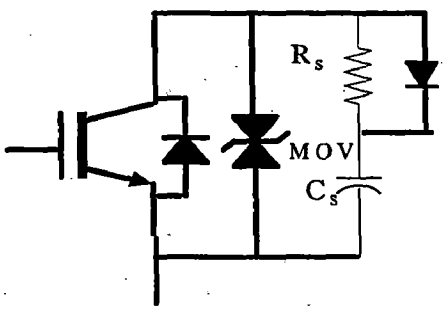

Figure 5.5. Snubber circuit of IGBT

(B) Over voltage protection

An additional protective device Metal-oxide-varistor (MOV) is used across each device to provide protection against the over voltages. MOV acts as a back-to-back zener and bypass the transient over voltage across the device. In general the voltage rating of MOV is kept equal are below the rating of IGBT to protect it from the over voltages.

(C) **Over heating protection**

Due to the ohmic resistance of IGBT and anti - parallel diode, I^2 R loss takes place as a result of the current conduction, which results the heat generation, thus raising the device temperature, this may be large enough to destroy the device. To keep device temperature within the permissible limits, all IGBTs are mounted on aluminum heat sink and is then dissipated to the atmosphere.

(D) **Short circuit protection**

The thermal capacity of semiconductor device is small. A surge current due to a short circuit may rise device temperature much above its permissible temperature rise limit which may instantaneously damage the device. Hence, the short circuit protection is provided by fast acting fuses in series with each supply line.

5.3.5 Current Sensor Circuit

Closed loop Hall Effect current transducer is used to sense the current. The transducer use the ampere turn compensation method to enable the measurement of current from DC to high frequency with an ability to follow rapidly changing level or wave shapes. The application of primary current (Ip) causes a change in flux in the air gap. This in turn produces a change in output from hall element away from the steady state condition. This output is amplified to produce a current (Is), which is passed through a secondary winding causing a magnetizing force to oppose that of the primary current, thereby reducing the air gap flux. The secondary current is increased until the flux is reduced to zero. At this point the hall element output will return increased until the flux is reduced to zero. At this point the hall element output will return to steady state condition and the ampere turn product of secondary circuit will match that of primary. The scaling of the current measurement is such that for 1 amp current at the input of the circuit their will be 1 volt voltage at the output of the circuit.

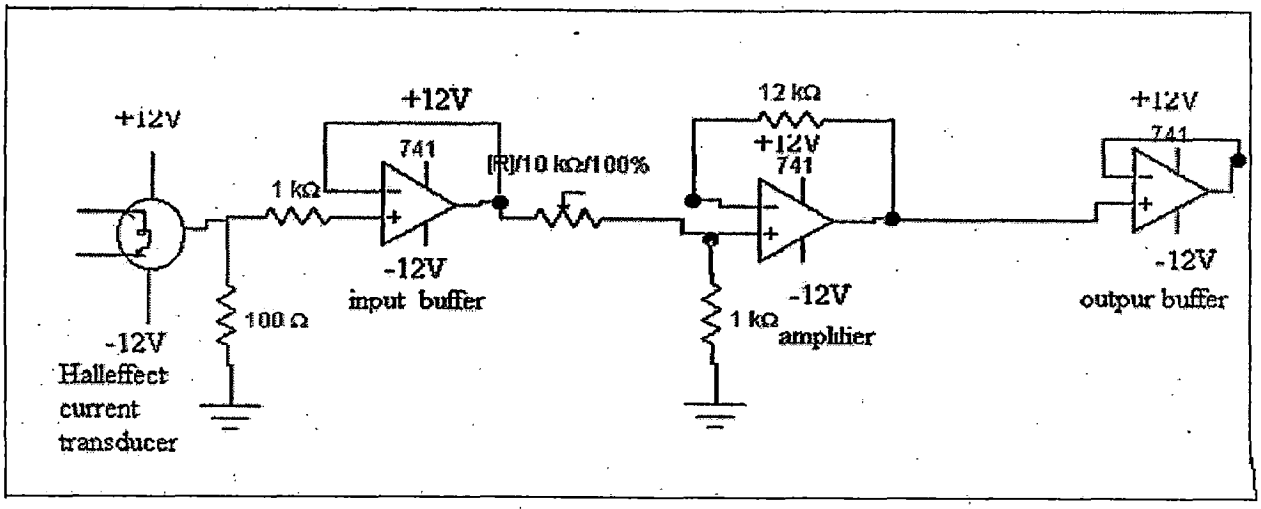

Figure 5.6 Current sensor circuit

The current that passes through the secondary winding is the output current. The transformation ratio is calculated by the standard current transformation equation

$$N_pI_p = N_sI_s$$

Where

N_p= primary current, Ns= secondary current

I_p= primary current, Is = secondary current.

5.3.6 DC Link Voltage Sensing Circuit

The dc output voltage of the capacitor is sensed through isolation amplifier AD202 for the voltage control of the inverter. We are using AD202 of DIP configuration. AD202 provide the total galvanic isolation between input and output stages of the isolation amplifier through the use of internal transformer coupling. It gives a bi-polar output voltage +5v, adjustable gain range from 1v/v to 100v/v, +0.025% max non-linearity, 130db of CMR and 75mw of power consumption. Circuit diagram is shown in *fig5.6*. In the shown figure output amplifier is made using op-amp which will be helpful in calibration. The transient response will deteriorate by using passive filter at the input side of AD202; but to reduce the ripples in measurement and control purpose it cannot be avoided.

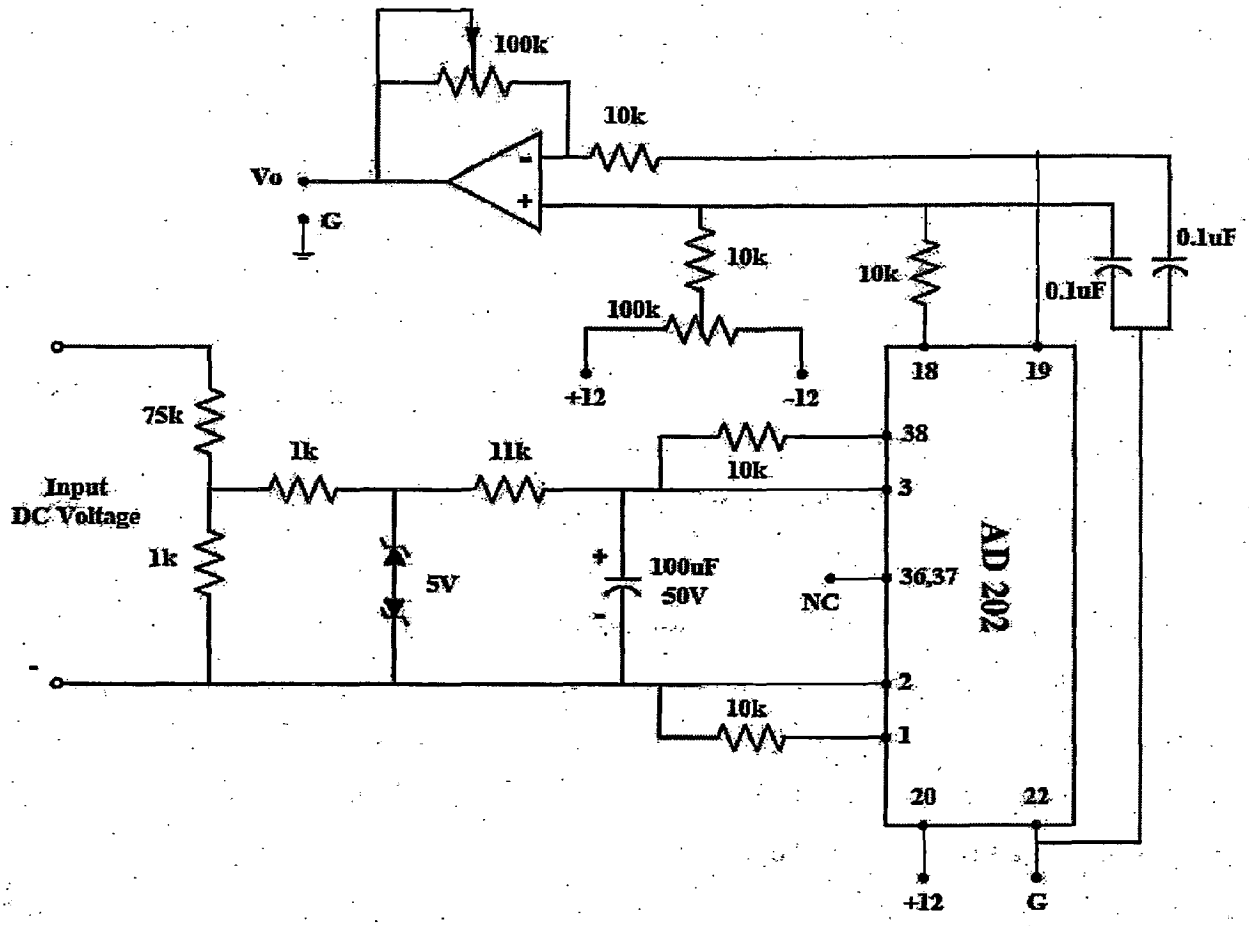

Figure 5.7 Circuit Diagram used for DC-Link Voltage Sensing and Calibration using AD 202.

5.3.7. Delay Circuit

Values of R and C are chosen to provide a delay around 5μs i.e. larger than turn off transition time of the IGBT. The switching signals from the lockout delay circuit are sent to the pulse amplification and isolation circuit.

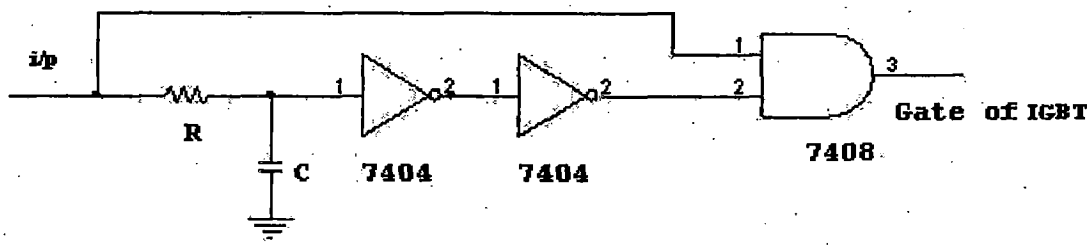

Fig.5.8. Delay Circuit

This circuit provides 5μS delay and R=5kΩ and C=0.001μF

5.4 Software Development using SBC6711 DSP Development board

Implementation of advanced motor drive systems requires the following features from a typical motor controller

- Capability of generating multiple high frequency, high-resolution PWM waveforms.
- Fast processing to implement advanced algorithms to minimize torque ripple, on line parameter adaptation, precise speed control etc.
- Implementing multiple features using the same controller (motor control, power factor correction, communication, etc.)
- Making the complete implementation as simple as possible (reduced component count, simple board layout and manufacturing etc.)
- Implementing a flexible solution so that future modification can be realized by changing software instead of redesigning a separate hardware platform.

A new class of DSP controllers has addressed these issues effectively. These controllers provide the computational capability of a DSP core and integrate useful peripherals on chip to reduce the total chip count. The TI's DSP2000 family controller is becoming a viable option for even the most cost sensitive applications like appliances, HVAC systems etc. In addition to traditional mathematical functions like digital filter, FFT implementations, this new class of DSPs integrates all the important power electronics peripherals to simplify the overall system implementation. This integration lowers over all part count of the system and reduces the board size. In my thesis the DSP controller board SBC6711 from Innovative Integration is used for motor control.

5.4.1 SBC6711 Hardware Functions

The SBC6711 is a stand alone digital signal processor (DSP) card based around the Texas Instruments TMS320C6711 processor. Implementing a modular I/O expansion system, the SBC6711 is particularly well suited to data acquisition and control tasks. The SBC6711 is also supported by a collection of I/O bus function cards, which provide hardware interfacing to real-world equipment.

The SBC6711's features include

- TMS320C6711 digital signal processor.
- External one wait-state SDRAM memory pools.
- FLASH memory.

- FIFO Port communications expansion capability.
- OMNIBUS I/O expansion compatible (two available slots).
- 32 bits of digital I/O.
- Synclink and clocklink trigger and clock sharing bus.
- Universal Serial Bus (USB) port.
- JTAG hardware emulation support.

The following figure gives a block diagram of the SBC6711.

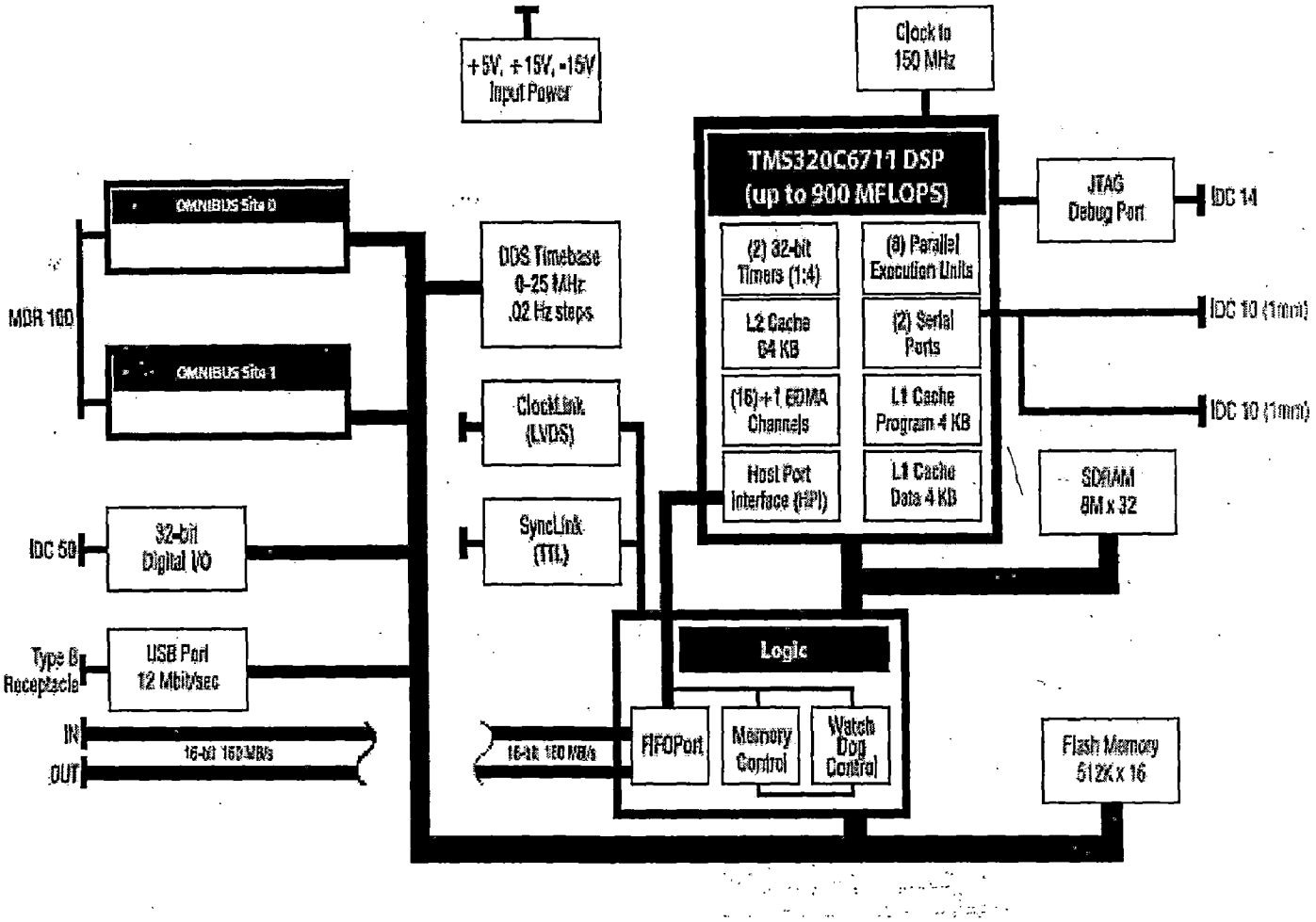

Fig 5.9 SBC6711 Block Diagram

A4D4 OMNIBUS Module

The A4D4 OMNIBUS module provides the target card processor with four channels of high speed 200 kHz, 16-bit resolution analog input to digital output conversion (A/D) per module slot. In addition, four channels of high speed 200 kHz, 16-bit

resolution digital input to analog output conversion (D/A). The A4D4 has analog I/O that is tightly coupled with the DSP, making it well suited for controls systems, process monitoring, and data acquisition applications. The A4D4 module uses two pairs of Analog Devices AD976AA A/Ds with each channel having independent input six-pole anti-alias filters and programmable gain amplifiers provide for flexible input. While two pairs of Analog Devices AD7846 D/As with output amplifiers and independent channel filtering, gain, and trim, provides for high speed data output signals.

The four analog inputs on the A4D4 module are successive approximation type A/D converters, which allows for low data latency that is critical in control applications and multiplexed channel configurations. In addition, each A/D channel is calibrated for offset and gain errors allowing accurate measurements for a variety of applications. The converters may be triggered via hardware timer or software access and are capable of interrupting the target processor in interrupt driven applications. The TERM card may be purchased to expand each of the A/D input with a multiplexer for a total of 32 single-ended channels or 16 differential channels of input to each A4D4 module. The TERM card is controlled by the OMNIBUS host DSP card so that the channel indexing is under software control.

The following block diagrams has been provided to show the conceptual arrangement of the component circuitry featured of the board.

The A4D4/TERM library functions can be divided into several groups:

- Sample rate control.
- A/D control.
- D/A control.
- Interrupt selection.
- Identification read back

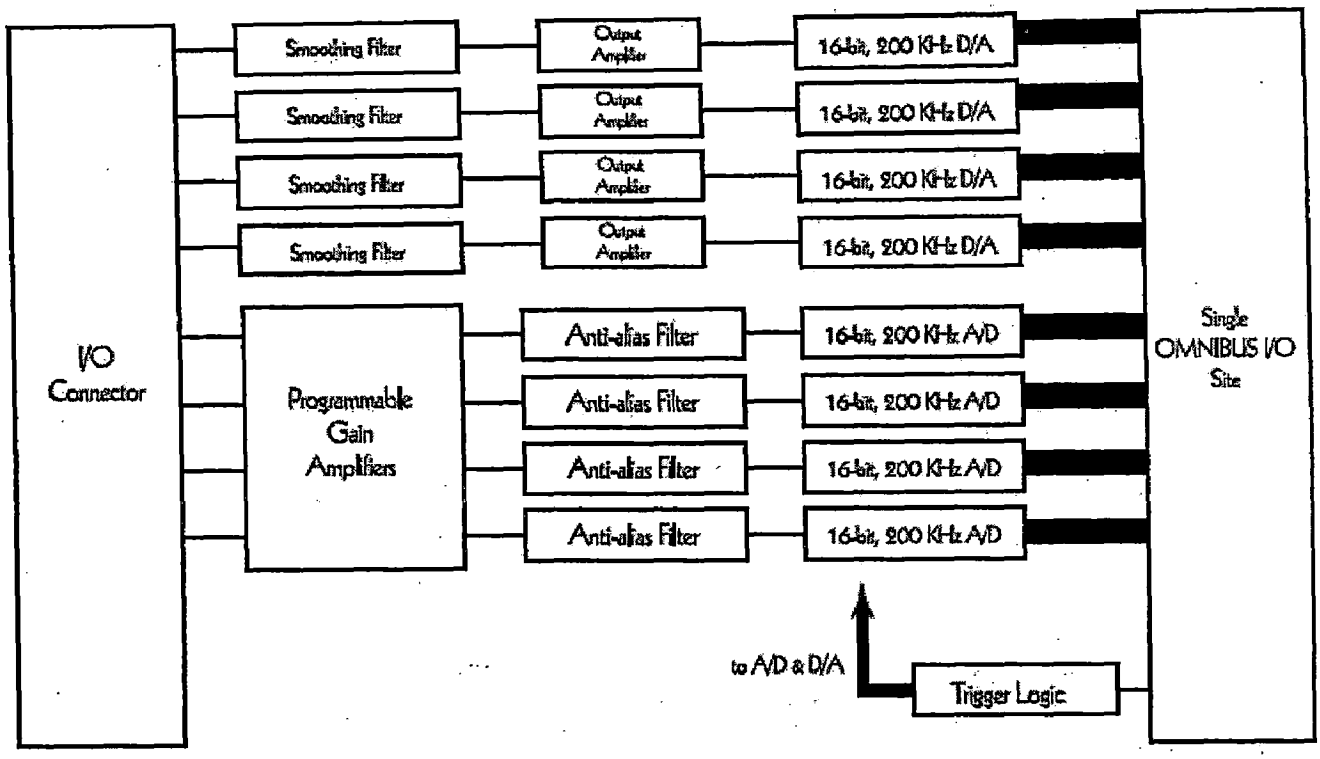

Fig 5.10 A4D4 Block Diagram

Analog Input

The analog to digital converters are 16-bit devices with a 5 us maximum conversion time (Analog Devices AD976A) capable of digitizing CD quality music, sensor outputs like thermocouples and accelerometers, and other demanding acquisition applications. Each A/D channel is an independent conversion path with independent filtering and input range. The default bipolar input range is +/-10V. The AD976A A/D converter is internally sampled prior to conversion and requires no external sample and hold circuitry. The ADC is self-timed and will typically convert in less than 5 us, which is the specified maximum conversion time for all conditions. The ADC also has its own internal precision voltage reference for accurate conversions. Do not use the reference output for any other device unless proper signal buffering is provided as this may adversely affect the conversion accuracy.

The A/D's are configured as pairs which read back with a single 32-bit read. Each 16-bit field within the readback value contains a single sample in two's-complement format. The devices may be read by a CPU read or by the DMA controllers.

Analog Output

Four channels of 16-bit instrumentation-grade digital-to-analog converters (D/A) are provided on the A4D4. The D/As are useful for analog signal outputs for both control and signal generation. Digital data is written to the D/As for output via a set of memory mapped locations. The data bus is connected to the D/As with each pair sharing a single load location with one device occupying the lower 16 bits of the bus and the other occupying the upper 16 bits. Data written to the D/A devices is in straight binary format, rather than two's complement. The inverting output stage of each D/A channel yields a [+10V ... -10V] output voltage for an input code range of [0..65535].

Digital I/O

The SBC6711 includes 32-bits of software programmable digital I/O for use in controlling digital instruments or acquiring digital inputs. The digital I/O port controls are mapped into memory space using two addresses: one to read/write the digital I/O data as a single 32-bit word, one for direction control and for each byte of the port and controlling the source of the clock edge used to latch input data into the digital I/O port register. The direction control register provides for software control of the drive direction of the port and the source of the input latch clock. The least significant four bits of the register control the four bytes available on the I/O port. Bit D0 sets the direction for the least significant eight bits if the port (port bits 0-7), D1 the next least significant bits (8-15), D2 the next least significant (16-23) and D3 the most significant (24-31).Each byte is individually controllable by writing a zero (to select output) or a one (to select input) to the respective bit in the direction control register. For example, if the value 0xC were written to the direction control register, bits 0-15 would act as inputs while bits 16-31 would act as outputs. All bytes default to input mode upon the board power-up or on reset.

Communications

RS232 Serial Port

The SBC6711 implements a single asynchronous serial port channel with RS232 drivers compatible with standard PC serial port interfaces. The serial port is implemented using a Texas Instruments TL16C750 UART and Maxim MAX3223 RS232 transceiver. The 16C750 external reset signal is automatically asserted on

power up and may be reasserted under software control via the SERIAL_RESET bit of the miscellaneous control register.

USB Port

A Universal Serial Bus (USB) compatible host interface port is included on the SBC6711 to support high data rate host communications requirements. Implemented using a ScanLogic SL811HST USB interface device, the port allows for communications on a USB network at up to 12 Mbits/sec (USB full speed bit rate). In-system real data rates will be determined by the USB data packet sizing, host bus rate and other limitations. Most systems can achieve from 4-8 Mbits/sec under Win2000 (Win98 is slower).The USB port supports USB specification 1.1 at 12 Mbit/sec or 1.5Mbit/sec data rates. Data rate is automatically sensed by the controller chip during the USB initialization. The SL811 provides an efficient dual-port memory interface between the DSP and serial engine with address auto-incrementing that allows the SBC6711 to achieve high data rates without unnecessary burden. The USB interface is accessed starting at address 0x90200000.

On-card memory

The SBC6711 has two types of external memory: synchronous DRAM (SDRAM), and flash EEPROM. The EEPROM memory is 512K x 16 (1Mbytes) and the SDRAM is organized as 8Mx32 (32 Mbytes). The flash EEPROM memory contains the SBC6711's start-up software. Shipped standard with Innovative's TALKER program installed for use with the SBC6711 Development Package, the EEPROM may be programmed with end user applications through the use of tools included in the Development Package. The EEPROM and boot process makes the SBC6711 a stand-alone processor board capable of remote control and data acquisition tasks. The EEPROM operates with several wait-states on the processor bus.

EEPROM memory is implemented on the SBC6711 with a single AMD 29F800 (compatible) flash device. In addition to its intended purpose as the boot device for application software, the 29F800 may also be used to store nonvolatile application-dependent data. The device is connected to the 'C6711 processor on the least significant sixteen bits of the processor bus, and responds to standard AMD programming sequences. The SBC6711 Development Package contains support software for erasing and programming the flash device.

The SDRAM memory provides a large, fast memory area for program and data storage. The 'C6711 has an advanced cache controller that is used to control the

SDRAM so that the programmer has a large virtual memory pool of very fast memory. The cache controller allows the SDRAM to operate at approximately 80% the efficiency of internal memory in many cases by caching instructions and data in on-chip memory for faster access. The 16 Mbyte SDRAM operates at one half the processor's bus rate, for a maximum throughput of 300 Mbytes/sec.

Power Supply

The SBC6711 processor board requires an off-board power supply capable of delivering three power supplies: +5V DC, +15V DC, and –15V DC. Power is delivered to the card via the main power connector. Innovative Integration supplies linear power supplies suitable for use with AC mains powered installations.

The software used for the system development is TI floating point C-compiler. The software code is written in code composer studio environment using c-language. After developing the c-code, it is converted into machine level code by using code composer studio. Here the terminal variables are can be sampled at high frequency. The optimized switching pattern which are selected based on the flux and torque are stored in lool-up table implemented using processor.

5.5Conclusion

In this chapter the implementation aspects of the conventional direct torque control for induction motor drive are discussed. Innovative integration sbc6711 DSP board is used for the implementation of the drive system. The fabrication of power circuit and the necessary sensing circuits are detailed.

Chapter 6

Conclusion and Future Scope

Conclusion

The presented work deals with the description of the principle of the direct torque controlled induction motor drive. The simulation and hardware implementation of the drive are discussed in detail. The simulation is implemented using MATLAB/SIMULINK toolbox with the speed sensor and without speed sensor. Various Fuzzy controllers for DTC based induction motor drives also simulated. The hardware needed for the drive is assembled.

The following conclusions are drawn from the present work.

1. A method for the simulation of the direct torque controlled drive is presented using MATLAB/SIMULINK toolbox.
2. The drive is simulated for the following cases
   - drive starting from rest
   - sudden changes in load torque
   - speed reversal
   - operation above the base speed with field weakening

3 The response of the simulations obtained is found to be well in agreement with results reported in literature.

4 A field weakening controller has been implemented and with this operation the speed of the drive has been increased above the base speed.

5 The rotor speed estimation method implemented is found to be suitable for the sensorless operation except at starting conditions where ripple is in estimated speed.

6 The hybrid fuzzy controller reduces the steady state error as compared with PI-type fuzzy logic controller (FLC), while keeping the merits of PI-type FLC. PI type fuzzy control and hybrid fuzzy control are nonlinear laws and with the integral mechanism, the associated drive system is robust to load disturbance and with less steady state error.

7 PD-type fuzzy control does not have integral mechanism; the associated system is with significant steady state error.

Future Scope

1. Reduction of the ripples in the torque and the flux by the use of methods other than the classical direct torque control.
2. The implementation of the direct torque controlled induction motor drive with speed sensor and without speed sensor.

References

[1]. Takahashi and T. Noguchi, "A New Quick Response and High efficiency Control Strategy of an Induction motor", IEEE Trans. Ind Appl, Vol.IA-22, No.5, pp.820827, 1986, September.

[2]. Hoang Le-Huy, "Modelling and simulation of electrical drives using MATLAB/Simulink and Power System Blockset," in Proc. IEEE IES'00, 2000, pp.1603-1611.

[3]. J.R.G. Schofield, "Direct torque control of induction motors," in Colloquium'95, 1995 IEE on Vector Control and Direct Torque Control of Induction motors, pp. 1/1-1/3.

[4] A.H.M. Yatim and N.R.N Idris, "Implementation of direct torque control of induction machine utilizing TMS320C31 digital signal processor," in Proc. IEEE Intl. Symposium on Signal Processing and its Applications, 2001, pp. 627-630.

[5]. Bibhu Prasad Panigrahi, Dinkar Prasad, Sabyasachi SenGupta," A simple hardware realization of switching table based direct torque control of induction motor" in Electric Power Systems Research xxx (2006) xxx–xxx.

[6]. N.Idris, A. H. M. Yatim, N. D. Muhamad and T. C. Ling, "Constant frequency Torque and Flux controllers for Direct Torque Control of Induction Machines"©2003 IEEE.

[7]. Nik Rumzi Nik Idris Abdul Halim Mohd Yatim Naziha Ahmad Azli "direct torque control of induction machines with constant switching frequency and improved stator flux" ieee transactions on industrial electronics, vol. 51, no. 4, august2004.

[8]. Nik Rumzi Nik Idris, *Senior Member, IEEE,* and Abdul Halim Mohamed Yatim, *Senior Member, IEEE"* Constant Frequency Torque and Flux controllers for Direct Torque control of induction machines" IEEE proc.0-9999-9999-0/03/$17.00 ©2003

[9]. Yen-Shin Lai, *Member, IEEE* and Jian-Ho Chen " New Approach to Direct Torque Control of Induction Motor Drives for Constant Inverter Switching Frequency and Torque Ripple Reduction" IEEE TANSACTIONS ON ENERGY CONVERSION, VOL. 16, NO. 3, SEPTEMBER 2001.

[10]. P. Marino, M. D'Incecco and N.Visciano "A Comparison of Direct Torque Control Methodologies for induction Motor "2001 IEEE Porto Power Tech Conference IO"' – 13'h Scptember, Porto, Portugal.

[11]. J. Rodr.´guez, J. Pontt, C. Silva, R. Huerta and H. Miranda "Simple direct torque control of induction machine using space vector modulation" ELECTRONICS LETTERS 1st April 2004 Vol. 40 No. 7

[12]. A. Arias; J.L. Romeral, E. Aldabas and M.G.Jayne"Fuzzy Logic Direct Torque Control "ISIE'2000, Cholula, Puebla, Mexico.

[13]. *Ji-Su Ryu, In-Sic Yoon, Kee-Sang Lee and Soon-Chan Hong* "direct torque control of induction motors using fuzzy variable switching sector" isie 2001, pusan, korea.

[14]. Malik Elbuluk "Torque Ripple Minimization in Direct Torque Control of Induction Machines" 2003 IEEE.

[15]. Yen-Shin Lai, *Senior Member, IEEE,* and Juo-Chiun Lin "New Hybrid Fuzzy Controller for Direct Torque Control Induction Motor Drives" IEEE TRANSACTIONS ON POWER ELECTRONICS, VOL. 18, NO. 5, SEPTEMBER 2003.

[16]. Junfeng Xu, Jianping Xu, Yinglei Xu, Fengyan Wang "Direct Torque Control of Induction Machines Using Discrete Space Vector Modulation Applied to Traction" 2003 IEEE.

[17]. J. Rodr.´guez, J. Pontt, C. Silva, R. Huerta and H. Miranda "Simple direct torque control of induction machine using space vector modulation" ELECTRONICS LETTERS 1st April 2004 Vol. 40 No. 7.

[18]. Nik Rumzi Nik, Idris Abdul Halim Mohd Yatim "Modeling of a New Torque Controller for Direct Torque Control of Induction Machines"2000 IEEE.

[19]. Domenico Casadei, *Member, IEEE,* Francesco Profumo, *Senior Member, IEEE,* Giovanni Serra, *Member, IEEE,* and Angelo Tani "FOC and DTC: Two Viable Schemes

for Induction Motors Torque Control" IEEE TRANSACTIONS ON POWER ELECTRONICS, VOL. 17, NO. 5, SEPTEMBER 2002.

[20]. Hoang Le-Huy "Comparison of Field-Oriented Control and Direct Torque Control for Induction Motor Drives" 1999 IEEE.

[21]. Mohammad Bagher Bannae Sharifian and Jawad Faiz "Implementation of sensor less DTC technique for speed control of induction motor using a novel switching pattern".

[22] J.Maes and J.Melkebeek, "Speed sensorless direct torque control of induction motors using adaptive flux observer", in Proc.IEEE IAS'99, 1999, pp.3-7, vol.4.

[23] Toshiyuki Kanmachi, Isao Takahasi "Sensorless Speed control of an induction motor with no influence of secondary resistance" IEEE IAS Ann.Mtg, pp408-413, 1993.

[24] A.monti, F.pironi, F.Sartogo and P.vas, "A new state observer for sensorless DTC control," in proc.IEE Power electronics and variable speed drives Intl.conf.1998 pp.11-317.

[25] Ma Xianmin, "Adaptive control system of speed sensorless AC motor variable speed drive," in Proc.IEEE world congress intelligent control and automation, 2000, pp.3141-3143.

[26] C.Lascu, I.Boldea and F.Blabjerg,"A modified direct torque control for induction motor senseless drive," in IEEE Trans.Industry applications, vol.36, pp. 122-130, jan-feb.2000.

[27] Maurizio Cirrincione, Marcello Pucci* "Sensorless direct torque control of an induction motor by a TLS-based MRASobserver with adaptive integration" *I.S.S.I.A-C.N.R. (Istituto di Studi sui Sistemi Intelligenti per l'Automazione), Section of Palermo, Viale delle Scienze snc, 90128 Palermo, Italy*

[28] Ralph Kennel a, Elwy E. El-kholy b,*, Sabry Mahmoud b, Abdou El-refaei c, Farouk Elkady "Improved direct torque control for induction motor drives with rapid prototyping system" Energy Conversion and Management 47 (2006) 1999–2010

[29].Yen-Shin Lai, *Senior Member, IEEE,* and Juo-Chiun Lin "New Hybrid Fuzzy Controller for Direct Torque Control Induction Motor Drives" IEEE TRANSACTIONS ON POWER ELECTRONICS, VOL. 18, NO. 5, SEPTEMBER 2003.

[30]. J. C. Trounce, S. D. Round, R. M. Duke "evaluation of direct torque control using space vector modulation for electric vehicle applications"ieee proc.

[31]. M´onica E. Romero, Julio H. Braslavsky and Mar´.a I.Valla "Ripple Reduction in Direct Torque and Flux Control of Induction Motors via Sliding Modes" *Preprint submitted to Elsevier Science 30 December 2003.*

[32].P.Vas, "Sensorless Vector and Direct Torque Control" Oxford, Oxford University press, 1998.

[32]. R. Krishnan "Electric Motor Drives Modeling, Analysis, and Control" Prentice-Hall of India.

[33]. B.K.Bose "Modern Power Electronics and AC Drives" Pearson Education.

[34].SBC6711 Development Package Manual, Innovative Integration board, November 26, 2002.

[35]. OMNIBUS User's Manual, Innovative Integration board, April 1, 2002.

Appendix A

Specification and the Parameters of Induction Motor:

415-v, 3-phase, 50Hz, 4-pole, Squirrel cage type

Machine's parameters:

Stator resistance/phase Rs=11.72Ω

Stator leakage inductance/phase = 0.03515H

Rotor resistance/phase =9.45Ω

Rotor leakage inductance/phase = 0.03515H

Magnetizing = 0.678H

Moment of inertia =0.001Kg-mt^2

Hall-Effect Current Transformers/Sensors

Closed-loop HALL-Effect current sensors are widely used in a variety of applications requiring an accurate, fast response signal proportional to the current being measured. Products are available for panel and PCB mounting covering primary current up to 1000A and provide complete galvanic isolation between the primary and the measuring circuit.

Closed-loop Hall effect current-sensors use the ampere-turn compensation method to enable measurement of current from dc to high frequency with the ability to follow rapidly changing level or wave shapes. The application of primary current (I_p) causes a change of the flux in the air-gap, this in turn produces a change in output from the hall element away from the steady-state condition. This output is amplified to produce a current (I_s) which is passed through the secondary winding causing a magnetizing force to oppose that of the primary current, there by, reducing the air-gap flux. The secondary current will increase until the flux is reduced to zero. At this point, the hall element output will have returned to the steady state condition and the ampere-turn product of the secondary circuit will match that of the primary. The current that passes through the secondary winding is the output current.

Main features of the current-sensor used are:

I. High accuracy.
II. Galvanic isolation between primary and secondary.
III. Non-Contact ness.
IV. Covers ac, dc and impulse current measurements.
V. Ease of installation.
VI. Wide dynamic range.

Linearity of the sensor is 0.1% of normal primary current and the operating temperature range is 0-70°C.

Voltage Sensors AD202/AD204

Features

I. Small Size: 4 Channels/inch
II. Low Power: 35mW (AD204)
III. High Accuracy: ±0.025% Max Nonlinearity (K Grade)
IV. High CMR: 130 dB (Gain = 100 V/V)
V. Wide Bandwidth: 5 kHz Full-Power (AD204)
VI. High CMV Isolation: ±2000 V_{PK} Continuous (K Grade)

(Signal and Power)

I. Isolated Power Outputs
II. Uncommitted Input Amplifier

Applications

I. Multi-channel Data Acquisition
II. Current Shunt Measurements
III. Motor Controls
IV. Process Signal Isolation
V. High Voltage Instrumentation Amplifier

General Description

The AD202 and AD204 are general purpose, two-port, and transformer- coupled isolation amplifiers that may be used in a broad range of applications where input signals must be measured, processed, and/or transmitted without a galvanic connection. These industry standard isolation amplifiers offer a complete isolation function, with both signal and power isolation provided for in a single compact plastic SIP or DIP style package. The primary distinction between the AD202 and the AD204 is that the AD202 is powered directly from a 15 V dc supply while the AD204 is powered by an externally supplied clock, such as the recommended AD246 Clock Driver.

The AD202 and AD204 provide total galvanic isolation between the input and output stages of the isolation amplifier through the use of internal transformer-coupling. The functionally complete AD202 and AD204 eliminate the need for an external, user-supplied dc-to-dc converter. This permits the designer to minimize the necessary circuit overhead and consequently reduce the overall design and component costs. The design of the AD202 and AD204 emphasizes maximum flexibility and ease of use, including the availability of an uncommitted op-amp on the input stage. They feature a bipolar ±5 V output range, an adjustable gain range of from 1V/V to 100 V/V, ± 0.025% max nonlinearity (K grade), 130 dB of CMR, and the AD204 consumes a low 35mW of power.

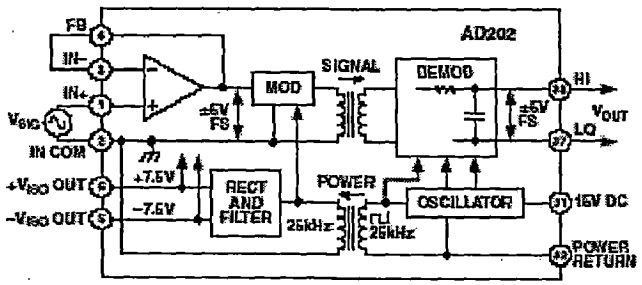

Figure A-1

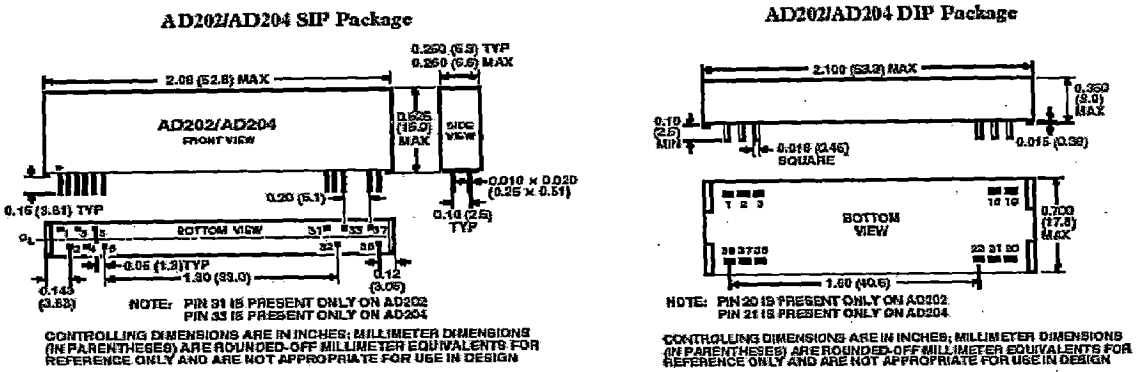

Figure A-2

The functional block diagram of AD202 is shown in *fig A-1* and *fig A-2* shows the pin configuration of AD202 in SIP and DIP package respectively.

Power Semiconductor Switches

Traditionally thyristors have been used as switches in converters. But the PWM technique requires forced-commutation of thyristors that necessitates the need for additional commutation circuitry, thus, adding to the cost, bulkiness and complexity of the converter circuit. Further more, the thyristors can't be switched at higher frequencies and this puts a limit on the switching frequency of the PWM converters. In recent years, more and more power semiconductor devices with high switching frequencies and/or power capability such as bipolar transistors, power MOSFETs, GTOs and IGBTs are becoming quite popular. This makes possible the easy use of the PWM technique to improve the quality of input current waveform and power factor.

Power Transistor

A power-transistor employed as a solid-state switching device and requires only one signal to turn it ON and it turns OFF automatically on the removal of this signal. Thus, in the PWM voltage-source converters, no commutation circuitry is required and the problems associated with the commutation (of thyristors) are automatically overcome. Further, the control circuitry is much simplified. Since the turn-ON and turn-OFF times of the order of 1μsec or less are achieved in power transistors, the devices can be operated at a high switching frequency. The power transistors suffer from a major problem of the second breakdown (SB), which is a destructive phenomenon, resulting from the current-flow to a small portion of the base and producing localized hotspots. If

the energy in these hotspots is sufficient, the excessive localized heating may damage the device. Other drawbacks are the sensitivity to transients and low overload capacity. The schematic block diagram is shown in *fig A-3*.

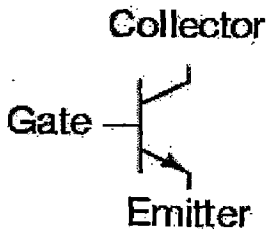

Figure A-3

Gate Turn OFF Thyristors (GTOs)

GTOs seems to hold a lot of promise fo the future. Presently their use is limited because of high cost and non-availability. A GTO can be turned-OFF by a negative gate-pulse and can be triggered by a positive gate-pulse. When a GTO has been turned-ON, it behaves as a thyristor. It can be manufactured for the highest voltage and current ratings (several kV and kA) and is mainly used for high power and/or high voltage equipment. With the obvious advantage of the non-requirement of a commutation circuit, which lays a restriction on the operating frequency of thyristors, the GTO has also some disadvantages. During turn-ON and turn-OFF, a GTO acts like a transistor, running a risk of second breakdown if the gate-pulse is insufficient. A GTO has a higher ON-state voltage as compared to a thyristor and the latching and holding currents are also high.

Power MOSFET

A Power Mosfet is a voltage-controlled device and requires only a small input current. The switching speed is very high and the switching times are of the order of nano-seconds. Power Mosfet's are finding increasing applications in low-power, high frequency converters. Mosfet's don't have the problems of the second breakdown as do the BJT's. Mosfet's are of two types

1) Deletion Mosfet's and,
2) Enhancement Mosfet's.

The main features of power Mosfet's are summarized as below:

I. Better reliability.

II. Simpler and cheaper driver circuitry.

III. Higher switching frequency (well above 1Mhz) due to fast switching speed and better efficiency, smaller overall circuit size and weight at high frequency.

IV. High overload and peak current handling capability.

V. Absence of second breakdown reduces the snubber circuitry in switching applications and

VI. Better temperature capability.

Like any other semiconductor device, Power Mosfet's do have their own subtleties and these must be recognized for the successful operation of the devices.

STATIC CHARGE: Power Mosfet's can be damaged by static charge when handling, testing or installing into a circuit. However, they have greater self-capacitance and are much more able to absorb the static charge. It is wise to employ the elementary precautions such as the grounded wrist straps, electrically grounded stations and grounded soldering irons.

GATE-VOLATGE TRANSIENTS: Excessive voltage applied to the gate of a power Mosfet's will punch through the gate oxide, thus causing a permanent damage. A typical gate-source voltage rating is ±20V. The simplest solution where the gate voltage transients are suppressed is to connect a clamping Zener diode between the gate and the source.

All the power Mosfet's have an integral body-drain diode built into their structure. This is shown in the *fig A–4.*

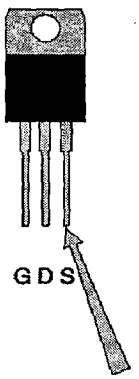

Figure A-4

INSULATED GATE BIPLOAR JUNCTION TRANSISTORS (IGBT'S)

An IGBT combines the advantages of the BJT's and Mosfet's. It has high input impedance like Mosfet's and low ON-state condition losses like BJT's. But there is no second breakdown problem like BJT's.

An IGBT is a voltage-controlled device like a power Mosfet. It has the advantages of ease of gate-drive, peak-current capability and ruggedness. It is inherently faster than a BJT. However, the switching speed is inferior to that of Mosfet's. They have three terminals, and they are Gate (G), Collector(C) and Emitter (E). IGBT's are finding increasing applications in medium-power applications such as dc and ac motor drives, power supplies, etc. The schematic diagram is shown in *fig A-5*.

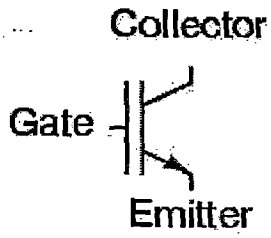

Figure A-5